

UCSF

UC San Francisco Electronic Theses and Dissertations

Title

MicroRNA regulation of Th2 cell function and asthma pathogenesis

Permalink

<https://escholarship.org/uc/item/3w4245m3>

Author

Simpson, Laura Jane

Publication Date

2015

Peer reviewed|Thesis/dissertation

MicroRNA regulation of Th2 cell function and asthma pathogenesis

by

Laura J. Simpson

DISSERTATION

Submitted in partial satisfaction of the requirements for the degree of

DOCTOR OF PHILOSOPHY

in

Biomedical Sciences

in the

GRADUATE DIVISION

of the

UNIVERSITY OF CALIFORNIA, SAN FRANCISCO

Copyright (2015)

by

Laura Simpson

Acknowledgements

I first want to thank my thesis advisor, Mark Ansel, for teaching me everything I know about how to be a good scientist. Thanks for teaching me to argue thoughtfully, self-criticize constructively, and experiment skillfully. Thanks for creating a supportive, fun, and challenging environment in the lab. I would like to thank the rest of the Ansel lab, especially Robin Kageyama, Yelena Bronevetsky, and Sana Patel, for helping me through the inevitable challenges we face in lab. I feel very lucky to have been able to call the Ansel lab my home.

Thank you also to my thesis committee, Dean Sheppard, Michelle Hermiston, and Robert Belloch, for sharing your expertise to make my project so much better. Thanks to our many collaborators, especially Prescott Woodruff, John Fahy, and Laura Koth, who have connected us to the clinical side of UCSF, and help us to bridge the gap between science and medicine. Thanks to the BMS program, especially Jason Cyster, Lisa Magargal, Monique Piazza, and Demian Sainz, for giving me the opportunity to learn.

Rob Judson, Rob Bell, Sean Bakker Kellogg, Sarah Bakker Kellogg, Julia Margulis, and Alina Bogdanov: thank you for keeping me sane, making me feel at home, and for challenging me to always be the best I can be. Thank you to my family, Mary Ann Simpson, Andrew Simpson, Diane Flood, Jason Flood, Drew and James, for always supporting me, and for making the distance seem much smaller. I love you all.

Finally, I want to thank Robin Kageyama for being my lab partner, my best friend, and my family. Thanks for helping me through the rough times in lab and in life, and for going on adventures with me. I love you and I like you.

Contributions of Co-authors to Presented Work

Chapter 2 of this thesis was published in *Nature Immunology* in 2014 as “A miRNA upregulated in asthma airway T cells promotes Th2 cytokine production.” The authors on this publication were Laura J. Simpson, Sana Patel, Nirav R. Bhakta, David F. Choy, Hans D. Brightbill, Xin Ren, Yanli Wang, Heather H. Pua, Dirk Baumjohann, Misty M. Montoya, Marisella Panduro, Kelly A. Remedios, Xiaozhu Huang, John V. Fahy, Joseph R. Arron, Prescott G. Woodruff, and Karl M. Ansel. L.J.S. designed, performed, and analyzed most experiments. S.P, D.F.C. H.D.B., X.R., Y.W., H.H.P, D.B., M.M.M., M.P., and K.A.R. helped design and perform some experiments. N.R.B. analyzed expression data. X.H., J.V.F., J.R.A., P.G.W. and K.M.A. helped design the clinical study and some experiments. L.J.S. wrote the manuscript. All authors reviewed and approved the manuscript.

Chapter 3 of this thesis is as yet unpublished. Nonetheless, the work would not have been possible without Laura Christian, who sorted most of the clinical samples, Suresh Garudadri, who processed BAL samples, Hannah MacLeod and Liam Barry, who processed sputum samples, and Jeanmarie Gonzalez and Sara Sun, who helped perform miRNA qPCR for our interim analysis for RITA. Erin Gordon, John Fahy, Prescott Woodruff, and Mark Ansel helped design the clinical studies and some experiments. All of these co-authors helped analyze and interpret most experiments.

MicroRNA regulation of T_H2 cell function and asthma pathogenesis

Laura J. Simpson

Abstract

MicroRNAs (miRNAs) exert powerful effects on immune function by tuning networks of target genes that orchestrate cell behavior. We sought to uncover miRNAs and miRNA-regulated pathways that control the T_H2 responses that drive pathogenic inflammation in asthma. Profiling miRNA expression in human airway-infiltrating T cells revealed miR-19a elevation in asthma. Modulating miR-19 activity altered T_H2 cytokine production in both human and mouse T cells, and T_H2 cell responses were markedly impaired in cells lacking the entire miR-17~92 cluster. miR-19 promotes T_H2 cytokine production and amplifies PI(3)K, JAK-STAT, and NF-κB signaling by direct targeting of PTEN, SOCS1, and A20. Thus, miR-19a upregulation in asthma may be an indicator and a cause of increased T_H2 cytokine production in the airways.

T_H2 cells are not the only lymphocyte involved in asthma pathogenesis. Other T-helper subsets, such as T_H1 and T_H17 cells, are present in asthmatic airways, and may be responsible for non- T_H2-driven asthma. Through collaborative clinical studies, we aim to profile miRNA expression in various T-helper cells in asthmatic and healthy airways to uncover pathways involved in T_H2-driven and non- T_H2-driven asthma pathogenesis. This study also allows us to immunophenotype healthy and asthmatic individuals by flow cytometry of bronchoalveolar lavage fluid and peripheral blood.

Although we have focused on lymphocyte functions in asthma pathogenesis, the role of innate immune cells cannot be overlooked. Type 2 innate lymphoid cells (ILC2s) and basophils are capable of producing T_H2 cytokines, and can respond to environmental cues of lung damage. Through a collaborative clinical study, we investigated the prevalence and function of ILC2s and basophils in asthma by flow cytometric immunophenotyping and gene expression of sputum cell pellets. Interestingly, ILC2s are equally rare in the sputum of healthy and asthmatic individuals, while basophils are more abundant in asthmatic individuals. The number of basophils positively correlates with sputum cell pellet expression of T_H2 cytokines, and correlates with asthma severity. These findings suggest a role for basophils in polarizing the lung environment towards T_H2 , and increasing asthma symptoms.

Table of Contents

Chapter 1: Introduction	1
Asthma pathogenesis and treatment.....	2
miRNA regulation of lymphocyte development and function.....	4
Overview of thesis work	18
Chapter 2: A miRNA upregulated in asthma airway T cells promotes Th2 cytokine production	28
Abstract	29
Introduction.....	30
Results.....	33
Discussion	40
Materials and Methods.....	46
Tables	53
Figures.....	54
Supplementary Figures and Tables.....	##
Chapter 3: Characterization of immune cell infiltration in asthma	85
Introduction.....	86
Results.....	89
Discussion	94
Materials and Methods.....	97
Figures.....	102

Chapter 4: Discussion, Conclusions, and Future Directions	122
Summary	123
miR-17~92 regulation of T-helper cells	123
Adaptive and innate immune regulation of asthma pathogenesis.....	124
References	127
Appendix 1: Interleukin-4 production by follicular helper T cells requires the conserved I4 enhancer hypersensitivity site V	136
Appendix 2: An integrated nano-scale approach to profile miRNAs in limited clinical samples	150

List of Figures

Chapter 1

- Figure 1** miRNAs set thresholds for lymphocyte development.....22
- Figure 2** miRNA regulation of the PI3K pathway24
- Figure 3** miRNAs as biomarkers or indicators of cellular processes.....26

Chapter 2

- Figure 1** miR-19a expression is elevated in CD4⁺ T cells from asthmatic lungs54
- Figure 2** The miR-17~92 cluster promotes T_H2 cytokine production.....56
- Figure 3** The miR-17~92 cluster promotes T_H2 cytokine production in a cell-intrinsic and proliferation-independent manner58
- Figure 4** miR-19a and miR-19b rescue the T_H2 cytokine defect in 17~92^{ΔΔ} cells60
- Figure 5** miR-19a promotes IL-13 production in human CD4⁺ T cells62
- Figure 6** Several miR-19 targets negatively regulate T_H2 cytokine production64
- Figure 7** The miR-17~92 cluster promotes T_H2-driven inflammation *in vivo*67
- Figure S1** Heatmap of all subjects and miRNAs analyzed by multiplex qPCR69
- Figure S2** miR-17~92 expression in 17~92^{ΔΔ} and 17~92^{+/+} naïve CD4 T cells71
- Figure S3** miR-19 activity in 17~92^{ΔΔ} and 17~92^{+/+} cells and effects of mimics and inhibitors73
- Figure S4** Effects of miR-17~92 members on proliferation75
- Figure S5** Identification of myeloid cells in BAL in the *in vivo* allergic airway inflammation model77

Chapter 3

Figure 1	Gating strategy for sorting T-helper subsets from PBMCs and BAL	102
Figure 2	Cytokine production by T-helper subsets in PBMCs	104
Figure 3	B2M expression analysis in RNA large fraction from RITA interim analysis	106
Figure 4	Transcription factor mRNA expression analysis in sorted clinical samples	108
Figure 5	miRNA expression in sorted clinical samples	110
Figure 6	FACS analysis of PBMCs and sputum cells from humans with asthma (CASA study)	112
Figure 7	Distribution of cell types and total ST2 expression in PBMC and induced sputum	114
Figure 8	Fluorescence Minus-One stains for ST2 antibody specificity	116
Figure 9	Distribution of ST2-expressing cell types in PBMCs and induced sputum .	118
Figure 10	Sputum basophils numbers correlate with PC20 and Th2 gene expression .	120

List of Tables

Chapter 2

Table 1	Healthy and asthmatic subjects providing bronchoalveolar lavage CD4 T cells for miRNA expression analysis	53
Table S1	List of miRNAs for each multiplex miRNA Taqman qPCR.....	79
Table S2	P-values and False Discovery Rate (FDR) calculations for miRNA expression analysis	81
Table S3	List of siRNAs used for target screening	84

Chapter 3

Table 1	Flow cytometry panel for sorting T-helper subsets – RITA	100
Table 2	Flow cytometry panel for analysis of sputum and PBMCs – CASA	101

Chapter 1

Introduction

Asthma pathogenesis and treatment

Asthma is a chronic pulmonary disorder defined by excessive inflammation in the airways leading to variable airway hyperresponsiveness and bronchospasm^{1,2}. The diagnosis of asthma in the United States and the developed world has increased over the last 20 years³.

Asthma is attributed to many genetic and environmental factors, without one clear cause initiating the disease. Most patients manage their asthma symptoms by long-term use of inhaled corticosteroids (ICS), leukotriene modifiers, or long-acting β_2 agonists. Use of acute rescue bronchodilators is limited to asthma attacks; these medicines include short-acting β_2 agonists, or oral or intravenous corticosteroids¹. However, responsiveness to therapy is highly variable between patients and within a patient over time. Disease severity is determined based on a patient's *impairment* and *risk*. 'Impairment' refers to the concurrent degree of control of asthma symptoms, and 'risk' refers to future events that should be prevented or reduced by the current treatment plan. Asthma can be further divided into atopic asthma and non-atopic asthma. Atopic asthma is allergen-driven, while non-atopic asthma has a less clear etiology.

The defining feature of asthma in all subtypes is underlying inflammation of the airways. Typical inflammatory cells involved are T lymphocytes, eosinophils, mast cells, and neutrophils. Inflammation contributes to variable airway obstruction and airway hyperresponsiveness (AHR), and promotes epithelial cell injury, which in turn induces more inflammation. Airway inflammatory cells contribute to the asthma phenotype by releasing inflammatory mediators such as cytokines, chemokines, and histamines⁴.

Atopic asthma is associated with increased numbers of activated T cells in the lung, which are skewed towards a T-helper type 2 (Th2) phenotype^{5,6}. Th2 cells are CD4-expressing T cells that differentiate from naïve CD4 T cells upon antigenic stimulation and in the presence of

the polarizing cytokine interleukin-4 (IL-4). When Th2 cells are fully differentiated and activated, they produce and secrete IL-4, IL-5, and IL-13. IL-13 acts directly on airway epithelium to promote AHR, mucus hypersecretion, and epithelial cell damage ⁷. IL-4 and IL-5 function primarily to promote infiltration of inflammatory cells. These key cytokines drive an immune response that is characterized by increased eosinophil infiltration in the airways and augmented production of immunoglobulin E (IgE) by B cells. IgE further drives the Th2 phenotype by activating mast cells and basophils that express the high affinity IgE receptor (FCER1) to release granules and produce Th2 cytokines ⁸. Type 2 innate lymphoid cells (ILC2s) also produce Th2 cytokines and are present in human airways ^{5,9}. The presence and function of ILC2s in asthma is the focus of part of our collaborative work in asthma clinical studies with John Fahy, M.D, covered in chapter 3.

Th2 cells are central in orchestrating and perpetuating the immune response in the airways by coordinating the infiltration and activation of other immune cells ^{10,11}. New therapeutic approaches to asthma should aim to modify the inflammatory pathogenesis, not just treat the symptoms, in an attempt to clear the inflammation from the airways. Th2 cells should be the focus for future therapeutic development; a therapy that targets Th2 cells in the asthmatic airway would likely alter many of the immune cells in the airway.

The balance between Th1 and Th2 cells has long been an area of research interest ¹². Both cell types differentiate from the same precursor CD4 T cells, and the microenvironment determines the cell fate. Th2 cells differentiate when IL-4 is present, while Th1 cells differentiate in response to IL-12 and IFN- γ . Each cell type has transcription factors that promote the cell fate decision; GATA3 promotes Th2 cell differentiation ¹³, while T-bet promotes Th1 differentiation.

Another layer of genetic regulation of cell fate decisions is post-transcriptional regulation of gene products by miRNAs, which we will focus on in this work.

miRNA regulation of lymphocyte development and function

The immune system imposes extensive regulation on lymphocyte development to prevent the survival and activation of autoreactive lymphocytes. Dysregulation of cell fate checkpoints in developing and mature lymphocytes can result in autoimmunity. Developing thymocytes go through several checkpoints that depend on the strength of signaling received through the T cell receptor (TCR)¹⁴. Similarly, the strength of B cell receptor (BCR) signaling determines whether developing B cells will survive and mature¹⁵. In the periphery, prevention of autoreactive B and T cell responses continues to depend on properly tuned signaling pathways, cell death and survival factors, and transcriptional and epigenetic regulation of effector cell differentiation. In addition, regulatory T cell (Treg) homeostasis and function is critical to restrain the activity of mature effector T cells, such as T-helper 1 (Th1), Th2, or Th17 cells¹⁶. All of these tolerance mechanisms depend on tunable responses that are sensitive to minor perturbations in the expression of cascades of proteins. In particular, antigen receptor signaling can be quantitatively manipulated by minor changes in the expression of limiting regulators of downstream signaling pathways, such as the PI3K and NFκB pathways. This type of manipulation is commonly carried out by microRNAs (miRNAs).

miRNAs are short noncoding RNA molecules that are transcribed alone or in polycistronic clusters in the genome, and sometimes appear within the introns or exons of coding genes¹⁷. Their primary transcripts are sequentially processed by DROSHA/DGCR8 and Dicer to produce mature miRNAs that are loaded into the miRNA-induced silencing complex (miRISC)

¹⁸. The miRNA guides the miRISC to target mRNAs by complementary base pairing, usually in 3' untranslated regions (UTRs), resulting in translational repression and/or mRNA degradation

¹⁹. miRNAs that share a similar seed sequence (nucleotides 2-8 of the mature miRNA) are defined as a family, and have significant overlap in their mRNA targets. miRNAs regulate networks of target genes. Each miRNA can target hundreds of distinct mRNAs, and most mRNA transcripts are predicted targets of multiple miRNAs.

Although miRNA regulation of each target results in small changes in gene expression, the network activity of miRNAs targeting hundreds of genes simultaneously can effect dramatic changes in cell behavior. These changes can be easily observed in the immune system, where miRNAs modulate many cell fate decisions made by developing and mature lymphocytes ²⁰⁻²².

miRNA regulation of early lymphocyte development

MicroRNAs are important nodes in the gene expression networks that govern lymphocyte development and the establishment of central tolerance. These processes operate through cell fate checkpoints that promote the maturation of cells that correctly recombine antigen receptor genes, while eliminating those that form strongly self-reactive receptors by apoptosis. Because these checkpoints rely on proper cellular interpretation of antigen signal strength, dysregulated TCR or BCR signaling can increase the survival of autoreactive lymphocytes and contribute to the development of autoimmune disease. miRNAs that regulate cell survival, antigen receptor signaling, and the availability of self antigens during lymphocyte development all play important roles in the development and selection of a repertoire of B and T lymphocytes bearing useful and safe antigen receptors.

Early research shows that the miRNA biogenesis pathway is critical for early B cell development, as ablation of *Dicer* leads to an almost complete block at the pro- to pre-B cell transition²³. A key function of pro-B cells is V(D)J recombination of BCR genes to generate a functional antigen receptor. *Dicer* deficiency does not alter the basic mechanism of V(D)J recombination, but it does alter the resulting BCR repertoire, suggesting that miRNAs play an important role in regulating the survival of potentially self-reactive B cells. Further analysis identified BIM (encoded by *Bcl2l1*) as a key miRNA target involved in the regulation of pro-B cell survival²³.

This work demonstrating the importance of the miRNA biogenesis pathway to B cell development was accompanied by further research that detailed the major role of miR-17~92²⁴. The miR-17~92 cluster is composed of six miRNAs belonging to four families: miR-17, miR-18, miR-19, and miR-92. Additional members of these miRNA families are expressed from two related genomic clusters. The miR-17~92 cluster promotes the survival of developing B lymphocytes at least in part through its ability to regulate PI3K signaling and genes expressed downstream of this pathway (**Figure 1A**). BIM is induced by PI3K signaling and is directly targeted by several miR-17~92 cluster miRNAs^{23,24}. The tumor suppressor PTEN, a potent negative regulator of the PI3K pathway, is also targeted by miR-17~92 miRNAs (**Figure 2**). When miR-17~92 is deleted from developing B cells, PTEN and BIM expression are elevated and cells undergo apoptosis, resulting in B cell deficiency. Conversely, miR-17~92 overexpression during B or T cell development leads to increased survival and promotes lymphoproliferative disease and autoimmunity²⁵.

In early stages of T cell development in the thymus, signaling through the newly formed TCR provides important survival signals. However, strong TCR signals in the thymus indicate

autoreactivity and induce apoptosis. Therefore, miRNAs that alter the strength of TCR signaling can increase the survival of cells that normally would have been deleted from the repertoire. miR-181 acts as a “rheostat” of TCR signal strength by targeting several phosphatases (**Figure 1B**), including PTPN22, SHP-2, DUSP5, and DUSP6²⁶, as well as PTEN²⁷. Early in development, double-negative (DN) thymocytes express high levels of miR-181, conferring high sensitivity to pre-TCR and TCR signals. miR-181 expression declines as thymocytes mature to the double-positive (DP) and single-positive (SP) stages, decreasing sensitivity to TCR ligation during positive and negative selection. Altering miR-181 expression dysregulates TCR signaling, and thymocytes that would normally be deleted from the repertoire survive instead²⁸. These findings suggested that miR-181 might be capable of regulating the onset and/or progression of T cell-mediated autoimmune disease. Indeed, thymic miR-181 expression is important for the elimination of self-reactive thymocytes responding to an endogenous positively-selecting self ligand²⁸.

miRNAs also affect central tolerance through their activity in thymic antigen presenting cells. Medullary thymic epithelial cells (mTECs) promiscuously express tissue-specific self antigens and present them to developing thymocytes, eliminating cells bearing TCRs reactive against self antigens. miRNA biogenesis in TECs is critical to the proper function of the thymus. *Dicer*^{29,30} or *Dgcr8*³¹ deletion specifically in TECs dramatically disrupts thymic architecture with increased TEC apoptosis and severely reduced thymic cellularity, particularly in the mature mTEC population^{30,31}. *Dicer* deletion in mTECs also leads to changes in promiscuous gene expression³⁰. In an inflammatory setting, miRNA-deficient mTECs do not prevent the maturation of self-reactive autoimmune uveitis-inducing IRBP-specific T cells³¹.

In addition, thymi with miRNA-deficient TECs undergo premature involution in response to IFN- α ²⁹. Deletion of the miR-29a cluster, consisting of miR-29a and miR-29b-1, partially replicates the defects seen in Dicer-deficiency. miR-29a is highly expressed in mTECs and targets *Ifnar1*, the mRNA that encodes the IFN- α receptor. Deletion of miR-29a increases IFNAR1 expression and downstream STAT1 phosphorylation, indicating that miR-29a regulates the strength of signaling through the IFN- α response pathway in mTECs²⁹.

These seminal studies demonstrate that miRNAs are essential regulators of lymphocyte development and selection. They regulate cell survival and critical signaling pathways in multiple key cell types, tuning response thresholds and developmental checkpoints. Further research will undoubtedly uncover additional miRNAs and target networks that contribute to the robust imposition of central tolerance.

miRNA regulation of lymphocyte effector functions

Mature autoreactive lymphocytes that have escaped central tolerance can become effector cells that drive autoimmune disease. Peripheral tolerance mechanisms restrict autoantibody production by B cells and tissue inflammation and destruction caused by T cells. These mechanisms are subject to miRNA regulation, and altering miRNAs that regulate peripheral lymphocyte fate decisions can lead to autoimmunity. Understanding how miRNAs regulate B and T cell activation, survival, proliferation, differentiation and effector functions can help to identify pathways that are dysregulated in autoimmune disease, or that could be targeted to prevent or dampen autoimmune pathology.

Immature B cells leave the bone marrow to complete their development and selection in the periphery. As in the bone marrow, the fate of immature B cells depends on BCR signals, and

dysregulation of BCR signal strength can skew the B cell repertoire and allow maturation of autoreactive cells³². Deletional tolerance and receptor editing eliminate BCRs that react strongly to peripheral self-antigens. Moderate BCR signals promote the generation of marginal zone (MZ) or transitional B cells, while weaker BCR signals promote the generation of follicular (FO) B cells³³. Ablation of Dicer late in B cell development leads to a significant decrease in the number of FO B cells, but relatively normal numbers of MZ and transitional B cells³⁴. miR-185 and several other miRNAs are more abundant in FO B cells compared to MZ or transitional B cells. Overexpression of miR-185 in FO B cells decreases expression of its target BTK, a kinase that transduces signals downstream of the BCR³⁴. Dicer ablation in peripheral B cells also increases class switch recombination and usage of certain J_H elements and positively-charged amino acids in the CDR3 implicated in autoreactivity. Female mice lacking Dicer in mature B cells spontaneously develop serum autoantibodies and deposition of immune complexes in the kidneys³⁴. Thus, miRNA regulation of BCR signal strength is necessary to prevent maturation of a self-reactive B cell repertoire and the onset of autoimmunity.

Recent work in leukemia revealed miRNA regulation of PI3K signaling downstream of BCR stimulation relevant to autoimmune disease. miR-150 expression is anti-correlated with severity of chronic lymphocytic leukemia (CLL)³⁵. miR-150 targets *Gab1*, which recruits PI3K to the plasma membrane upon BCR stimulation, and *Foxp1*, a negative feedback regulator of PI3K signaling. miR-34a also targets *Foxp1*, suppresses B cell development, and is a candidate gene in the *Idd9.3* locus that protects mice from type 1 diabetes (T1D)^{36,37}.

PTEN has proven to be a multipotent miRNA target, having effects in many different immune cell types^{27,38-41}. A subset of mature B cells implicated in CLL progression express increased miR-22, which targets PTEN, leading to increased PI3K activity and proliferation⁴².

PTEN^{+/-} mice develop splenomegaly and lymphadenopathy, have increased serum IgG and anti-ssDNA antibodies, and develop lung and kidney inflammation⁴³. Interestingly, PTEN expression is decreased in SLE patient B cells, and this correlates with increased expression of miR-22 and two other miRNAs, miR-7 and miR-21, that also target PTEN⁴⁴.

While B cells mature in the spleen and lymph node into antibody-secreting cells, T cells differentiate into several lineages of effector cells, such as CD4⁺ T-helper cells (Th1, Th2, Th17) and cytotoxic CD8⁺ T lymphocytes. miRNAs are involved in the differentiation of these lineages, and recent work has focused particularly on the Th17 lineage, thought to be involved in the pathogenesis of MS and other autoimmune diseases⁴⁵. Mice lacking miR-155 in T cells do not develop severe EAE, and have a significant decrease in the production of IL-17A, a critical cytokine for EAE pathogenesis⁴⁶. miR-155-deficient mice are also resistant to collagen-induced arthritis, and have impaired Th17 differentiation⁴⁷. More recently, the mechanism behind miR-155 induction of Th17 differentiation was more clearly defined by its targeting of *Jarid2*, a component of the polycomb complex that mediates gene repression⁴⁸. While miR-155 encourages Th17 differentiation, miR-210 restrains the production of IL-17 by Th17 cells, and contributes to autoimmune pathogenesis in a mouse model of inflammatory bowel disease⁴⁹. miR-210 also restricts autoantibody development in aged mice, and overexpression of miR-210 decreases class switch recombination, suggesting that miR-210 limits autoimmune responses in both B and T cells⁵⁰.

The miR-17~92 cluster is also involved in Th17 differentiation and function by targeting PTEN and IKZF4. Deletion of the miR-17~92 cluster decreases Th17 differentiation and reduces EAE pathogenesis⁵¹. However, the miR-17 family member miR-20b suppresses IL-17 production in Th17-polarizing cultures by targeting ROR γ t and STAT3⁵². Overexpression of

miR-17~92 in T cells induces anti-dsDNA autoantibodies, multiorgan inflammation, splenomegaly and lymphadenopathy⁴⁰. This may be related to miR-17~92 promotion of Tfh cell differentiation mediated in part by targeting of PTEN and the PKB phosphatase PHLPP2^{39,40}.

miRNA regulation of Treg function

miRNAs are necessary to maintain peripheral tolerance through their essential roles in regulatory T cell (Treg) homeostasis and function. Genetic ablation of mouse *Dicer* or *Drosha* in Foxp3-expressing cells leads to fatal systemic autoimmune disease. Despite normal thymic Treg development in these mice, miRNA-deficient Tregs exhibit diminished homeostatic potential and are unable to adequately perform their suppressive functions⁵³⁻⁵⁵. Some of these defects can now be at least partly attributed to specific miRNAs expressed in Tregs.

miR-155 is highly expressed in Tregs in a FoxP3-dependent manner, and miR-155 deficiency impairs Treg development and homeostasis^{56,57}. Tregs lacking miR-155 have increased expression of the miR-155 target Suppressor of Cytokine Signaling 1 (SOCS1) and reduced responses to IL-2, a critical regulator of Treg homeostasis. However, miR-155 may be dispensable for Treg suppressive functions, since miR-155-deficient Tregs are capable of preventing autoimmune disease in mice^{56,57}.

The miR-17~92 cluster limits induced Treg (iTreg) differentiation in vitro through the combined activity of miR-17 and miR-19⁵⁸. Although miR-17~92 is dispensable for thymic Treg development and homeostasis in vivo, it is required to support IL-10 production by antigen-specific Tregs in EAE⁵⁹.

miR-10a is expressed in Tregs but not in conventional effector T cells⁶⁰. This expression is reinforced by retinoic acid signaling and correlates inversely with autoimmune disease

susceptibility in mouse strains, with highly susceptible mice having the lowest expression of miR-10a, and resistant mice having the highest⁶¹. miR-10a stabilizes the Treg gene expression program through repression of non-Treg genes such as Bcl6 and Ncor2^{60,61}. However, genetic ablation of miR-10a does not induce Treg defects or autoimmunity⁶¹, suggesting redundancy with other miRNAs such as miR-10b or perhaps miRNAs of the related miR-99/100 family. Like miR-10a, miR-99a expression is induced in Tregs by retinoic acid, and its overexpression promotes iTreg differentiation in vitro [Warth et al, EMBO Journal, *in press*]. Surprisingly, miR-99a cooperates with miR-150 through an as yet unknown mechanism to repress mTOR.

These studies have given some insight into the roles of specific miRNAs in Treg functions, but the question of how miRNAs affect T cell signaling pathways in Tregs remains unclear. The PI3K pathway in particular is influenced by miRNA regulation (**Figure 2**), and is a central node in regulating the differentiation of a CD4 T cell into either an effector T-helper cell or a Treg. Dicer ablation in CD4 T cells increases mTOR activity and sensitivity to TCR stimulation⁶². mTOR is activated by the PI3K pathway, and is a key integrator of signals from antigen receptors, cytokine receptors, and toll-like receptors⁶³. Increased PI3K signaling in mice leads to an expansion of non-Treg effector CD4 T cells⁶⁴. In fact, increased PI3K signaling blocks FOXP3 expression in Tregs⁶⁵, and key negative regulators of the PI3K pathway, such as Cbl-b⁶⁶ and PTEN⁶⁷, are essential to proper FOXP3 expression⁶⁸. Premature termination of PI3K signaling confers FOXP3 expression and Treg behavior⁶⁷, indicating that manipulation of the time period of PI3K signaling can lead to alterations in the balance between Tregs and T-effector cells. Cbl-b-deficient mice develop spontaneous T cell activation and are predisposed to autoimmune disease¹⁴. Cbl-b is induced by NFkB in response to TCR stimulation, and it negatively regulates not only the PI3K pathway, but also the NFkB and MAPK pathways⁶⁶.

Since negative regulation of these pathways promotes Treg gene expression programs, future research will likely uncover additional miRNAs that affect Treg generation and function by regulating PI3K, NFkB, or MAPK signaling.

While miRNAs generally function in a cell-autonomous manner by post-transcriptional regulation of gene expression programs, recent work has highlighted a non-cell-autonomous role of miRNAs. Many cells, including T cells and other immune cells, release miRNAs into the extracellular space within exosomes. These vesicles can transfer miRNAs into recipient cells, enabling RNA-mediated intercellular communication. Recent evidence suggests that this process may operate as a mechanism of immune suppression by Tregs and other immune suppressive lymphocytes^{69,70}. Exosomes released from Tregs in culture can transfer suppressive miRNAs into recipient Th1 cells⁶⁹. Tregs lacking both Rab27a and Rab27b are unable to secrete exosomes, and also fail to suppress effector T cell responses in in vitro co-culture and in vivo colitis experiments. Further work is needed to clarify the direct role of transferred miRNAs in enforcing immune tolerance, and to determine whether other Treg suppressive functions remain intact in Rab27-deficient Tregs. Extracellular miRNAs released from CD8 T cells also suppressed T cell responses in a mouse model of high-dose antigen tolerization to contact sensitivity⁷⁰.

miRNAs as biomarkers and active players in immune-mediated disease pathogenesis

The emergence of miRNAs as useful diagnostic and prognostic biomarkers in cancer has inspired extensive efforts to profile miRNA expression in human autoimmune disease⁷¹.

Depending on the how these studies are conducted, they also have the potential to provide insight into disease pathogenesis and the roles of specific miRNAs (**Figure 3**). As described in the

previous sections, most of our current understanding of miRNA function in immunity was established by combining mouse genetics with cell culture methods and disease models. The conservation of many (but not all) miRNAs and their target networks make these approaches productive and valuable. However, it is also important to study miRNAs in the context of human disease, and blended approaches have been successful at connecting disease-associated miRNA expression patterns with clear disease-associated functions.

Many studies have determined miRNA expression in blood, an abundant and easily obtained biospecimen that consists of mixed populations of hematopoietic cells. miR-155 expression is decreased in PBMCs of juvenile SLE patients⁷². Transfection of miR-155 into PBMCs from juvenile SLE patients rescued IL-2 secretion, suggesting a functional role of miR-155. More work needs to be done to determine which cell type requires miR-155 for IL-2 secretion. miR-146a is also downregulated in PBMCs from SLE patients, and its expression anti-correlates with disease activity⁷³. Overexpression of miR-146a by transfection of an expression vector in PBMCs from SLE patients reduced the excessive production of IFN-a and IFN-b. A recent meta-analysis of genome-wide association studies found miRNA polymorphisms that confer risk for SLE (miR-146a rs57095329) and RA (miR-499 rs3746444)⁷⁴. The polymorphism associated with SLE risk at the promoter for miR-146a decreased the binding of ETS1 to the promoter, thus reducing miR-146a expression⁷⁵.

miRNA expression profiling in PBMCs⁷⁶⁻⁷⁸, whole blood^{79,80}, and serum⁸¹ revealed miRNAs that may be involved in MS. miR-326 is highly expressed in PBMCs from relapsing MS patients compared to remitting MS patients or healthy subjects⁸². miR-326 expression correlates with disease severity and IL-17 production, suggesting a role for miR-326 in Th17 cell function. In mice, overexpression of miR-326 during EAE leads to increased Th17 cell

differentiation. Interestingly, miR-326 was also found to be upregulated in PBMCs from autoantibody-positive T1D patients⁸³, suggesting a more general role for miR-326 in autoimmunity.

Differential expression of a miRNA in complex specimens such as whole blood may reflect changes in cellular composition as well as changes in miRNA expression within one or more cell types. Importantly, the high expression of miR-326 in MS was limited to the CD4 T cell compartment, and especially in CCR6-expressing Th17 cells⁸². Identifying the cell type harboring high miR-326 expression as the Th17 cells that are involved in the autoimmune process provided stronger evidence for miRNA function in MS pathogenesis. In another study, circulating CD4 T cells from MS patients expressed more miR-17-5p, and lower levels of miR-17 targets in the PI3K pathway⁸⁴.

Several studies have identified miRNA expression changes in specific cell types from blood. miRNA expression analysis of circulating CD4 T cells from SLE patients revealed elevated miR-21 and miR-148a expression, which contribute to DNA hypomethylation by targeting DNMT1 and RASGRP1⁸⁵. miR-223 is upregulated in circulating T cells from RA patients^{86,87}. miR-223 expression is highest in naïve RA CD4 T cells, but nearly undetectable in non-naïve RA CD4 T cells and in naïve CD4 T cells from healthy subjects⁸⁶. miR-223 targets IGF-1R, resulting in decreased IL-10 secretion in response to IGF-1 stimulation⁸⁷. Another study found upregulation of miR-143 and miR-223 in CD4 T cells, as well as upregulation of miR-10a and miR-345 in CD19 B cells in SLE patients⁸⁸.

Dysfunction of Tregs plays a critical role in autoimmune disease pathogenesis, and a better understanding of the cellular processes leading to their dysfunction will aid the development of Treg-based therapies. In MS, miRNA expression profiling of circulating Tregs

revealed differential expression of some members of the miR-106b~25 cluster ⁸⁹. In RA, miRNA expression profiling of circulating naïve and memory Tregs and Teffs defined a miRNA signature of naïve and memory Tregs ⁹⁰. This paper did a very careful analysis of specific cell types, and leaves many open questions about the role of these miRNAs in Treg function. In T1D, miR-510 is upregulated and miR-342 is downregulated in circulating Tregs from T1D patients compared to their effector T cells ⁹¹. miR-146a is upregulated in Tregs in both T1D patients and healthy subjects, suggesting that miR-146a has a role in Tregs in normal and disease states.

Isolating cells from the inflammatory setting, such as the lungs in asthma or the joint synovium in RA, provides even more direct evidence connecting miRNA expression changes to their role in disease pathogenesis. Obtaining specific cell types involved in disease pathogenesis often involves invasive procedures and complex downstream cell separation protocols. The ability to profile miRNA expression in very small cell numbers is often essential. For example, in our own work we profiled miRNA expression in airway-infiltrating T cells sorted by flow cytometry from research bronchoscopy specimens in observational clinical studies of asthma ^{41,92}. miR-19a is significantly upregulated in CD4 T cells from asthmatic airways compared to CD4 T cells from healthy airways. Mouse miR-17~92 conditional-knockout CD4 T cells produce significantly less Th2 cytokines compared to wild-type cells, and this defect is rescued when miR-19a was added back to the cells. In a mouse model of ovalbumin-induced airway inflammation, CD4 T cells lacking the miR-17~92 cluster do not induce eosinophilia or mucus secretion in the airway. This suggests that blocking miR-19a might ameliorate the pathogenic inflammation observed in asthma ⁴¹.

Very few studies have looked for functionally relevant miRNA expression differences in immune cells in sites of autoimmune inflammation. miRNA expression profiling of CD4 T cells

in the synovial fluid of a small number of RA patients revealed upregulation of miR-146a⁹³. The upregulation of miR-146a may contribute to the resistance of RA synovial fluid CD4 T cells to apoptosis, at least in part through targeting Fas Associated Factor 1 (FAF1). Overexpression of miR-146a in mice induces symptoms similar to human autoimmune lymphoproliferative syndrome (ALPS)⁹⁴. miRNA expression changes in structural cells such as synoviocytes in RA and lung epithelial cells in asthma can also contribute to disease pathogenesis, but these studies do not contribute to our understanding of lymphocyte involvement in autoimmunity⁹⁵⁻⁹⁷.

Additional studies are needed to understand how miRNAs function in pathogenic lymphocytes in these sites of inflammation. Such studies would advance our understanding of gene regulation in the immune system, and may also point the way to novel therapies for autoimmune diseases. miRNAs are viable drug targets, and sequence-specific miRNA inhibitors are both easy to design and proven to work in patients⁹⁸. Although it has so far proven challenging to deliver these molecules to immune cells, some preclinical studies have indicated that local or systemic miRNA inhibitor administration may be a viable approach to treating autoimmune and allergic diseases⁹⁹⁻¹⁰¹.

Overview of thesis work

miRNAs that are differentially expressed in CD4 T cells from asthmatic airways represent potential targets for new therapeutics aimed at modifying the underlying disease process in asthma. Chapter 2 discusses our involvement in the MAST study that led to identification of differentially expressed miRNAs in asthma, and establishment of a role for miR-17~92 in regulation of Th2 cytokine production. We identified miRNAs that are differentially expressed in CD4 T cells in human asthma by multiplex microfluidic miRNA qPCR of RNA from T cells sorted from research bronchoscopies. We found significant upregulation of miR-19a in CD4 T cells from asthmatic airways compared to CD4 T cells from healthy airways. miR-19a is a member of the miR-17~92 cluster, which is involved in the development and function of both B and T lymphocytes, and has roles in lymphomagenesis¹⁰². Surprisingly, the other members of the miR-17~92 cluster, miR-17, miR-18a, miR-19b, and miR-20a (miR-92a failed to pass our quality control thresholds for this analysis) were not differentially expressed between asthma and healthy CD4 T cells.

To understand the functional role of miR-19a in Th2 cell biology, I analyzed the ability of mouse miR-17~92-deficient CD4 T cells to differentiate into Th2 cells in vitro compared to miR-17~92-sufficient CD4 T cells. CD4 T cells lacking the miR-17~92 cluster produced significantly less of the Th2 cytokines IL-4, IL-5, and IL-13 compared to wild-type cells. Interestingly, CD4 T cells overexpressing the miR-17~92 cluster produced significantly more of the Th2 cytokine IL-13 compared to wild-type cells, although there was no difference in IL-4 or IL-5 production by these cells. We also found that the Th2 cytokine defect was cell-intrinsic, and independent of the slight proliferation defect observed in CD4 T cells lacking the miR-17~92 cluster.

miR-17~92-deficient T cells lack all 6 mature miRNAs in the cluster. To understand the specific role of miR-19a in Th2 cytokine production, we transfected mature miRNA mimics corresponding to each miRNA in the cluster into miR-17~92-deficient T cells. miR-19a and miR-19b completely rescued both IL-4 and IL-13 production by miR-17~92-deficient T cells, while other members of the cluster did not fully rescue either cytokine. This implies that miR-19 is the primary component of the miR-17~92 cluster that promotes Th2 cytokine production.

miR-19a proved to have a functional role in Th2 cytokine production in human CD4 T cells as well. We overexpressed or knocked down miR-19a using transfectable miRNA mimics or inhibitors in human CD4 T cells from cord blood during the course of Th2 differentiation. When miR-19a was overexpressed, human T cells made significantly more IL-13. When miR-19a was inhibited, human T cells made less IL-13. However, alterations in miR-19a activity did not result in changes in IL-4 production.

We then screened known miR-19 targets that are expressed in CD4 T cells for their ability to alter Th2 cytokine production by transfecting siRNA against each target into miR-17~92-deficient T cells. Through this analysis, we identified three functionally relevant targets: PTEN, SOCS1, and A20. Knockdown of each of these targets individually rescued IL-13 and IL-4 production.

In vivo, miR-17~92 expression in Th2 cells was essential to promoting eosinophilic infiltration into the airways in an ovalbumin (OVA)-induced allergic airway inflammation model. Mice that received miR-17~92-deficient OTII (OVA-specific) Th2 cells prior to OVA challenge oropharyngeally did not develop airway hyperresponsiveness, eosinophilia, or goblet cell hyperplasia. Surprisingly, transfecting miR-19a into miR-17~92-deficient OTII Th2 cells

prior to transfer significantly increased eosinophilia in the airways, and showed a trend toward increased mucus secretion and airway inflammation.

These experiments confirmed our hypothesis that identifying miRNAs that are differentially expressed in asthmatic airway T cells could lead to a better understanding of the regulation of Th2 cell biology, and give insights into possible therapeutic targets for asthma. We also hoped to gain a better understanding of the immunology of asthma through clinical studies at UCSF with John Fahy and Prescott Woodruff. Chapter 3 discusses our involvement in two clinical studies to understand the role of the immune system in asthma pathogenesis. One of these studies aims to characterize the types of inflammatory cells present in the airways, with a particular focus on innate immune cells (basophils and ILC2s in particular). The other aims to characterize T-helper cell subsets in the airways of asthmatic patients by flow cytometry of bronchoalveolar lavage fluid obtained from research bronchoscopies. Later, we will analyze sorted specimens from these subjects to identify miRNA and gene expression changes in each T-helper cell subset.

My work in the Ansel lab began with studying epigenetic regulation of T cell function. Appendix 1 contains my first publication with the Ansel lab. This paper addresses the Site V enhancer that alters IL-4 production by Tfh cells. My work in this project is in Figure 7. Using chromatin immunoprecipitation experiments, we showed decreased H3K4 dimethylation (activated chromatin marker) and increased H3K4 trimethylation (silenced chromatin marker) in the *Il4* gene locus in the absence of Site V in Th2 or Tfh cells. Appendix 2 contains my second publication with the Ansel lab. This paper is a technical analysis of the miRNA taqman qPCR technique that I later used for my first-author publication. My work in this project appears in Figure 7 and 11 of the paper, and was focused on qPCR confirmation of miRNA expression

differences identified by microarray and by microfluidic qPCR. These two projects gave me invaluable experience in the techniques and cell types I would be analyzing later in my thesis project.

Figure 1: miRNAs set thresholds for lymphocyte development

A) miR-17~92 sets a threshold for B cell survival during development. miR-17~92 targets several genes in the PI3K pathway, including the pro-apoptotic molecule BIM. Mice deficient in miR-17~92 in the B cell lineage develop B cell lymphopenia. Mice with overexpression of miR-17~92 in the B cell lineage develop self-reactive B cells. **B)** miR-181 sets a threshold for TCR signal strength during T cell development in the thymus. miR-181 expression decreases as thymocytes differentiate from double negative (DN) to double positive (DP) to single positive (SP) thymocytes. miR-181 expression confers greater sensitivity to TCR stimulation by modulating the targets PTPN22, SHP2, DUSP5, DUSP6 and PTEN.

Figure 1

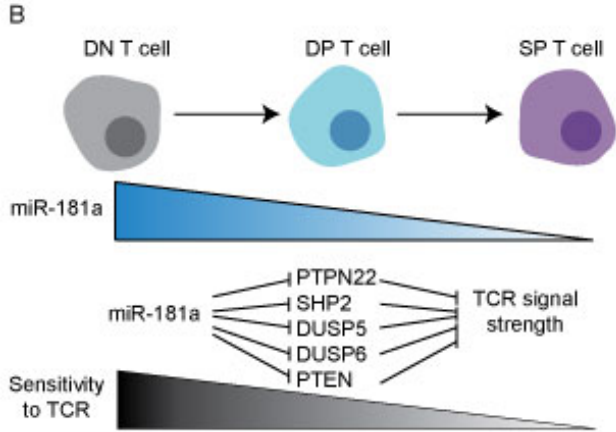
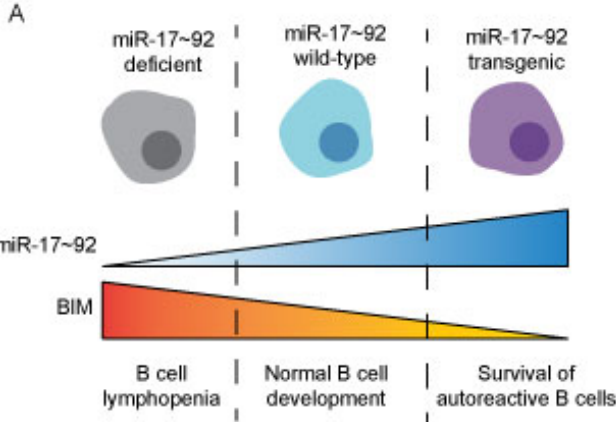


Figure 2: miRNA regulation of the PI3K pathway

PI3K inhibitors are currently in clinical trials for leukemia, lymphoma, myeloma, asthma, and chronic rhinitis [clinicaltrials.gov], and preclinical data support their therapeutic potential in autoimmune diseases as well ¹⁰³. The immune system is highly sensitive to manipulation of PI3K signaling, and this pathway is subject to several layers of regulation that permit fine tuning of signal output. Just a 2-fold change in PI3K signal activity through Akt is sufficient to alter lymphocyte homeostasis and induce autoimmunity in mice ⁴³. This degree of fine-tuning falls well within the range of regulation mediated by miRNAs. The PI3K pathway is strictly regulated by the phosphatases PTEN and SHIP, which dephosphorylate PI3K products and/or limit substrate availability. PTEN is a prominent target of many miRNAs (miR-17~92 and miR-181 family members) in many different immune cell types (Th1, Th2, Th17, Tfh, CD8 T cells, B cells). SHIP is a prominent target of miR-155, and appears to play an important role in its proinflammatory functions in several cell lineages. MicroRNAs also modulate PI3K signaling by targeting downstream signaling mediators and inhibitors. Understanding which miRNAs are expressed in specific cell types, as well as understanding the varying limiting roles played by their targets will lead to a more comprehensive understanding of miRNA regulation of cell fates and behaviors.

Figure 2

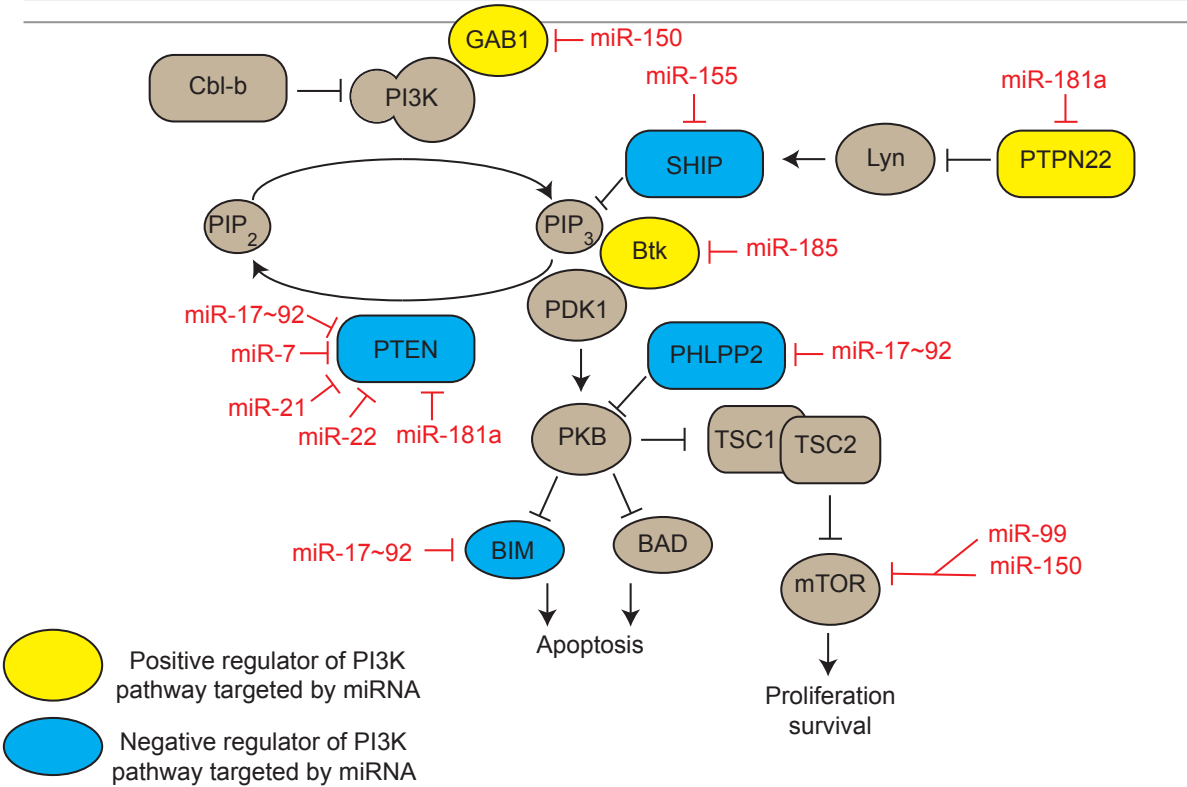
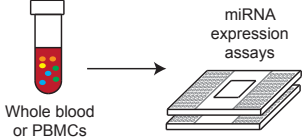
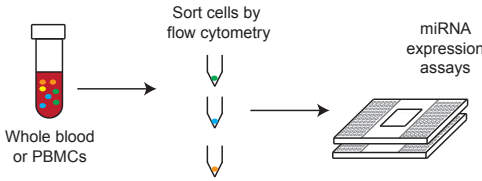
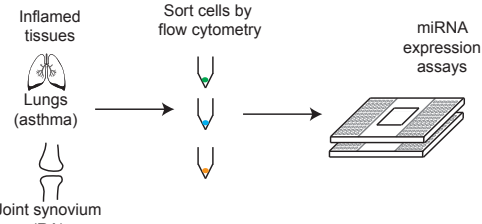


Figure 3: miRNAs as biomarkers or indicators of pathogenic processes

miRNA expression analysis can be a useful tool to identify biomarkers of disease, or to generate mechanistic hypotheses about disease pathogenesis. Useful biomarkers are identified from abundant biospecimens like blood with little sample processing before miRNA expression analysis. To generate mechanistic hypotheses, more sample processing is necessary to determine the cell type specificity of miRNA expression changes. Even stronger support for the role of a particular miRNA in disease pathogenesis can be obtained using tissue-infiltrating immune cells at the sites of autoimmune or allergic inflammation. The invasiveness of these procedures limits their utility for biomarker identification.

Figure 3

Procedure	Biomarker Discovery	Mechanistic hypothesis generation
 <p>Whole blood or PBMCs</p> <p>miRNA expression assays</p>	<p>↑ high utility +Simple procedure +Abundant tissue source</p>	<p>↓ low utility -Mixed cell populations</p>
 <p>Whole blood or PBMCs</p> <p>Sort cells by flow cytometry</p> <p>miRNA expression assays</p>	<p>↓ low utility -Costly and time consuming</p>	<p>↑ high utility +Abundant tissue source +Specific circulating cell populations</p>
 <p>Inflamed tissues</p> <p>Lungs (asthma)</p> <p>Joint synovium (RA)</p> <p>Sort cells by flow cytometry</p> <p>miRNA expression assays</p>	<p>↓ low utility -Costly and time consuming -Invasive procedure -Few cells</p>	<p>↑ high utility +Specific tissue cell populations involved in pathogenesis +miRNA expression changes imply function</p>

Chapter 2

A miRNA upregulated in asthma airway T cells promotes T_H2 cytokine production

Simpson LJ, Patel S, Bhakta NR, Choy DF, Brightbill HD, Ren X, Wang Y, Pua HH, Baumjohann D, Montoya MM, Panduro M, Remedios KA, Huang X, Fahy JV, Arron JR, Woodruff PG, and Ansel KM. A miRNA upregulated in asthma airway T cells promotes Th2 cytokine production. *Nature Immunology*. 2014;15(12):1162–1170.

Abstract

MicroRNAs (miRNAs) exert powerful effects on immune function by tuning networks of target genes that orchestrate cell behavior. We sought to uncover miRNAs and miRNA-regulated pathways that control the T_H2 responses that drive pathogenic inflammation in asthma. Profiling miRNA expression in human airway-infiltrating T cells revealed miR-19a elevation in asthma. Modulating miR-19 activity altered T_H2 cytokine production in both human and mouse T cells, and T_H2 cell responses were markedly impaired in cells lacking the entire miR-17~92 cluster. miR-19 promotes T_H2 cytokine production and amplifies PI(3)K, JAK-STAT, and NF-κB signaling by direct targeting of PTEN, SOCS1, and A20. Thus, miR-19a upregulation in asthma may be an indicator and a cause of increased T_H2 cytokine production in the airways.

Introduction

Asthma is a respiratory disorder characterized by reversible airflow limitation, bronchial hyperresponsiveness, and airway inflammation^{2,5}. Although it is clear that asthma is a heterogeneous syndrome, a prominent subset of asthma is characterized by type 2 inflammation with infiltration of T helper type 2 (T_H2) cells to the airways and lung parenchyma, and a molecular signature of airway epithelial cell exposure to T_H2 cytokines, especially interleukin 13 (IL-13) (ref. ^{10,104}). IL-13 coordinates allergic lung inflammation through receptors on both structural and inflammatory cells. It induces epithelial cell hyperplasia and mucus production, airway smooth muscle cell hyperresponsiveness, and the recruitment and survival of eosinophils, which is enhanced by another T_H2 cytokine, IL-5 (ref. ¹⁰⁵). IL-13 is a key driver of airway inflammation in mouse models of asthma ⁷, and biomarkers of type 2 inflammation predict enhanced clinical benefit from treatment with antibodies that block IL-13 signaling such as lebrikizumab ¹⁰⁶ and dupilumab ¹⁰⁷.

The external signals and transcription factors that regulate T_H2 cell differentiation are well understood. The cytokine IL-4 is both the canonical product of T_H2 cells and a powerful driver of T_H2 cell differentiation. Naive CD4 T cell precursors require concurrent T cell antigen receptor (TCR) and cytokine signals to induce T_H2 differentiation. TCR ligation activates T cells through a broad signaling cascade that includes the PI(3)K and NF-κB pathways. IL-4 receptor signals activate STAT6, which upregulates GATA-3 in activated T cells. Together these two key transcription factors promote T_H2 cell differentiation and cytokine production ¹³. Because T_H2 cell differentiation is governed by a cytokine and transcription factor positive feedback loop, it is very sensitive to minor changes in cytokine production, the strength of TCR stimulation, and other intrinsic and environmental factors. Our extensive knowledge of the signals that control T

cell differentiation and our ability to reproducibly manipulate this process *in vitro* make it an attractive system for the study of basic principles that govern gene expression networks and cell identity.

MicroRNAs (miRNAs) regulate gene expression programs by reducing the translation and stability of target mRNAs¹⁹. miRNAs are grouped into families that share a network of predicted mRNA targets. Although the quantitative effect produced by each miRNA-target interaction is small, the combined effect of the network of miRNA-target interactions produces substantial changes in cell behavior. Several studies have attempted to understand miRNA functions in asthma by analyzing miRNA expression in whole lung, airway epithelial cells, or mixed peripheral blood lymphocytes from humans with asthma or mice subjected to allergic airway inflammation models^{95,100,108,109}. These studies provide insight into the effect of airway inflammation on miRNA expression patterns, but they do not define cell-intrinsic effects of miRNA regulation on disease pathogenesis.

In T cells, miRNAs regulate proliferation, survival, activation, differentiation, and cytokine production²⁰. The miR-17~92 cluster has emerged as a particularly potent and pleiotropic regulator of T cell responses. This cluster is transcribed as a single primary miRNA transcript that is processed to produce six mature miRNAs belonging to four miRNA families: miR-17, miR-18, miR-19, and miR-92 families¹⁰². Primary miR-17~92 and the corresponding mature miRNAs are upregulated in activated CD4 T cells and can promote T cell proliferation and survival^{25,58,110,111}. Although they are expressed without apparent cell-type specificity, miRNAs in the miR-17~92 cluster regulate the differentiation and function of several distinct T cell subsets. Both miR-17 and miR-19b promote T_H1 and T_H17 cell differentiation^{51,58}. These two miRNAs also inhibit inducible T_{reg} cell differentiation *in vitro*⁵⁸, but the cluster as a whole is

required for normal T_{reg} cell function *in vivo*⁵⁹. T_{FH} cell responses are reduced and dysregulated in the absence of miR-17~92^{39,40}. However, miRNA regulation of T_H2 cell differentiation and cytokine production remains poorly understood.

We hypothesized that miRNAs that are differentially expressed in airway-infiltrating T cells in asthma regulate T_H2 cell function and promote lung inflammation. We used a highly sensitive nanoscale microfluidic qPCR approach to profile miRNA expression in $CD4^+$ T cells isolated from human asthmatic airways^{92,112}. miR-19a, a member of the miR-17~92 cluster, was significantly upregulated in asthma. Using genetically engineered mice, we found that miR-17~92 promotes T_H2 cytokine production *in vitro* and type 2 inflammation *in vivo*. We mapped miR-17~92 regulation of T_H2 cytokine production to the miR-19 family using transfectable miRNA mimics and inhibitors in primary human and mouse T cells. A functional screen of the miR-19 target network in T_H2 cells revealed several signaling inhibitors that restrain IL-13 and IL-4 production. Taken together, our data indicate that the observed increase in T cell miR-19a expression in humans with asthma augments T_H2 responses in their airways.

Results

miRNA expression in airway CD4 T cells

To investigate miRNA expression in airway-infiltrating T cells, we profiled the expression of a panel of 190 miRNAs in CD4⁺ T cells sorted from bronchoalveolar lavage (BAL) fluid from 8 healthy, 13 steroid-naive asthmatic, and 21 steroid-using asthmatic subjects (**Table 1**)⁹⁵. RNA was extracted from sorted CD3⁺ CD4⁺ T cells, and miRNA expression was determined by nanoscale microfluidic qPCR on 100 pg RNA from each subject (**Supplementary Fig. 1a, Supplementary Table 1**). Our analysis revealed few differences in miRNA expression between asthmatic and healthy CD4⁺ T cells from BAL with one notable exception (**Supplementary Fig. 1b, Supplementary Table 2**). Of the 89 miRNAs that were detected in at least 60% of the subjects, miRNA-19a was the most significantly elevated in asthma (**Fig. 1a, Supplementary Table 2** $p = 0.0199$). miR-19a expression was consistently elevated in all of the steroid-naive asthmatic subjects with very little variability, and was similarly elevated in the steroid-using asthmatic subjects that were treated with the inhaled corticosteroid (ICS) budesonide (**Fig. 1c**). This miRNA remained elevated in CD4⁺ T cells from steroid-naive asthmatics upon 6 weeks of ICS treatment (**Fig. 1d**), indicating that it is resistant to gene expression changes induced by steroid treatment. Because miR-19a is a member of the miR-17~92 cluster, a highly conserved cluster of 6 miRNAs transcribed in one polycistronic pri-miRNA, we investigated the expression of other members of the cluster. Only miR-19a, and not miR-19b, miR-17, miR-18a, or miR-20a, was differentially expressed between asthmatic and healthy CD4⁺ T cells (**Fig. 1e**). These data demonstrate that miR-19a is specifically elevated in airway T cells in asthma, and indicate that individual members of the miR-17~92 cluster are differentially regulated in this setting.

miR-17~92 promotes T_H2 cytokine production

The miR-17~92 cluster regulates the differentiation and effector functions of several helper T cell subsets including T_H1, T_H17, T_{FH} and T_{reg} cells with varying degrees of potency^{25,39,40,51,59,111}. However, the cluster's role in T_H2 cell differentiation and cytokine production, important features of the asthmatic immune response, has not been investigated. To this end, we cultured miR-17~92-deficient CD4⁺ T cells (called '17~92^{Δ/Δ}' here), miR-17~92-sufficient control CD4⁺ T cells (called 17~92^{+/+} here), and transgenic miR-17~92-overexpressing CD4⁺ T cells (called 17~92^{GFP/+} here) in T_H2 polarizing conditions. Intracellular cytokine staining revealed that 17~92^{GFP/+} cells produced more of the type 2 cytokine IL-13 compared to 17~92^{+/+} controls (**Fig. 2a**). Conversely, fewer 17~92^{Δ/Δ} cells produced the type 2 cytokines IL-13, IL-5, and IL-4 compared to 17~92^{+/+} controls (**Fig. 2a-b**). This defect in T_H2 differentiation and cytokine production did not result in increased T_H1 cytokine production, as measured by IFN-γ production (**Fig. 2c**). 17~92^{Δ/Δ} cells produced substantially more TNF, which is a known direct target of miR-19 (**Fig. 2c**), suggesting that these cells are capable of efficient cytokine production in T_H2-polarizing conditions, and that the defect is limited to type 2 cytokines. 17~92^{Δ/Δ} cells produced less T_H2 cytokines even in established GATA-3^{hi} T_H2 cells (**Fig. 2d**). Thus, the miR-17~92 cluster positively regulates T_H2 cytokine production.

To determine whether the T_H2 cytokine defect was cell-intrinsic, we co-cultured congenically marked 17~92^{Δ/Δ} and 17~92^{+/+} CD4⁺ T cells in T_H2 conditions. After 5 days in culture, the CD45.1⁺ 17~92^{Δ/Δ} T cells produced less IL-13 and IL-4 compared to the CD45.2⁺ 17~92^{+/+} cells (**Fig. 3a**), demonstrating that the cytokine defect is cell-intrinsic and does not

entirely depend on feedback from IL-4 or other products produced by the mutant T cells in culture.

We observed a slight proliferation defect in 17~92^{ΔΔ} T_H2 cell cultures compared to 17~92^{+/+} controls, and a slight increase in proliferation in 17~92^{GFP/+} cells (**Fig. 3b**). To test whether the frequency of T_H2 cytokine-producing cells among 17~92^{ΔΔ}, 17~92^{+/+}, and 17~92^{GFP/+} CD4⁺ T cells was an indirect result of their rate of proliferation, we labeled the cells with CellTrace Violet (CTV) and analyzed cytokine production at each division after 5 days of culture in T_H2 polarizing conditions. IL-13 and IL-5 production did increase with each cell division in 17~92^{+/+} cells. However, 17~92^{ΔΔ} cells produced significantly less IL-13, IL-5, and IL-4 at each cell division compared to 17~92^{+/+} cells (**Fig. 3c,d**). In contrast, 17~92^{GFP/+} cells produced more IL-13 and IL-5 at each division, but an equal amount of IL-4 as compared to 17~92^{+/+} cells (**Fig. 3c,d**). Together these data indicate that the miR-17~92 cluster promotes type 2 cytokine production in a cell-intrinsic and proliferation-independent manner.

miR-19 augments T_H2 differentiation

To understand the mechanism of miR-17~92 control of T_H2 cell cytokine production, the functions of individual miRNA members of the cluster need to be addressed. Therefore, we transfected mature miRNA mimics corresponding to each of the six miRNAs in the miR-17~92 cluster into 17~92^{ΔΔ} CD4⁺ T cells on days 1 and 4 of T_H2 polarizing cultures. Transfection of either miR-19a or miR-19b was sufficient to completely rescue T_H2 cytokine production (**Fig. 4a-c**). Other miRNAs within the cluster conferred only partial rescue of T_H2 cytokine production compared to miR-19a or miR-19b. These data indicate that miR-19 is the primary component of the miR-17~92 cluster that augments T_H2 differentiation.

All of the miR-19a and the large majority of miR-19b expressed in T cells derive from the miR-17~92 cluster (**Supplementary Fig. 2**). Consistent with this finding, specific retroviral sensors of miR-19a and miR-19b activity were strongly repressed in 17~92^{+/+} cells, but not 17~92^{ΔΔ} cells (**Supplementary Fig. 3**). T cell activation induces increased transcription of the miR-17~92 cluster, and all of the miRNAs in the cluster remain highly expressed during T_H2 cell differentiation¹¹³ (and data not shown). A single transfection either early in the culture (day 1) or late (day 4) did not rescue T_H2 cytokine production (**Fig. 4d,e**). We conclude that miR-19 is required throughout T_H2 cell polarization to support robust T_H2 cell differentiation and cytokine production. miR-19 mimics also modestly increased proliferation of 17~92^{ΔΔ} cells in T_H2 conditions (**Supplementary Fig. 4**).

We next tested whether modulating the activity of miR-19 alone was sufficient to alter type 2 cytokine production in miR-17~92-sufficient T cells with normal endogenous expression of the other miRNAs in the cluster. Transfection of miR-19a and miR-19b inhibitors into 17~92^{+/+} T cells specifically increased the expression of corresponding GFP sensors of miR-19a and miR-19b activity and decreased expression of IL-13 (**Supplementary Fig. 3**). These inhibitors also significantly reduced IL-13, but not IL-4, production when transfected into human cord blood CD4⁺ T cells in T_H2-polarizing cultures (**Fig. 5a,b**). Conversely, transfection with miR-19a mimic was sufficient to increase IL-13 expression, but not IL-4, in human cord blood CD4⁺ T cells (**Fig. 5c,d**). Similarly, 17~92^{+/+} mouse CD4 T cells had increased IL-13 production, but not IL-4, when transfected with miR-19a or miR-19b mimics in non-polarizing conditions (**Supplementary Fig. 3**). We conclude that changes in miR-19 expression, such as those seen in human asthmatic airway T cells, are sufficient to modulate the abundance of IL-13 produced in primary human and mouse CD4⁺ T cells.

miR-19 targets *Pten*, *Socs1*, and *Tnfaip3*

Because a large number of direct miR-19 targets have been validated in B cell lymphomas and other cell types, we took a candidate approach to uncover how miR-19 augments T_H2 differentiation. We individually inhibited the 38 previously validated¹¹⁴⁻¹¹⁶ miR-19 targets that are expressed in T cells¹¹⁷ with siRNA SmartPools in 17~92^{ΔΔ} CD4⁺ T cells during T_H2 polarization (**Supplementary Table 3**). IL-13 and IL-4 z-scores were calculated for each of the transfections (**Fig. 6a,b**). The top 8 candidate genes that when inhibited increased IL-13 and IL-4 were characterized further by inhibition with 3 individual siRNAs per gene in 17~92^{ΔΔ} CD4⁺ T cells during T_H2 polarization to confirm the rescue of IL-13 and IL-4 (**Fig. 6c,d**). The type 2 cytokine defect of 17~92^{ΔΔ} cells was rescued by inhibition of *Pten*, *Socs1*, and *Tnfaip3* (which encodes A20) with at least 2 out of 3 individual siRNAs (**Fig. 6e**). Each of the top 8 candidate genes was confirmed to be inhibited by miR-19 expression by qPCR of 17~92^{ΔΔ} cells transfected with miR-19a, -19b, or control mimics, compared to 17~92^{+/+} cells (**Fig. 6f**). Furthermore, to test whether genetic depletion of PTEN expression in 17~92^{ΔΔ} cells could rescue T_H2 cytokine production, we deleted one allele of *Pten* in 17~92^{ΔΔ} cells (17~92^{ΔΔ} *Pten*^{Δ+}). Genetic depletion of PTEN moderately rescued the cytokine defect of 17~92^{ΔΔ} T cells (**Fig. 6g**).

Pten, *Socs1*, and *Tnfaip3* are negative regulators of T cell signaling pathways that are important for all T helper cell subsets. To test whether each of these targets regulated other T helper cell cytokines, such as IFN-γ, IL-17A, and IL-17F, we transfected 17~92^{ΔΔ} cells with individual siRNAs against *Pten*, *Socs1*, and *Tnfaip3* under non-polarizing (T_HN), T_H17, and T_H2-polarizing conditions (**Fig. 6h-j**). Consistent with previous reports^{51,58}, *Pten* inhibition increased

the production of all T helper cytokines tested, but reducing *Socs1* or *Tnfrsf25* expression enhanced production of T_H2 cytokines, but not IFN- γ or IL-17. Thus, miR-19 specifically regulates T_H2 responses through distinct limiting mRNA targets.

miR-17~92 augments T_H2 cell function *in vivo*

We next tested whether reduced T_H2 cytokine production by 17~92 ^{$\Delta\Delta$} T cells would result in altered airway type 2 inflammation *in vivo*. We transferred 17~92 ^{$\Delta\Delta$} or 17~92^{+/+} ovalbumin (OVA)-specific OT-II T_H2 cells to *Cd28^{-/-}* mice, and challenged the mice every 24 h oropharyngeally with OVA for 3 days (**Supplementary Fig. 5a**). 18 h after the last challenge, we analyzed pulmonary resistance in response to increasing doses of acetylcholine. Mice that received either no OT-II cells or 17~92 ^{$\Delta\Delta$} OT-II T_H2 cells had significantly lower pulmonary resistance than mice that received 17~92^{+/+} OT-II T_H2 cells (**Fig. 7a**), indicating that T_H2 cells that lack the miR-17~92 cluster are less capable of inducing allergic airway hyperresponsiveness. Histological analysis of lung sections from these mice revealed increased mucus-secreting goblet cells and more severe inflammation in mice that received 17~92^{+/+} OT-II T_H2 cells compared to those that received 17~92 ^{$\Delta\Delta$} OT-II T_H2 cells (**Fig. 7b-d**). Mice that received 17~92 ^{$\Delta\Delta$} OT-II T_H2 cells transfected with miR-19a mimic showed a trend toward increased inflammation and mucus secretion (**Fig. 7b-d**). To better characterize and quantify airway inflammation, we analyzed BAL from the recipient mice by flow cytometry (**Supplementary Fig. 5b**). Mice that received 17~92 ^{$\Delta\Delta$} OT-II T_H2 cells had significantly reduced eosinophilia in the airways compared to mice that received 17~92^{+/+} OT-II T_H2 cells (**Fig. 7e**). However, 17~92 ^{$\Delta\Delta$} OT-II T_H2 cells transfected with miR-19a induced airway eosinophil infiltration similar to that seen in recipients of 17~92^{+/+} OT-II T_H2 cells (**Fig. 7e**).

Macrophage and neutrophil numbers were relatively similar in all three groups of recipients, suggesting that the differences in airway inflammation were restricted to effects induced by type 2 cytokines. We conclude that the miR-17~92 cluster, and miR-19a specifically, has a role in the *in vivo* function of T_H2 cells as inducers of the allergic inflammatory phenotype associated with asthma.

Discussion

Guided by miRNA expression in T cells present in the airways in human asthma, we identified a miRNA that augments T_H2 cytokine production and allergic inflammation via coordinate regulation of cytokine and antigen receptor signaling pathways. Our data demonstrate that the miR-17~92 cluster, and specifically miR-19a, promotes T_H2 cytokine production by simultaneously targeting inhibitors of the NF- κ B, JAK-STAT, and PI(3)K pathways. In the context of previous studies of the miR-17~92 cluster, these findings illustrate basic principles of miRNA regulation, including the network logic of miRNA function, and how complex biological processes such as effective T cell-mediated immune responses emerge from coordinate miRNA regulation of diverse aspects of cell behavior.

The miR-17~92 cluster has many established functions in lymphocytes¹¹⁸. The cluster as a whole promotes T cell proliferation and survival, and the differentiation and function of several committed effector T cell subsets^{25,39,40,51,58,59}, making it an important coordinator of T cell responses. T_{FH} responses involve the concerted action of all 4 miRNA families in the miR-17~92 cluster^{39,40}. miR-17 and miR-92 family miRNAs support T cell proliferation in the absence of other miRNAs¹¹¹. In our experiments, miR-19 as well as miR-17 and miR-92 family miRNAs partially rescued 17~92 ^{Δ/Δ} T cell proliferation. Both miR-17 and miR-19b promote T cell survival and T_H1 and T_H17 cell differentiation, while limiting iT_{reg} cell differentiation^{51,58}. However, no specific functions have previously been attributed to miR-19a in T helper cells. We mapped the T_H2 cytokine-promoting activity of the miR-17~92 cluster to miR-19, as both miR-19a and miR-19b (but not other miRNAs in the cluster) rescued IL-13 and IL-4 production in 17~92 ^{Δ/Δ} T cells.

Our study emphasizes an important concept regarding the mechanism of miRNA regulation of cell behavior: a single miRNA can be expressed in and regulate many different cell types through distinct but overlapping networks of targets. Each target may play a limiting role in distinct differentiation environments, or may play a similar role in a variety of contexts. For example, miR-19 regulated T_H2 cytokine production in part through PTEN, a target that has widespread effects on T helper cell effector programs^{25,39,51,58}. In contrast, SOCS1 and A20 were limiting factors for T_H2, but not T_H1 or T_H17 cytokine production. The same concept applies to transcription factors and their target genes. For example, c-Maf regulates both T_H2 and T_H17 cytokine production through distinct molecular pathways. Similarly, GATA-3 is the principle determinant of T_H2 cell differentiation and a direct regulator of *Il13* and *Il5*, but it also regulates T cell development in the thymus and survival in the periphery. Our findings demonstrate that careful dissection of target networks can reveal not only the mechanisms through which transcription factors and miRNAs mediate their functions, but also novel or unexpected limiting requirements for downstream genes and pathways that coordinate T cell-mediated immunity.

We identified at least three important pieces of the miR-19 target network in T_H2 cells: *Pten*, *Socs1*, and *Tnfrsf3*. Each of these target mRNAs encodes an inhibitor of a distinct signaling pathway, indicating that miR-19 augments T_H2 cytokine production by simultaneously amplifying PI(3)K, JAK-STAT, and NF-κB signaling. However, our analysis revealed a limiting independent role for each target, since depleting each one individually was sufficient to markedly increase T_H2 cytokine production. These pathways are all essential components of the antigen and cytokine signaling that induce T cell differentiation and effector function. As such, the importance of PTEN, SOCS1, and A20 for T_H2 cytokine production have been inferred or assumed, but never tested.

PTEN inhibits the PI(3)K pathway, which promotes T cell proliferation and cell survival¹¹⁹, and deletion of one allele of *Pten* results in autoimmunity and lymphoproliferative disease in mice⁴³. PTEN is an important miR-17~92 target in T_H1, T_H17 and T_{FH} cell differentiation^{39,40,51,58}, but its effects on cytokine production by T_H2 cells were previously unknown. Genetic rescue of PTEN overexpression in 17~92^{Δ/Δ} cells partially rescued T_H2 cytokine production, indicating that both PTEN and other targets significantly contribute to the T_H2 phenotype.

SOCS1 inhibits the JAK-STAT pathway downstream of cytokine receptors¹²⁰, and favors T_H17 over T_H1 differentiation by repressing IL-12 and IFN- γ signaling^{121,122}. Both IFN- γ and IL-4-producing CD4⁺ T cells are increased in SOCS1-deficient mice¹²³ and SOCS1 inhibits IL-4 signaling in macrophages¹²⁴. These findings have led to speculation that SOCS1 may inhibit T_H2 responses¹²⁵, but this possibility had remained untested prior to our experiments. Furthermore, SOCS1 has not previously been found to be an important miR-17~92 target in regulating the differentiation and effector functions of any helper T cell subset.

Tnfrsf25 encodes A20, a constitutively expressed negative regulator of the NF- κ B pathway in T cells. A20 was identified as an important miR-19 target in macrophages¹¹⁶. Inhibition of A20 increases IL-2 production in Jurkat cells¹²⁶, but its effect on T_H2 cytokine production had not yet been described. While identification of these three targets leads to better understanding of the intracellular components that regulate Th2 cytokine production, genome-wide approaches to determine the full miR-19 target network in T_H2 cells would likely reveal additional targets involved in helper T cell biology.

We hypothesized that miRNA expression profiling in airway-infiltrating T cells could reveal functionally relevant miRNAs and pathways that are directly involved in asthma

pathogenesis. Indeed, we identified miR-19a as a candidate regulator of T_H2 responses through miRNA profiling^{92,112} in the small number of CD4 T cells that can be recovered from bronchoalveolar lavage. Previous studies identified miRNAs of interest by profiling expression in complex cell mixtures, such as whole lungs in animal models¹⁰⁹, epithelial cell brushings⁹⁵, or mixed lymphocytes from peripheral blood of asthmatic subjects^{108,127}. Interpretation of data from unseparated tissues can be ambiguous. Differential miRNA expression may reflect changes in cellular composition of samples from asthmatic subjects, and formation of mechanistic hypotheses about disease pathogenesis requires further work to identify which cell type(s) exhibit differential expression of any miRNA of interest. Future studies will be needed to confirm the observed increase in miR-19a in airway CD4⁺ T cells in asthma, and to determine whether this change is limited to T_H2 cells in this context. Larger studies may also identify correlation between miR-19a expression and asthma severity, lung function, response to corticosteroid treatment, or biomarkers of T_H2 inflammation that stratify asthma phenotypes^{2,128}.

Although clusters of miRNAs are transcribed as a single polycistronic primary miRNA (pri-miRNA) transcript, each mature miRNA in the cluster is not necessarily expressed at the same abundance in a given cell type and condition. Nevertheless, we were surprised to find a specific increase in miR-19a, but not other members of the miR-17~92 cluster, in airway-infiltrating T cells in asthma. miR-19a and miR-19b were also preferentially increased in premalignant cells in a mouse model of B cell lymphoma and in human Burkitt's lymphoma cell lines¹⁰². A specific increase in miR-19a may be mediated by preferential processing from the polycistronic miR-17~92 pri-miRNA transcript, or by a sequence-specific increase in the efficiency of some other step in miR-19a biogenesis. Alternatively, mature miR-19a may be specifically stabilized in T cells in inflamed lungs. Regardless of the mechanism, the observed

increase in miR-19a abundance should have a significant impact on secretion of IL-13, since altering miR-19a activity by overexpression or depletion in both human and mouse primary T cells altered IL-13 production *in vitro*.

The identity and function of miRNAs that regulate type 2 inflammation in a T cell-intrinsic manner have remained uncertain. miR-155 has been a major focus because miR-155-deficient T cells have a modest bias toward T_H2 differentiation *in vitro*^{129,130} and miR-155-deficient mice develop partially penetrant spontaneous airway remodeling with some of the characteristics of asthma¹²⁹. However, these mice are resistant to experimentally induced airway inflammation¹³¹, suggesting that miR-155 may have a role in cell types other than T_H2 cells in this model. Our data suggest that miR-19a upregulation in T cells in asthmatic airways may be an indicator and a cause of increased IL-13 production, and likely contributes to type 2 inflammation in asthma. Indeed, 17~92^{ΔΔ} T_H2 cells induced far less airway eosinophilia than 17~92^{+/+} T_H2 cells in an allergic airway inflammation model, and restoration of miR-19a was sufficient to rescue this defect.

Our study links miR-19a activity with human asthma and uncovers mechanisms of miR-19a function in T cells, suggesting that miR-19 may be an attractive drug target. Previous animal model studies have validated the concept of miRNA-based therapy by using intranasal administration of sequence-specific miRNA inhibitors to ameliorate allergic airway inflammation^{100,132-134}. In addition, uncovering the target networks through which miRNAs act may be an effective path to the development of novel therapies. For example, our findings lend weight to the argument that NF-κB inhibitors might be effective in asthma and other allergic diseases¹³⁵. Through coordinate repression of several mRNA targets, miR-19 amplifies signals that augment production of T_H2 cytokines, the principle drivers of asthma pathogenesis.

Acknowledgements

This work was supported by the U.S. National Institutes of Health (HL107202, HL109102), the Sandler Asthma Basic Research Center, a Scholar Award from The Leukemia & Lymphoma Society, L.J.S. is a National Science Foundation predoctoral fellow (2010101500), the Swiss Foundation for Grants in Biology and Medicine (PASMP3-142725), the National Multiple Sclerosis Society, and the UCSF Program for Breakthrough Biomedical Research, which is funded in part by the Sandler Foundation. The authors would like to thank Mike McCune, Yelena Bronevetsky, and Elisabeth Krow-Lucal for help with human biospecimens, and Robin Kageyama for helpful discussion of the manuscript.

Author contribution statement

L.J.S. designed, performed, and analyzed most experiments. S.P, D.F.C. H.D.B., X.R., Y.W., H.H.P, D.B., M.M.M., M.P., and K.A.R. helped design and perform some experiments. N.R.B. analyzed expression data. X.H., J.V.F., J.R.A., P.G.W. and K.M.A. helped design the clinical study and some experiments. L.J.S. wrote the manuscript. All authors reviewed and approved the manuscript.

Materials and Methods

Human subjects

Bronchoalveolar lavage (BAL) fluid was obtained from three groups of subjects: asthmatic subjects that had not been treated with inhaled corticosteroids (ICS) for 6 weeks prior to the study start date, called “steroid-naïve” here; asthmatic subjects that were treated continuously with ICS, called “steroid-using” here, and healthy control subjects. BAL was obtained from steroid-naïve subjects at baseline and again after 8 weeks of ICS treatment, 200µg budesonide twice a day. BAL was obtained from steroid-using subjects after standardizing their ICS treatment to a regimen of 200µg budesonide twice a day for 8 weeks. This study, called the Study of the Mechanisms of Asthma (MAST), was registered on clinicaltrials.gov: NCT00595153. A power calculation was used to determine the number of subjects needed to measure differences in expression of 3 biomarker genes of IL-13 exposure in the airway. We utilized all sorted T cell samples available from this completed study. Inclusion and exclusion criteria for human subjects are provided on clinicaltrials.gov. Written informed consent was obtained from all subjects, and all studies were performed with approval from the UCSF Committee on Human Research.

Sorting of clinical BAL samples

Investigators were blinded to the group allocation of subjects during cell sorting and sample processing. Live CD3⁺ CD4⁺ T cells were sorted using a FACSAria flow cytometer (BD Biosciences, San Jose, CA) from BAL cells transported in ice cold PBS with 5% FCS within approximately four hours of collection. CD3-PE (cat# MHCD03044) was purchased from Invitrogen (Carlsbad, CA). CD4-Cy7 (cat# 557852), CD8-APC-Cy7 (cat# 557834), and PI (cat#

51-66211E) were purchased from BD Biosciences (San Jose, CA). The average purity of the sorted cells, confirmed by flow cytometric analysis, exceeded 95%. Sorted cells were washed in ice cold PBS with 2% FCS and 2mM EDTA and then lysed in RLT buffer (Qiagen, Valencia, CA) prior to being snap-frozen and stored at -80°C.

High-throughput multiplex qPCR

High-throughput multiplex qPCR was performed according to a previously described protocol⁹². Briefly, CD4 T cells sorted by flow cytometry from clinical samples were lysed and stored in RLT buffer (Qiagen) at -80°C until all samples were collected. Frozen lysates were thawed and loaded onto QIAshredder homogenizer columns (Qiagen). Using a low concentration of ethanol (35% v/v), the large fraction of RNA (>150nt) was precipitated and captured on collection columns (RNeasy, Qiagen). The small fraction of RNA (<150nt) does not bind with low concentration of RNA, and so the flow-through from the first column was brought up to a concentration of 75% v/v ethanol and RNA was precipitated and collected on a fresh column (MinElute, Qiagen). Both RNA fractions were treated with DNase per manufacturer's recommendations (Qiagen). 2µl of RNA from each large fraction, as well as a standard curve of RNA from *in vitro*-derived T_H2 cells, were reverse transcribed using the SuperScript III kit (Invitrogen). RNA was then quantified by qPCR using primers for *β2m* and comparing to the standard curve of RNA. We calculated 100pg RNA from the small fraction for each sample for multiplex reverse transcription using 2 separate mixes of 96 miRNA stem loop reverse primers at a final concentration of 1nM (Supplemental table 1). Reverse transcription and 20 cycles of preamplification were performed according to previous protocols^{92,112}. Excess primers were removed from samples using 9µl ExoSAP-IT (USB) per sample, and then 15µl of each sample

was purified on Illustra AutoScreen-96 Well Plates (GE Healthcare). MiRNA qPCR data was collected on the BioMark system (Fluidigm) using a 96.96 Dynamic Array Integrated Fluidic Circuit (IFC).

Fluidigm Biomark qPCR data analysis

Data was first analyzed on Real Time PCR Analysis software (Fluidigm) with the quality threshold set at 0.5, baseline correction set to linear (derivative), and Ct threshold method set to auto (detectors). The data was further analyzed in R (version 2.14.1) through the following pipeline: Ct values < 5 or >28 were removed per Fluidigm recommendations; miRNAs that were detected in less than 60% of patient samples were removed from analysis; missing Ct values were replaced with the limit of detection (highest Ct value within the standard curve) + 0.1, and 4) the data were global mean-normalized per plate to account for inter-plate differences.

Mice

Mice with loxP-flanked alleles encoding miR-17~92 (*Mirc1*^{fl/fl}, 008458, The Jackson Laboratory), and *Rosa26*-miR-17~92-transgenic mice (Gt(ROSA)26Sor^{tm3(CAG-MIR17-92,-EGFP)Rsky}, 008517, The Jackson Laboratory) were crossed to CD4-Cre mice (4196, Taconic) to generate CD4-Cre;*Mirc1*^{fl/fl} (called ‘17~92^{Δ/Δ}’ here), CD4-Cre;Gt(ROSA)26Sor^{tm3(CAG-MIR17-92,-EGFP)Rsky} (called ‘17~92^{GFP/+}’ here), and CD4-Cre;*Mirc1*^{+/+} or *Mirc1*^{fl/fl}; (collectively called ‘17~92^{+/+}’ here). OT-II mice (004194), and mice heterozygous for the *Rora*^{sg} mutation (002651) were from The Jackson Laboratory. Mice with loxP-flanked *Pten* alleles have been described¹³⁶. *Cd28*^{-/-} mice (002666) were from The Jackson Laboratory. All mice were housed and bred in the specific pathogen-free

barrier facility at the University of California, San Francisco. The Institutional Animal Care and Use Committee at the University of California, San Francisco, approved all animal experiments.

***In vitro* human cord blood T cell polarization**

Peripheral blood mononuclear cells (PBMCs) from anonymous human cord blood donors were isolated by Lymphoprep gradient (Accurate Chemical & Scientific Corp; cat # 1114545). CD4⁺ T cells were isolated from PBMCs using the Dynabeads Untouched Human CD4⁺ T Cell Isolation Kit (Invitrogen). Cells were stimulated for ~65 h on plates coated with 1 μg/ml anti-CD3 (UCSF Monoclonal Antibody Core; clone OKT-3) and 2 μg/ml anti-CD28 (UCSF Monoclonal Antibody Core; clone 9.3) at an initial density of 0.7x10⁶ cells/ml. After stimulation, the cells were rested for two days in media containing 20 units/ml recombinant human IL-2 (NCI). For T_H2 polarizing conditions, 12.5 ng/ml recombinant human IL-4 (PeproTech; cat # 200-04) was added throughout the 5 days. T cell culture was in RPMI-1640 media with 10% FCS, pyruvate, nonessential amino acids, L-arginine, L-asparagine, L-glutamine, folic acid, beta mercaptoethanol, penicillin, and streptomycin.

***In vitro* mouse primary T cell polarization**

CD4⁺ T cells were isolated from spleen and lymph nodes of young mice (4-8 weeks old) using the Mouse CD4 Dynabeads Isolation kit (Invitrogen; L3T4). For experiments including CellTrace Violet (Invitrogen), cells were stained at 5 μM in PBS for 20 minutes at 37°C, quenched with 5 volumes of media with 10% FCS for 5 minutes, and washed twice in media prior to culture. For all conditions, cells were activated with hamster anti-mouse anti-CD3 (clone 2C11, 0.25 μg/ml) and anti-mouse CD28 (clone 37.51, 1 μg/ml) antibodies on a plate coated with

goat anti-hamster IgG (0.3mg/ml in PBS; MP Biomedicals) for ~65 h at an initial density of 0.7×10^6 cells/ml, and then rested in media with 20 units/ml recombinant IL-2 (National Cancer Institute) for 48-72 h. For T_H2 polarizing conditions, 500 units/ml IL-4 supernatant and 5 μ g/ml anti-IFN- γ (clone XMG1.2) were added to the culture throughout the 5-6 days. “Low T_H2 ” conditions included only 5 units/ml IL-4, and “ T_HN ” conditions received no polarizing cytokines or antibodies. T_H17 polarizing conditions received 5ng/ml recombinant human TGF- β (Peprotech), 25ng/ml recombinant murine IL-6 (Peprotech), 10ug/ml anti-IL-4 (clone 11B11), 10ug/ml anti-IFN-g, and 20ng/ml recombinant murine IL-23 (R&D Systems) throughout the 5 days of culture. All cultures used DMEM high glucose media supplemented with 10% FCS, pyruvate, nonessential amino acids, MEM vitamins, L-arginine, L-asparagine, L-glutamine, folic acid, beta mercaptoethanol, penicillin, and streptomycin.

miRNA mimics, miRNA inhibitors, siRNA, and miRNA sensors

During *in vitro* polarization, human or mouse primary CD4⁺ T cells in culture were transfected with miRNA mimics, inhibitors, or siRNAs (Dharmacon) at 24 and 96 h of culture. miRIDIAN miRNA mimics were used at 500nM per transfection. miRIDIAN miRNA Hairpin Inhibitors were also used at 500nM. siGENOME SmartPools and ON-TARGETplus Individual siRNA were used at 500nM. Cells were transfected using the Neon Transfection system by Invitrogen as described¹¹¹. Retroviral miRNA sensors containing 4 perfectly complementary binding sites for miR-1, miR-19a, and miR-19b were constructed and transduced at 48 h as described¹¹¹.

Intracellular cytokine and transcription factors stains

For cytokine staining, cells were restimulated with 20nM PMA and 1 μ M ionomycin for 4 hours, and 5 μ g/ml brefeldin A was added during the last 2 hours of restimulation. Cells were stained with the viability dye eFluor780 (eBiosciences; Cat # 65-0865-14), and then fixed in 4% paraformaldehyde for 8 minutes at room temperature. Cytokine staining was done in permeabilization buffer containing 0.05% saponin. For transcription factor staining, unstimulated cells were fixed, permeabilized, and stained using the FoxP3 Staining Kit (eBiosciences; Cat # 00-5523-00). Samples were analyzed with a flow cytometer (BD LSR II). Mouse antibodies: IL-13-PE (eBiosciences; eBio13A), IL-4-APC (eBiosciences; 11B11), IL-5-PE (Biolegend; TRFK5), IFN γ -FITC (eBiosciences; XMG1.2), TNF α -AlexaFluor700 (BD Biosciences; MP6-XT22), and GATA-3-PE (eBiosciences; E50-2440). Human antibodies: IL-13-FITC (eBiosciences; PVM13-1), IL-4-APC (BD Biosciences; 8D4-8), IL-17A-eFluor450 (eBiosciences; eBio17B7), and IL-17F-PE (BD Pharmingen; 079-289).

***In vivo* allergic airway inflammation model**

For each *in vivo* experiment, we used at least 5 mice per group to gain power for statistical analysis, and repeated the model to pool data and determine reproducibility. Mice received 3 different cell types in rotation such that each cage had 1-2 recipients for each cell type. Mice were challenged in random order and were tested for pulmonary resistance in rotating order through each group. One mouse was removed from analysis due to low body weight and lack of movement; histological analysis confirmed signs of emphysema. Six- to eight-week old sex-matched littermate *Cd28^{-/-}* mice were injected retro-orbitally with 2x10⁵ *in vitro* T_H2-polarized 17 \sim 92^{+/+} or 17 \sim 92 ^{$\Delta\Delta$} OT-II cells. The mice were challenged oropharyngeally with 50 μ g ovalbumin (OVA) in PBS at 24, 48, and 72 hours post transfer to induce allergic airway

inflammation. 18 hours after the final challenge, mice were anesthetized with ketamine/xylazine, and pulmonary resistance was measured by trachea cannulation in response to intravenous acetylcholine, as previously described¹³⁷. BAL was collected by 5 lavages of 0.8ml of PBS for flow cytometry, and lungs were filled with 10% buffered formalin and fixed for histology. BAL cells were washed, counted, and surface stained for analysis by flow cytometry. Antibodies used for myeloid cell enumeration: CD11b-AlexaFluor488 (eBiosciences; M1/70), CD11c-PE-Cy7 (Biolegend; N418), Ly6G-V450 (BD Biosciences; 1A8), SiglecF-PE (BD Biosciences; E50-2440). Two paraffin-embedded 5µm sections of the whole lung from each mouse were stained with H&E and PAS. To quantify inflammation, H&E-stained lung sections were de-identified for blinding and scored for peribronchial and perivascular inflammatory cell infiltration: grade 0, no infiltration; grade 1, <25% of examined area; grade 2, 25-50%; grade 3, 51-75%; and grade 4, >75%. To quantify goblet cell hyperplasia, PAS stained lung sections were de-identified for blinding and scored for the percentage of PAS positive cells among airway epithelial cells: grade 0: none; grade 1 <25% of airway epithelial cells; grade 2, 25-50%; grade 3, 51-75%; and grade 4, >75%.

Table 1: Healthy and asthmatic subjects providing bronchoalveolar lavage CD4 T cells for miRNA expression analysis

	Healthy	Steroid-naïve Asthma	Steroid-using Asthma
Sample size (M/F)	8 (4/4)	14 (5/9)	21 (9/12)
Age, y	40.3 (25-56)	30.1 (20-56)	37.3 (18-55)
FEV1 % predicted	100 (88-128)	90 (61-103)	80 (59-110)
Methacholine PC ₂₀ mg/ml	>10	0.8 (0.08-4.3)	2.1 (0.14-8.1)
Sorted CD4 ⁺ T cells (x10 ³)	215 (24-440)	243 (29-1,250)	277 (45-2,200)

Figure 1. miR-19a expression is elevated in CD4⁺ T cells from asthmatic lungs

(a) Taqman qPCR analysis of miRNA expression in sorted CD4 T cells. Circles represent global-mean-normalized average miRNA expression in asthma compared to healthy subjects. Dashed lines represent 2-fold higher or lower expression. (b) qPCR analysis of miR-19a expression normalized to the global mean. Circles represent individual subjects. Line represents mean expression for each group. (c) qPCR analysis of miR-19a expression in CD4⁺ T cells from individual asthmatic subjects pre- and post- 6 weeks of inhaled corticosteroid (ICS) treatment. $n = 5$. (d) qPCR analysis of the expression of miR-17, miR-18a, miR-19b, and miR-20a (members of the miR-17~92 cluster; miR-92a was not detected in this experiment) normalized to the global mean. Circles represent individual subjects. Lines represent mean expression for each group. (a-d) Data are pooled from 2 experiments with $n = 8$ Healthy, 13 steroid-naïve (SN) asthma, and 21 steroid-using (SU) asthma. (b, d) One-way ANOVA with Dunnett's post test (compared to healthy). (c) Paired 2-tailed t-test. * $p < 0.05$, ** $p < 0.0001$, ns = not significant.

Fig. 1

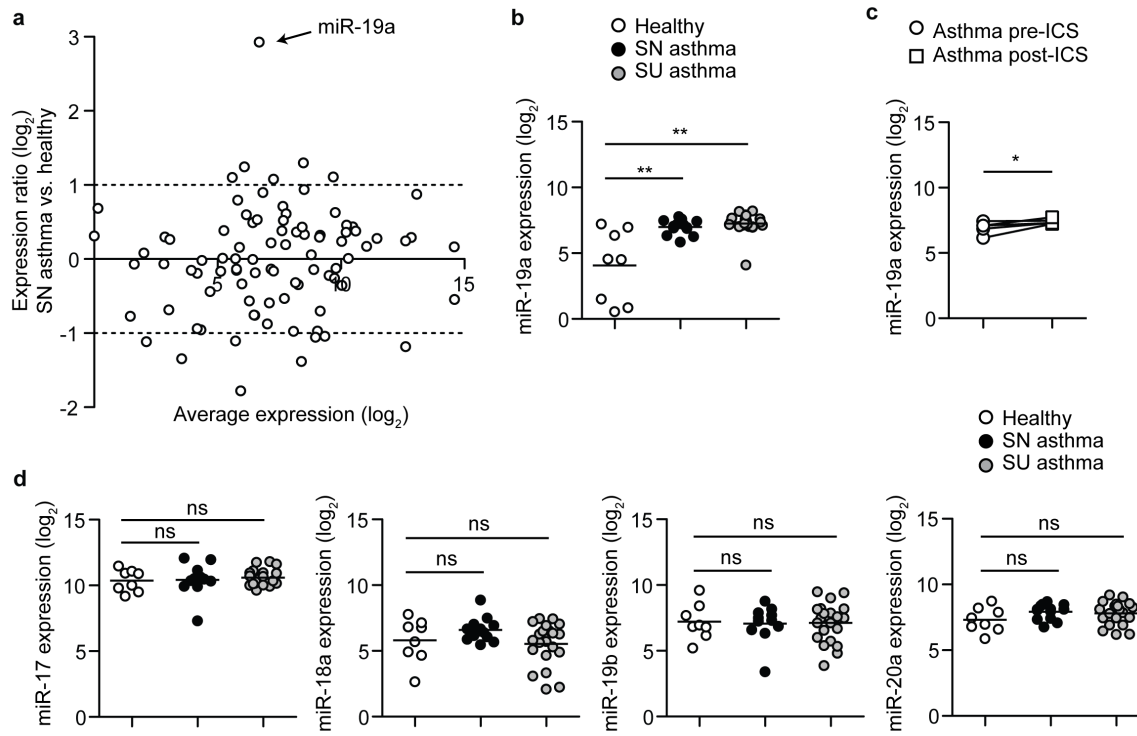


Figure 2. The miR-17~92 cluster promotes T_H2 cytokine production

(a-c) Intracellular cytokine staining and pooled analysis of day 5 T_H2-polarized CD4⁺ T cells from 17~92^{ΔΔ} (left), 17~92^{+/+} (middle), and 17~92^{GFP/+} (right) mice. Numbers in quadrants indicate percentage of cells producing the indicated cytokine among live singlets. Bar graphs indicate total cytokine⁺ cells as a percentage of live singlets. Error bars are mean ± SEM. **(a)** Flow cytometry data is representative of 11 independent experiments. *n* = 12 17~92^{ΔΔ} (black), 17 17~92^{+/+} (grey), and 6 17~92^{GFP/+} (white) mice pooled from 11 independent experiments. **(b)** Flow cytometry data is representative of 7 independent experiments. *n* = 8 17~92^{ΔΔ} (black), 10 17~92^{+/+} (grey), and 4 17~92^{GFP/+} (white) mice pooled from 7 independent experiments. **(c)** Flow cytometry data is representative of 11 independent experiments. *n* = 12 17~92^{ΔΔ} (black), 17 17~92^{+/+} (grey), and 7 17~92^{GFP/+} (white) mice pooled from 11 independent experiments. **(d)** Flow cytometry of GATA-3 expression in day 5 T_H2-polarized CD4 T cells from 17~92^{ΔΔ} (black line), 17~92^{+/+} (grey filled), and 17~92^{GFP/+} (black dashed line) mice. Data are representative of 2 experiments. Bar graph indicates mean fluorescence intensity (MFI) of GATA-3 expression in live singlets of 17~92^{ΔΔ} (black), 17~92^{+/+} (grey), and 17~92^{GFP/+} (white) mice. Error bars are mean ± SEM. *n* = 4, 4, 4 (2 mice in each group with duplicate cultures from 2 independent experiments). **(a, c, d)** One-way ANOVA with Dunnett's post test. **(b)** One-way ANOVA Kruskal-Wallis test (for groups with unequal variance) and Dunn's post test. **p* < 0.05, ***p* < 0.001, ns = not significant.

Fig. 2

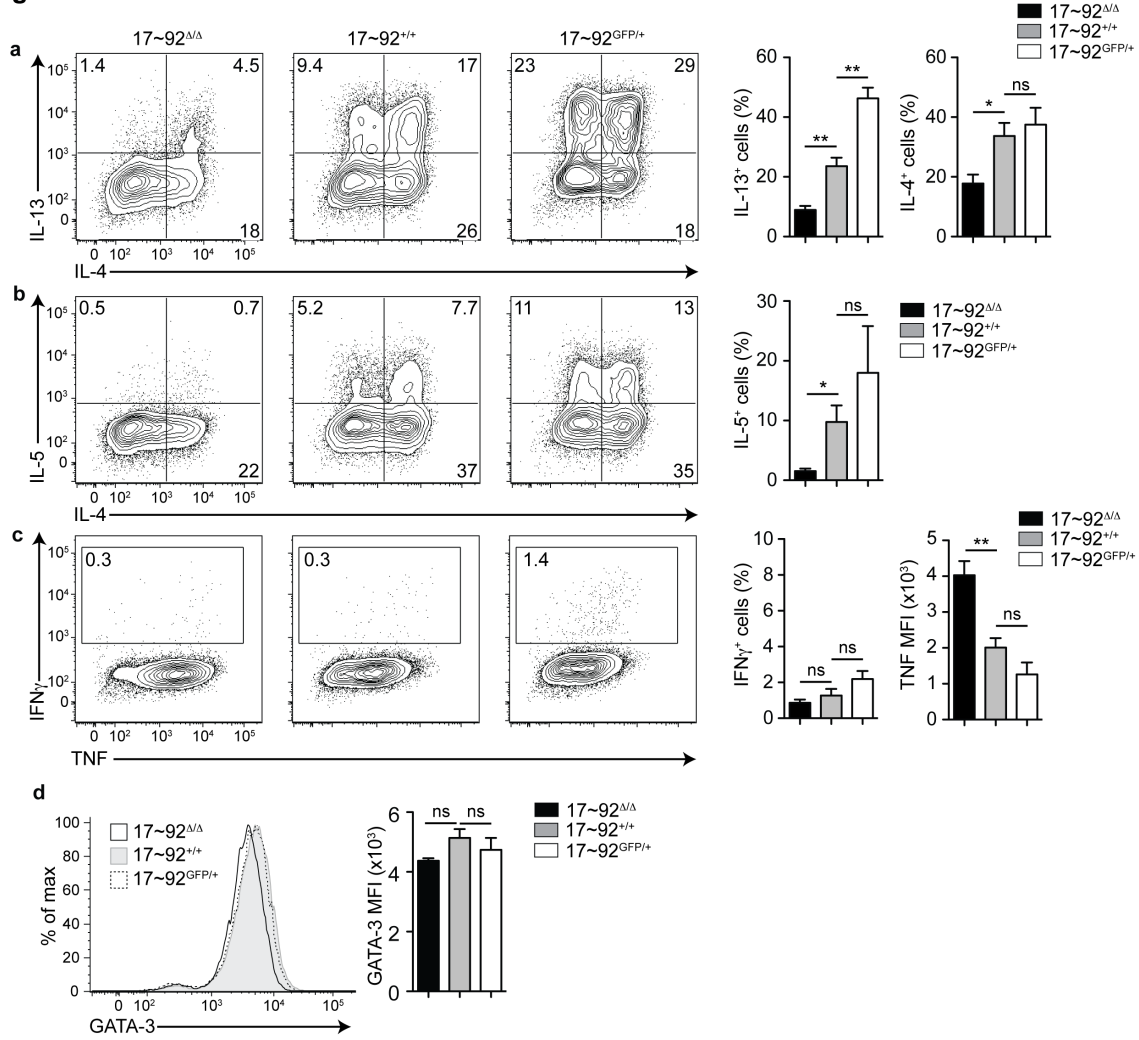


Figure 3. The miR-17~92 cluster promotes T_H2 cytokine production in a cell-intrinsic and proliferation-independent manner

(a) Intracellular cytokine staining of CD4⁺ T cells from CD45.1⁺ 17~92^{Δ/Δ} and CD45.2⁺ 17~92^{+/+} mice, co-cultured in T_H2 polarizing conditions for 5 days. Numbers indicate percentage of cytokine-producing cells (above the dotted line) in either the CD45.1⁺ or the CD45.1⁻ gate (solid boxes). Data are representative of 2 independent experiments with 2 mice each and duplicate cultures. **(b)** CellTrace Violet (CTV) stain indicating proliferation of day 5 T_H2-polarized 17~92^{Δ/Δ} (black line), 17~92^{+/+} (grey filled), and 17~92^{GFP/+} (black dashed line) CD4⁺ T cells. Numbers above peaks indicate division number relative to an undivided control. **(c)** Intracellular cytokine staining of CTV-labeled 17~92^{Δ/Δ} (left), 17~92^{+/+} (middle), and 17~92^{GFP/+} (right) day 5 T_H2-polarized CD4⁺ T cells. Solid box indicates cytokine-positive gate used for quantification in **(d)**. **(d)** Quantification of **(c)** showing cytokine-positive cells (as a percentage of live singlets) at each division in 17~92^{Δ/Δ} (black bars), 17~92^{+/+} (grey bars), and 17~92^{GFP/+} (white bars) cells. Data are from one representative experiment. Error bars are mean with range. *n* = 2 replicate cultures from one mouse of each genotype. *p* < 0.0001 by 2-way ANOVA comparing 17~92^{Δ/Δ} and 17~92^{+/+} in IL-13, IL-5, and IL-4. *p* < 0.0001 by 2-way ANOVA comparing 17~92^{+/+} and 17~92^{GFP/+} in IL-13 and IL-5. *p* = 0.3153 by 2-way ANOVA comparing 17~92^{+/+} and 17~92^{GFP/+} in IL-4. **(b-d)** Data are representative of 6 independent experiments with 17~92^{Δ/Δ} and 17~92^{+/+} (*n* = 6 mice each), and 2 experiments with 17~92^{+/+} and 17~92^{GFP/+} (*n* = 2 mice each).

Fig. 3

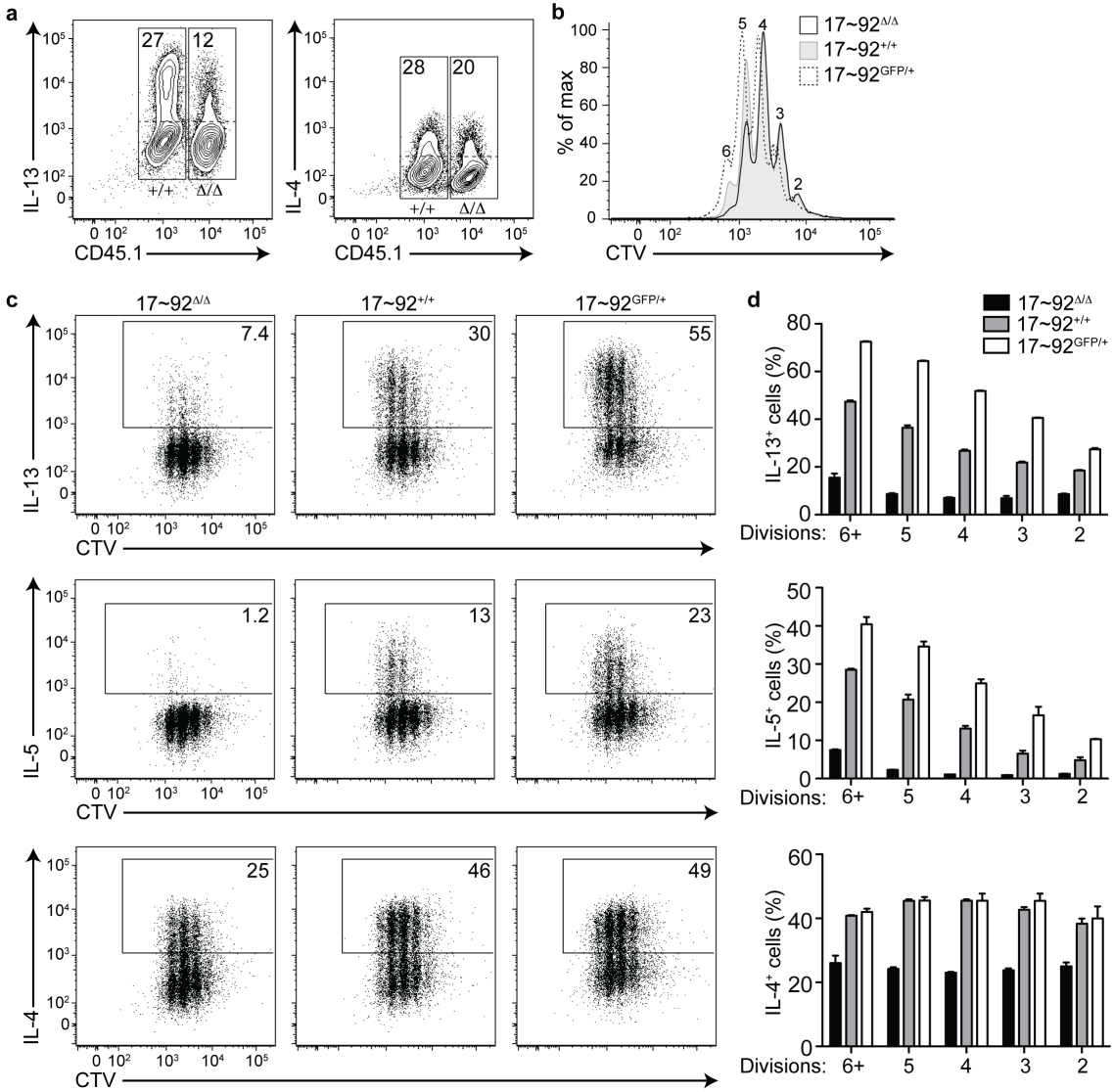


Figure 4. miR-19a and miR-19b rescue the T_H2 cytokine defect in 17~92^{ΔΔ} cells

(a) Intracellular cytokine staining of 17~92^{+/+} or 17~92^{ΔΔ} CD4 T cells transfected with control mimic (CM), miR-19a, -19b, -17, -18a, -20a, or -92a mimics. Cells were transfected on days 1 and 4 of T_H2 polarization, and analyzed on day 5. Numbers in each quadrant indicate percentage of cells producing the indicated cytokine. Data are representative of 3 independent experiments.

(b-c) Quantification of IL-13 **(b)** or IL-4 **(c)** production at day 5 after transfection with miRNA mimics. Bars represent mean ± SEM for 3 individual transfections for each condition. Data are representative of 3 independent experiments. **(d-e)** 17~92^{+/+} or 17~92^{ΔΔ} CD4⁺ T cells were

transfected with CM, miR-19a, or -19b on day 1 only, day 4 only, or both day 1 and 4.

Quantification of IL-13 **(d)** or IL-4 **(e)** production at day 5 of T_H2 polarization. Error bars are mean ± SEM for 3 individual transfections for each condition. Data are representative of 2 independent experiments.

(b, c) One-way ANOVA with Dunnett's post test (comparing each column to 17~92^{ΔΔ} + CM). **(d, e)** $p < 0.0001$ by 2-way ANOVA with Bonferroni post test

(comparing each column to 17~92^{ΔΔ} + CM per time point). ns = "not significant", * $p < 0.05$, **

$p < 0.01$, *** $p < 0.001$, **** $p < 0.0001$.

Fig. 4

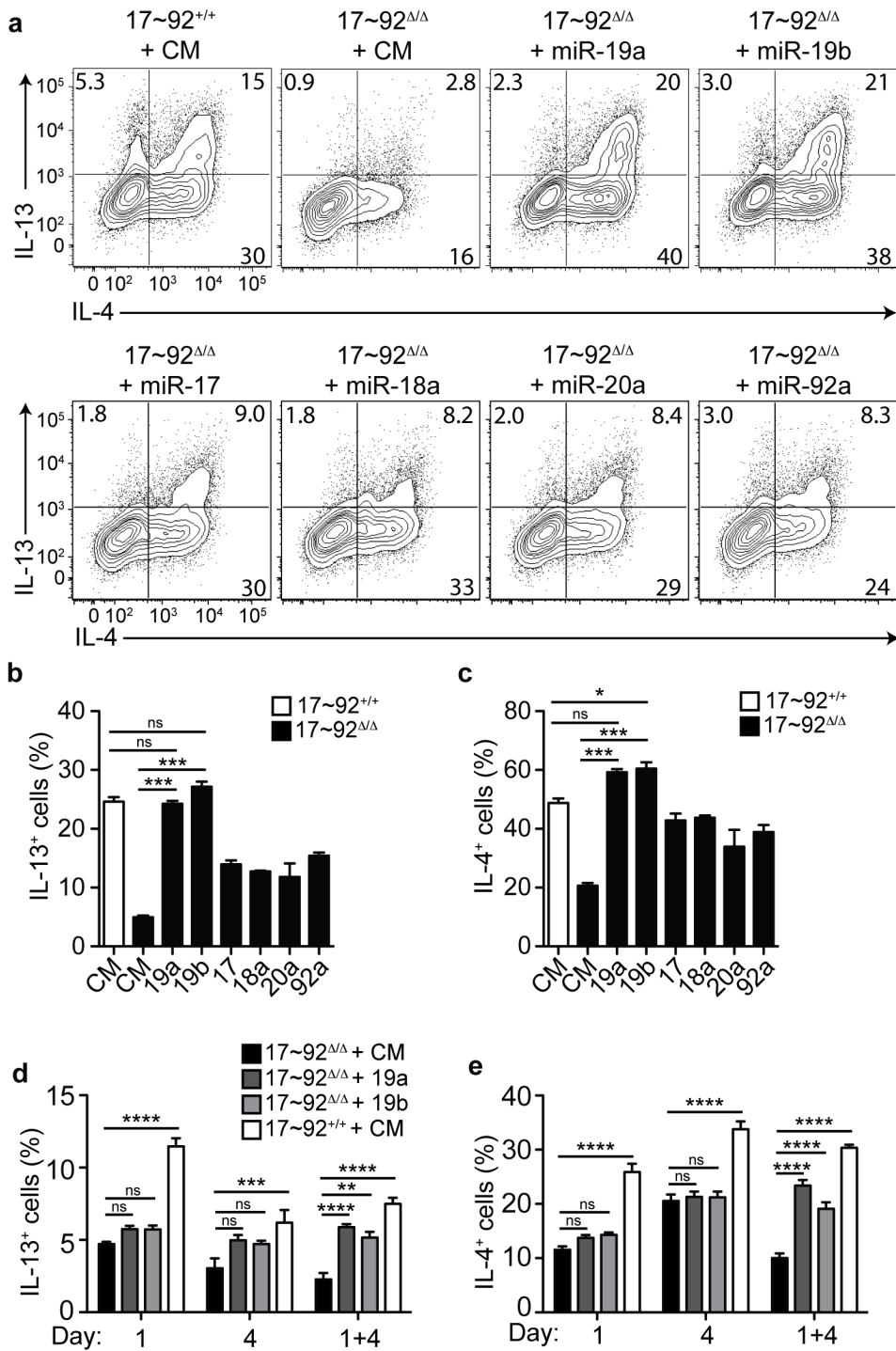


Figure 5. miR-19a promotes IL-13 production in human CD4⁺ T cells

(a) Intracellular cytokine staining of CD4⁺ T cells isolated from human cord blood and transfected with control inhibitor or anti-miR-19 inhibitor on days 1 and 4 in T_H2 polarizing conditions, analyzed on day 5. Numbers in each quadrant indicate percentage of cytokine-positive cells. Data are representative of 3 experiments with 8 cord blood samples. (b) Quantification of IL-13 (left) or IL-4 (right) producing human CD4⁺ T cells upon transfection with control inhibitor (CI) or anti-miR-19 inhibitor (Anti-19). Circles represent the mean of 2 individual transfections of each inhibitor. Lines connect individual cord blood donors receiving either inhibitor. *n* = 8 cord bloods in 3 experiments. (c) Intracellular cytokine staining of CD4⁺ T cells isolated from human cord blood and transfected with control mimic or miR-19a mimic on days 1 and 4 in T_H2 polarizing conditions, analyzed on day 5. Numbers in each quadrant indicate percentage of cytokine-positive cells. Data are representative of 3 experiments with 8 cord blood samples. (d) Quantification of IL-13 (left) or IL-4 (right) producing human CD4⁺ T cells upon transfection with control mimic (CM) or miR-19a mimic (19a). Circles represent the mean of 2 individual transfections of each mimic. Lines connect individual cord blood donors receiving either mimic. *n* = 8 cord bloods in 3 experiments. (b, d) Two-tailed paired t-test. **p* < 0.01, ***p* < 0.001, ns = not significant.

Fig. 5

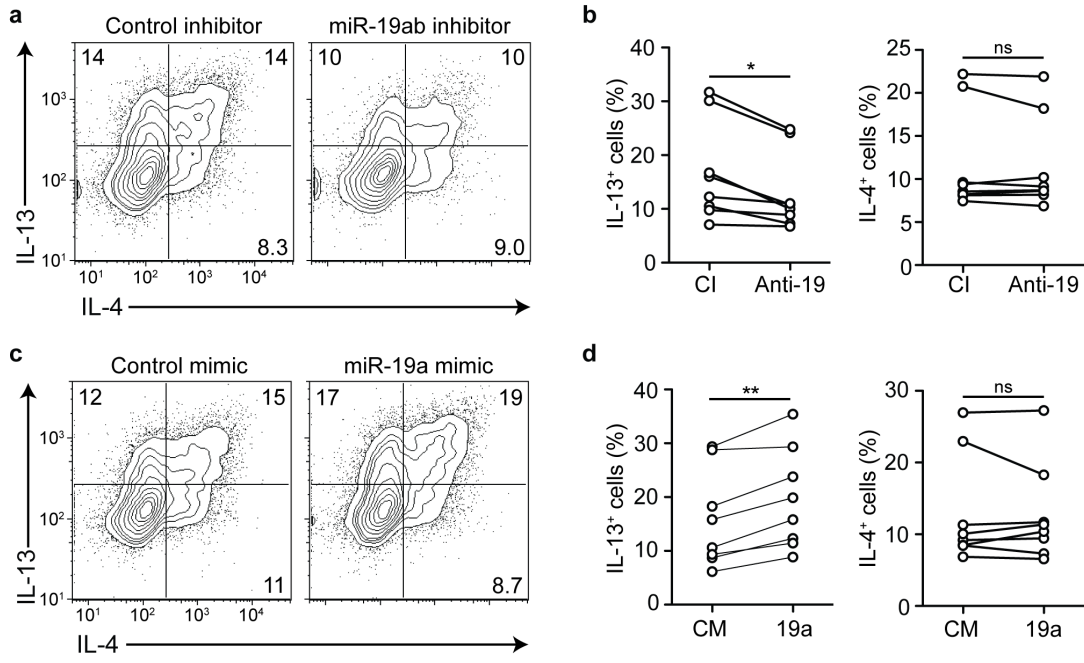


Figure 6. Several miR-19 targets negatively regulate T_H2 cytokine production

(a-b) Primary screen of miR-19 targets that alter IL-13 and IL-4 production. Analysis of intracellular cytokine staining of 17~92^{ΔΔ} cells transfected with 38 siRNA smartpools. Bars indicate IL-13 z-score ($z = x - \text{mean}/\text{SD}$ where x represents the IL-13⁺ cells (%) for each siRNA **(a)** or IL-4 z-score **(b)**). The white bar indicates siRNA nontargeting control (siNegCtl), and the black bar indicates miR-19a mimic positive control. The shaded grey area highlights the 8 genes with further analysis in **(c)** and **(d)**. Data are representative of two independent experiments. **(c-d)** Analysis of intracellular cytokine staining of 17~92^{ΔΔ} cells transfected with 3 individual siRNAs against the top 8 candidate genes identified in **(a)** and **(b)**. Bars indicate IL-13⁺ **(c)** and IL-4⁺ **(d)** cells as a percentage of live singlets. The white bar indicates siNegCtl, and the black bar indicates miR-19a mimic. Dashed lines indicate the range between the negative and positive controls. Data are representative of 2 independent experiments. **(e)** Intracellular cytokine staining of 17~92^{ΔΔ} cells transfected with individual siRNAs against *Socs1*, *Tnfrif3*, and *Pten* compared to siNegCtl. Numbers in each quadrant indicate percent of cytokine-positive cells. Data are representative of 4 independent experiments. **(f)** qPCR expression of the top 8 candidate miR-19a targets in 17~92^{ΔΔ} cells transfected with control (CM, black bars), miR-19a (dark grey bars), miR-19b (light grey bars) mimics, or 17~92^{+/+} cells transfected with CM (white bars). Data are normalized to *Gapdh*. Data are representative of 2 independent experiments. Error bars represent mean with range of 2 technical replicates. **(g)** Intracellular cytokine stain of day 5 “Low T_H2”-polarized cells from 17~92^{ΔΔ} *Pten*^{+/+} (left), 17~92^{ΔΔ} *Pten*^{+/-} (middle), and 17~92^{+/+} *Pten*^{+/+} mice. Numbers in each quadrant indicate percent of cytokine-positive cells. Data are representative of two experiments. **(h-j)** Analysis of intracellular cytokine staining of 17~92^{ΔΔ} cells in non-polarizing **(h)**, T_H17 polarizing **(i)**, or T_H2 polarizing **(j)** conditions transfected

with individual siRNAs against *Socs1*, *Tnfrsf25*, and *Pten*, compared to siNegCtl. Bars represent mean with range. $n = 2$ transfections for each condition. Data are representative of 2 independent experiments.

Fig. 6

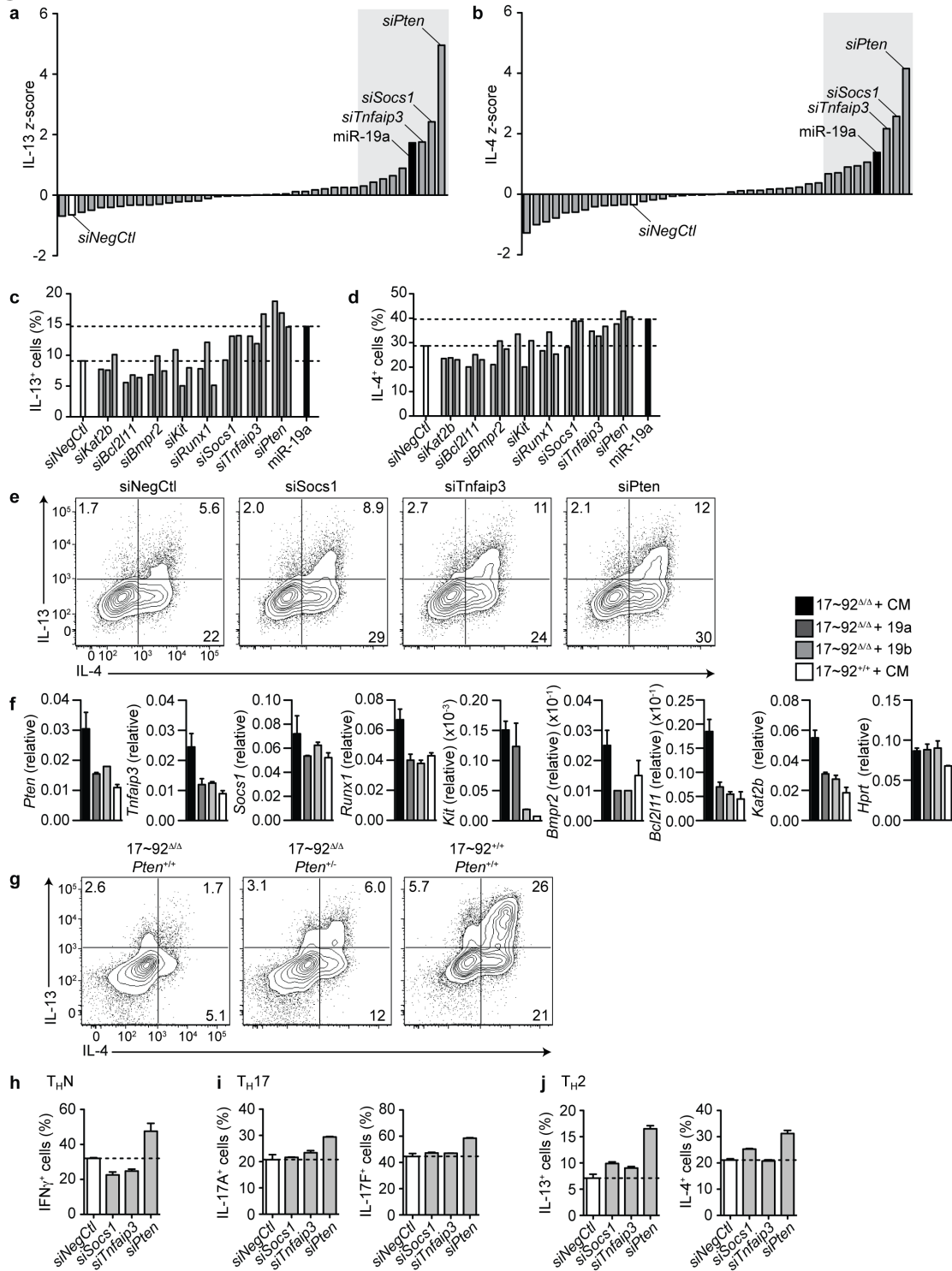


Figure 7. The miR-17~92 cluster promotes T_H2-driven inflammation *in vivo*

(a) Pulmonary resistance measures at day 4 in response to increasing doses of acetylcholine.

Circles represent mean of 10 mice receiving 17~92^{+/+} OT-II cells (black line open circles), 10 mice receiving 17~92^{ΔΔ} OT-II cells (black line black circles), and 6 mice receiving no cells (grey dashed line open circles). Error bars represent mean ± SEM. Statistics on the plot indicate differences at the highest dose of acetylcholine. Data from 2 experiments were combined. (b)

Representative Periodic Acid Schiff (PAS) staining of lung sections from recipient mice with 17~92^{+/+} OT-II cells transfected with control mimic (CM) (left; *n* = 10), 17~92^{ΔΔ} OT-II cells transfected with CM (middle; *n* = 10), or 17~92^{ΔΔ} OT-II transfected with miR-19a mimic (right; *n* = 9). Images are representative of 2 experiments. Black arrowheads mark PAS⁺ cells. The area between the dotted lines indicates immune cell infiltration. (c-d)

Histologic scores of PAS

staining (c) to quantify mucus-secreting cells, and H&E staining (d) to quantify airway

inflammation. Error bars represent median with interquartile range. Analyses use a scale 0-4 and

are analyzed by a blinded observer. (e) Analysis of flow cytometry of inflammatory cells in the

BAL on day 4. Eosinophils (CD11b⁺Siglec F⁺, left), neutrophils (CD11b⁺Ly6G⁺, middle), and

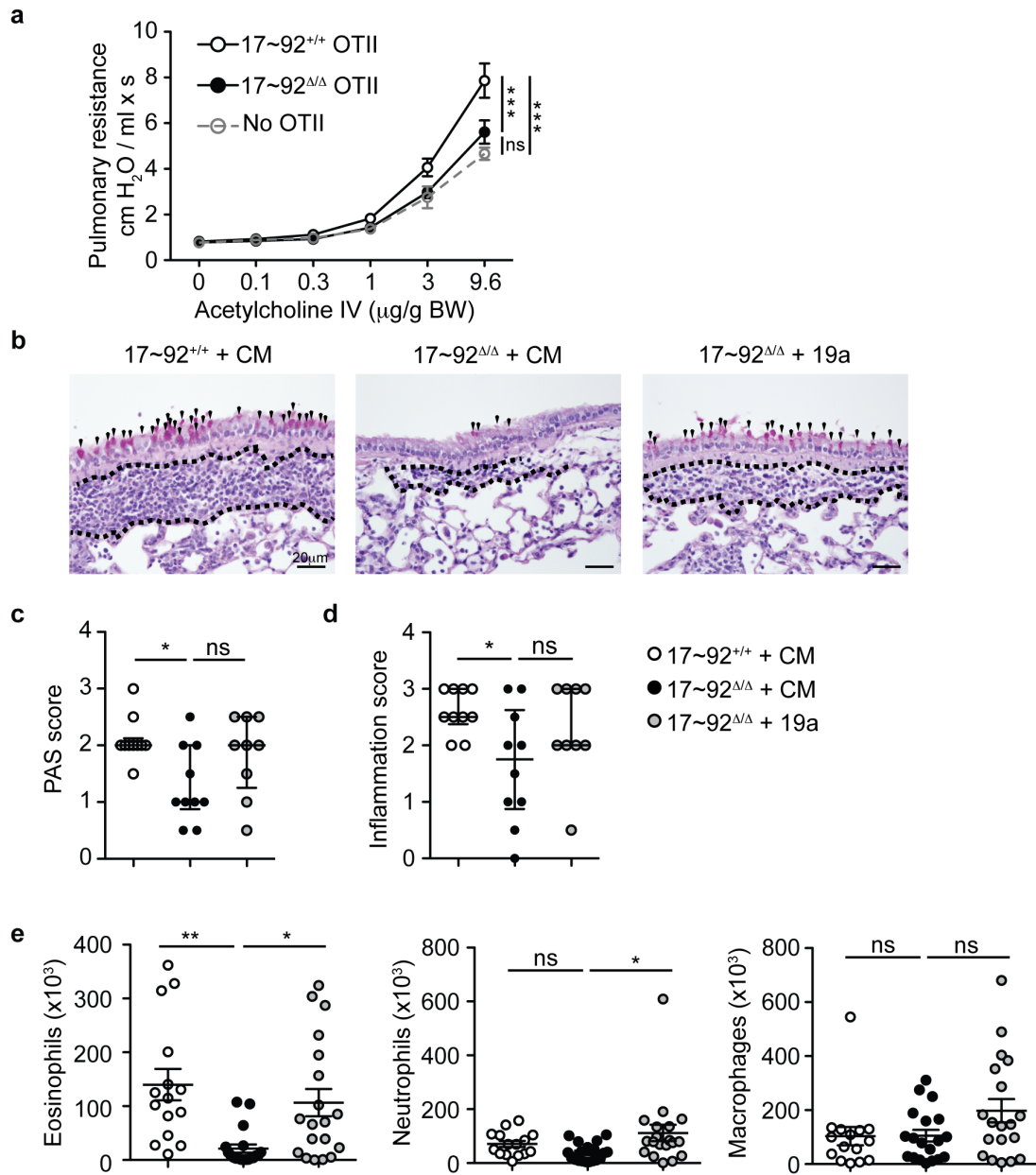
alveolar macrophages (CD11c⁺Siglec F⁺, right) were quantified as the product of their frequency

among live cells and the total BAL cell count. Error bars represent mean ± SEM. *n* = 15, 19, and

19. (a) Two-way ANOVA with Bonferroni post-tests. (c-e) One-way ANOVA with Dunnett's

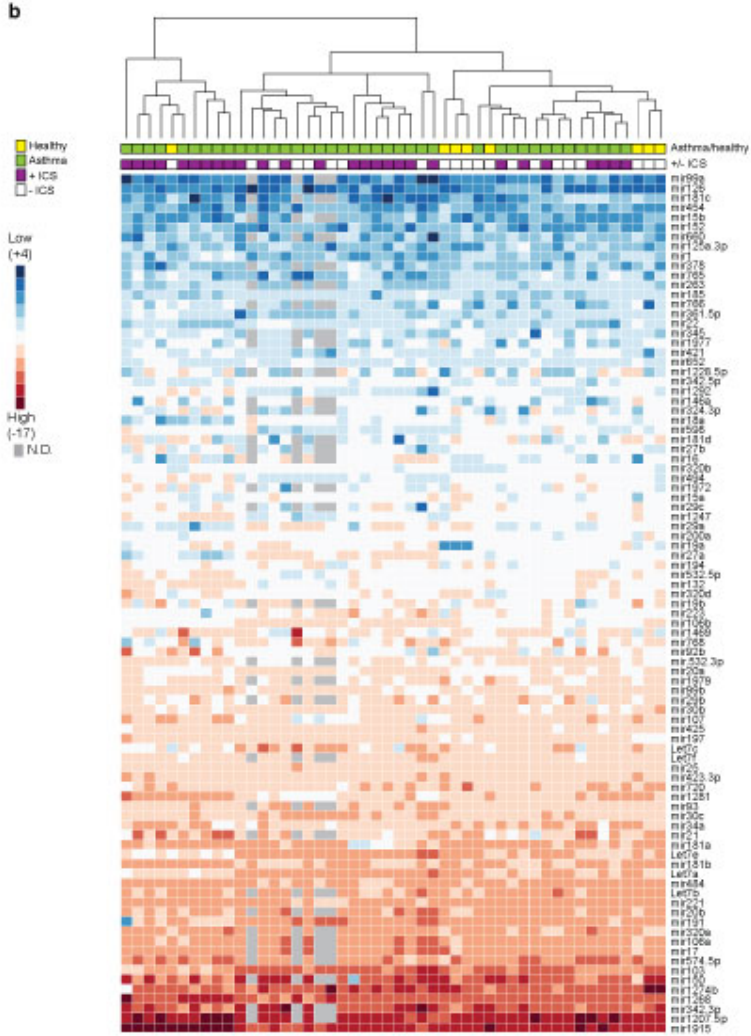
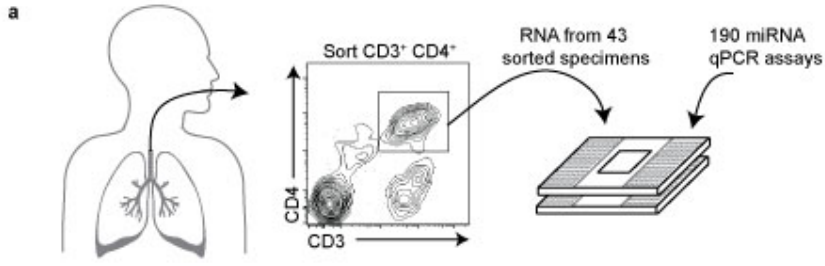
post test. **p* < 0.05, ***p* < 0.001, ****p* < 0.0001. ns = not significant.

Fig. 7



Supplemental Figure 1. Heatmap of all subjects and miRNAs analyzed by multiplex qPCR

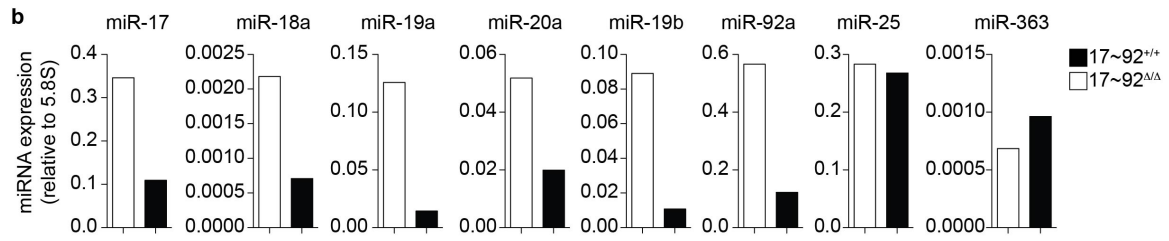
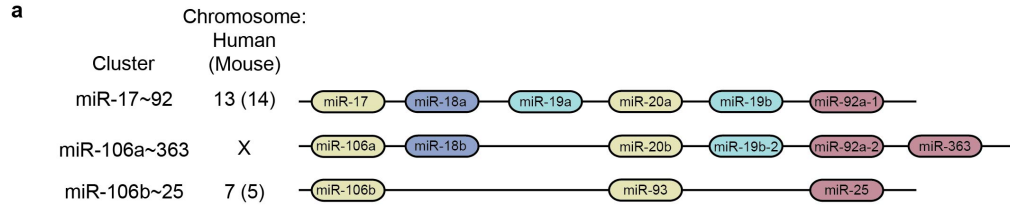
(a) Method shown for isolation of RNA from CD3⁺ CD4⁺ T cells from BAL fluid from healthy and asthmatic subjects. RNA was reverse transcribed and preamplified, and miRNA expression was analyzed using the Fluidigm Biomark qPCR system. (b) Unsupervised hierarchical clustering using the 23 most variable miRNAs (between healthy and steroid-naïve asthma) was determined in R (version 2.14.1) using the *hclust* function with “complete” method. The heatmap (R version 2.14.1; *heatmap* function) was generated using the hierarchical clustering above, including expression of all miRNAs determined by multiplex qPCR using the Biomark system (Fluidigm). In the heatmap, red indicates expression level higher than the mean across all subjects, blue denotes expression level lower than the mean, and grey indicates expression not determined (N.D). In the first row, green indicates asthmatic subjects, and yellow indicates healthy subjects. In the second row, purple indicates inhaled corticosteroid (ICS) treatment, and white indicates no ICS. miRNAs are arranged by average expression across all subjects (lowest to highest). Significance was determined by Welch t-test comparing the healthy and SN asthma groups. (Full table of *p*-values is provided in **Supplementary Table 2.**)



Supplementary Figure 2. miR-17~92 expression in 17~92^{ΔΔ} and 17~92^{+/+} naïve CD4 T cells

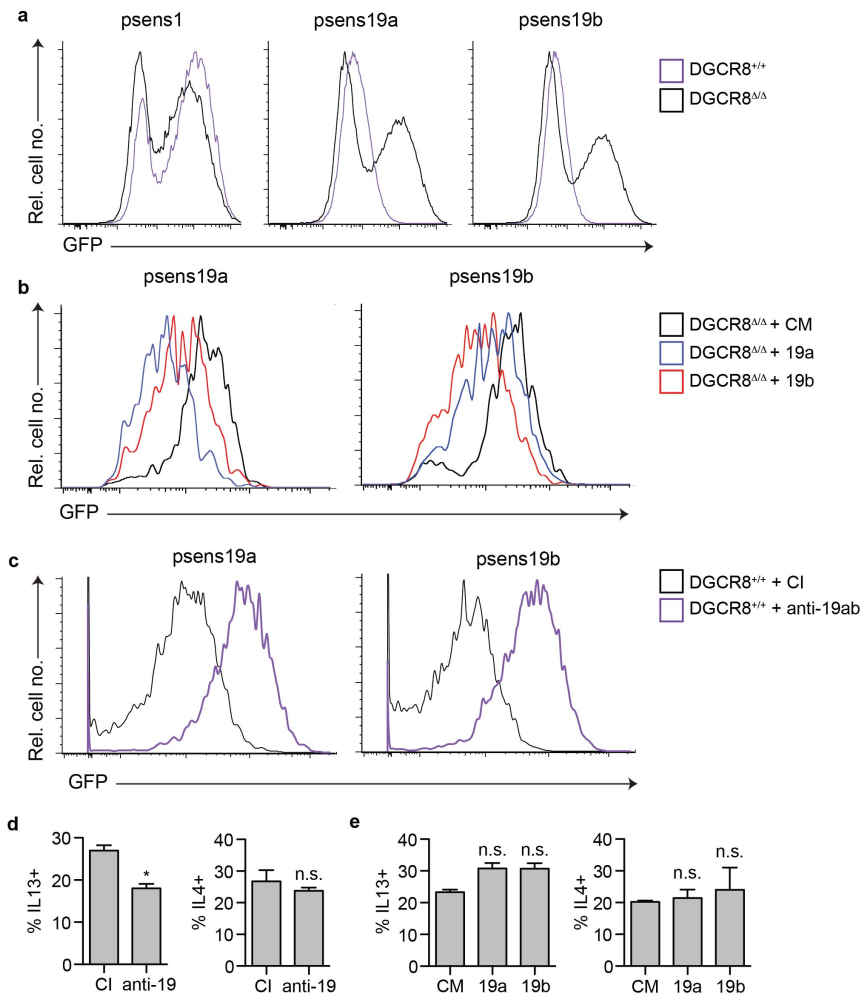
(a) Schematic of the genomic loci of the miR-17~92, miR-106a~363, and miR-106b~25 clusters.

Colors indicate miRNAs belonging to the same family; yellow = miR-17 family, blue = miR-18 family, teal = miR-19 family, pink = miR-92 family. (b) miRNA expression was determined by SYBR qPCR in 17~92^{+/+} (black bars) and 17~92^{ΔΔ} (white bars) naïve CD4 T cells. Expression was normalized to 5.8S rRNA in each sample. Data are representative of 2 experiments.



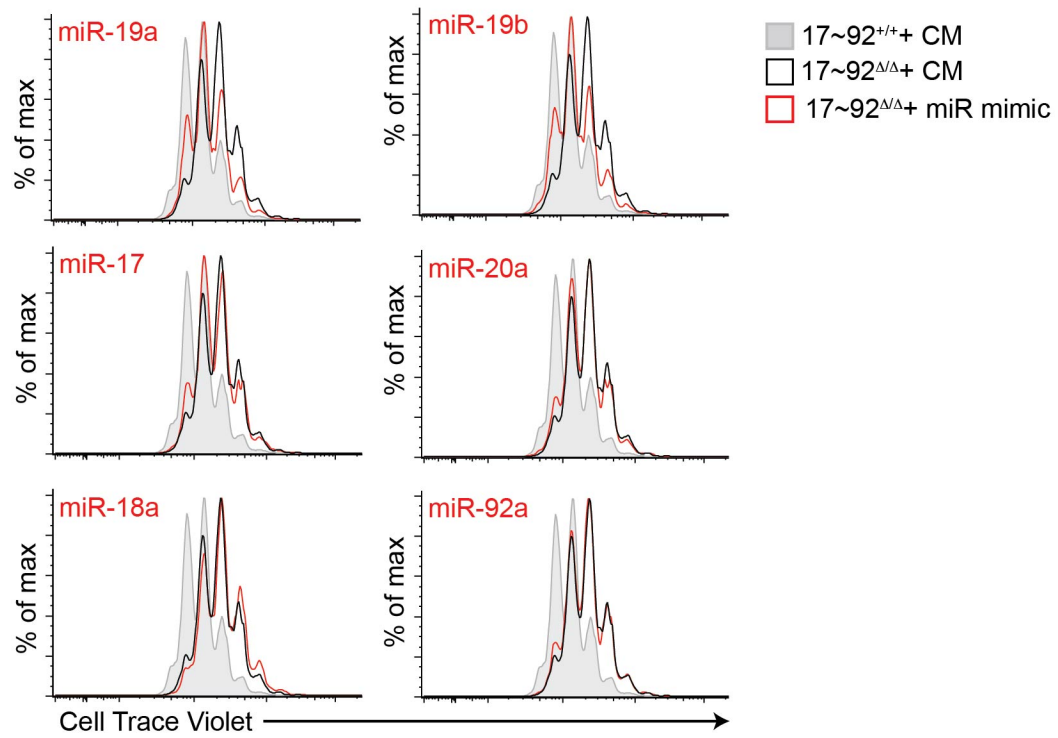
Supplementary Figure 3. miR-19 activity in 17~92^{Δ/Δ} and 17~92^{+/+} cells and effects of mimics and inhibitors

(a) DGCR8^{+/+} and DGCR8^{Δ/Δ} CD4 T cells transduced with retroviral sensors expressing GFP with 4 perfectly complementary binding sites for miR-1 (psens1), miR-19a (psens19a), or miR-19b (psens19b) in the 3'UTR. (b) DGCR8^{Δ/Δ} CD4 T cells transduced with miR-19a (psens19a) or miR-19b (psens19b) sensors and transfected with control mimic (CM), miR-19a mimic (19a), or miR-19b mimic (19b). (c) DGCR8^{+/+} CD4 T cells transduced with psens19a or psens19b, and transfected with control inhibitor (CI) or anti-miR-19a and anti-miR-19b inhibitors (anti-19ab). (d) Analysis of cytokine expression by flow cytometry in DGCR8^{+/+} CD4 T cells cultured for 5 days in nonpolarizing conditions and transfected with control inhibitor (CI), and anti-miR-19b inhibitors (anti-19). Data represent mean +/- SEM. * p = 0.03. (e) DGCR8^{+/+} CD4 T cells cultured for 5 days in nonpolarizing conditions and transfected with control mimic (CM), miR-19a mimic (19a), or miR-19b mimic (19b). Data represent mean +/- SEM.



Supplementary Figure 4. Effects of miR-17~92 members on proliferation

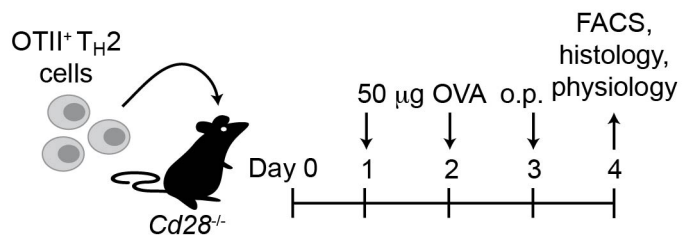
Analysis (day 5) of cell proliferation by flow cytometry of Th2-polarized cells labeled with CellTrace Violet (CTV). Grey filled histogram represents 17~92^{+/+} cells transfected with control mimic (CM), black histogram represents 17~92^{ΔΔ} cells transfected with control mimic (CM), and red histogram represents cells transfected with the corresponding miRNA mimic. Data are representative of 3 independent experiments, with 3 technical replicates in each experiment.



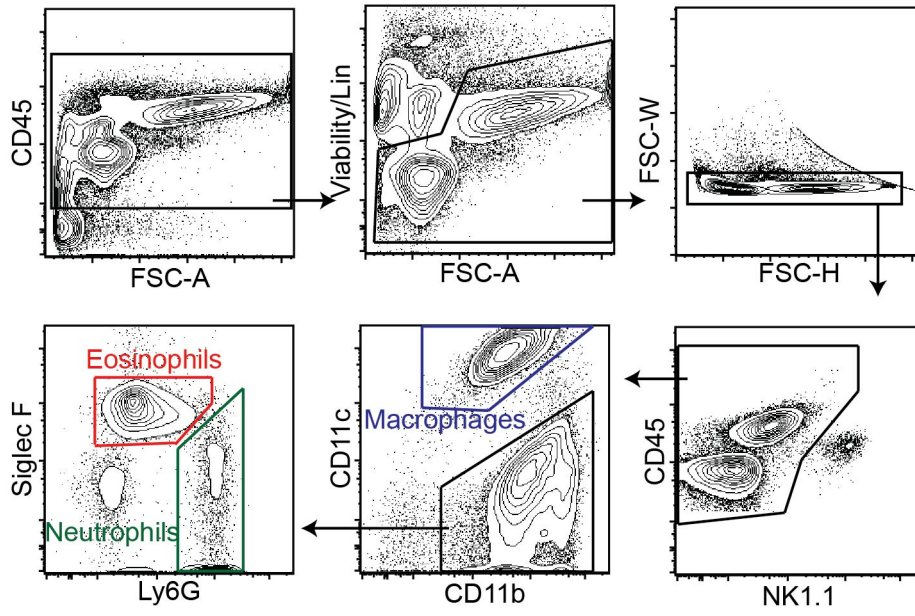
Supplementary Figure 5. Identification of myeloid cells in BAL in *in vivo* allergic airway inflammation model

(a) Method for T_H2 OT-II cell adoptive transfer model of allergic airway inflammation. See Materials and Methods for details. (b) Gating strategy used to identify eosinophils (CD45⁺ CD11b⁺ Siglec F⁺), neutrophils (CD45⁺ CD11b⁺ Ly6G⁺), and alveolar macrophages (CD45⁺ CD11c⁺ Siglec F⁺) in bronchoalveolar lavage (BAL) fluid from mice that received 17~92^{+/+} or 17~92^{ΔΔ} OT-II Th2 cells and were challenged with ovalbumin for 3 consecutive days. Cells are first gated as CD45⁺, Live (eF780 viability dye-/CD4-/CD8-/CD19-), singlet, NK1.1-, and then divided into the above mentioned cell types. Numbers of each cell type are determined by the product of the frequency of that cell type (as a percentage of live cells) and the total BAL cell count determined by Coulter Counter.

a



b



Supplementary Table 1. List of miRNAs for each multiplex miRNA Taqman qPCR

#	Plate 1	Plate 2	#	Plate 1	Plate 2
1	Let7a	Let7b	39	mir30c	mir29b
2	Let7c	Let7d	40	mir30d	mir29c
3	Let7e	Let7f	41	mir32	mir301a
4	Let7i	Let7g	42	mir328	mir30a
5	mir1	mir1	43	mir331	mir30e
6	mir101	mir100	44	mir340-5p	mir320a
7	mir103	mir103	45	mir34a	mir33a
8	mir106b	mir107	46	mir361-5p	mir330-3p
9	mir107	mir10a	47	mir365	mir335-5p
10	mir125a 3p	mir122	48	mir374b	mir339 5p
11	mir126	mir125b 5p	49	mir421	mir342-3p
12	mir128	mir130b	50	mir423-3p	mir263
13	mir132	mir142 5p	51	mir425	mir378
14	mir141	mir146a	52	mir484	mir423-5p
15	mir142 3p	mir148a	53	mir494	mir451
16	mir148b	mir150	54	mir532-5p	mir-532-3p
17	mir152	mir151 5p	55	mir590-5p	mir574-5p
18	mir15a	mir15b	56	mir652	mir590-3p
19	mir181a	mir16	57	mir744	mir1280
20	mir181b	mir17	58	mir92b	mir671-5p
21	mir185	mir181c	59	mir99b	Mir7a
22	mir18a	mir181d	60	mir1225 5p	mir874
23	mir190b	mir186	61	mir1246	mir93
24	mir191	mir191	62	mir1247	mir98
25	mir194	mir192	63	mir1248	mir99a
26	mir197	mir193a-3p	64	mir1268	mir106a
27	mir19a	mir195	65	mir1274b	mir1207 5p
28	mir200a	mir199-5p	66	mir1281	mir1228 5p
29	mir20a	mir19b	67	mir1285	mir1260
30	mir22	mir20b	68	mir1290	mir1274a
31	mir221	mir21	69	mir1292	mir1275
32	mir223	mir210	70	mir146b-5p	mir140
33	mir23a	mir222	71	mir151 3p	mir18b
34	mir25	mir23b	72	mir155	mir193b
35	mir26a	mir24	73	mir193a-5p	mir31
36	mir27a	mir26b	74	mir320b	mir320c
37	mir29a	mir27b	75	mir320d	mir324-3p
38	mir30b	mir28 5p	76	mir339 3p	mir345

#	Plate 1	Plate 2
77	mir342-5p	mir361-3p
78	mir362-5p	mir374a
79	mir454	mir 424
80	mir497	mir483-5p
81	mir768	mir486-5p
82	mir580	mir505
83	mir582	mir513a -5p
84	mir589	mir593-3p
85	mir598	mir 625
86	mir627	mir629
87	mir638	mir651
88	mir643	mir660
89	mir663	mir663b
90	mir720	mir766
91	mir765	mir92a
92	mir769-5p	mir95
93	mir1469	mir1908
94	mir1915	mir1972
95	mir1973	mir1977
96	mir1978	mir1979

Supplementary Table 2. P-values and False Discovery Rate (FDR) calculations for miRNA expression analysis.

mir	number.A	number.H	logFC	pval	FDR
mir197	13	8	1.299708392	0.000724557	0.06448555
mir361-5p	13	8	-0.955886846	0.012802531	0.35971674
mir27a	13	8	0.896706608	0.019377641	0.35971674
mir19a	13	8	2.927611875	0.019900427	0.35971674
mir1281	13	8	-0.971030553	0.025465949	0.35971674
mir532-5p	13	8	-0.59254465	0.029151878	0.35971674
mir107	13	8	-1.381753871	0.030904628	0.35971674
mir1292	13	8	-1.10656942	0.032334089	0.35971674
mir223	13	8	1.076910016	0.044269656	0.41463526
Let7e	13	8	1.107050534	0.055553443	0.41463526
mir221	13	8	-0.355880347	0.066835861	0.41463526
mir34a	13	8	-0.701560197	0.071540629	0.41463526
mir720	13	8	-1.053771947	0.071718502	0.41463526
mir425	13	8	0.431670044	0.07265129	0.41463526
mir194	13	8	-0.875290805	0.073348997	0.41463526
mir181d	10	8	-1.779317354	0.075027766	0.41463526
mir181a	13	8	-0.220820981	0.086088242	0.41463526
mir152	13	8	-1.115509599	0.087124144	0.41463526
mir1979	10	8	-0.97484687	0.090008929	0.41463526
Let7a	13	8	0.626786956	0.100162689	0.41463526
mir191	13	8	0.457546157	0.108799248	0.41463526
mir1274b	13	8	-1.180384411	0.112498991	0.41463526
mir1247	13	8	-0.757694746	0.112864207	0.41463526
mir181b	13	8	-0.259591749	0.115763927	0.41463526
mir20a	13	8	0.610545395	0.127850763	0.41463526
mir765	13	8	-1.343815014	0.130386893	0.41463526
mir200a	13	8	0.533199548	0.135359668	0.41463526
mir1915	13	8	-0.543604256	0.139015074	0.41463526
mir342-3p	10	8	0.876244796	0.139697961	0.41463526
mir16	10	8	1.246087607	0.143846876	0.41463526
mir320b	13	8	0.599978259	0.144423519	0.41463526
mir1	13	8	-0.686137737	0.164049752	0.45626337
mir30b	13	8	-0.344707963	0.183045596	0.49366843
mir21	10	8	-1.042524581	0.227666588	0.58998359
Let7c	13	8	0.937749551	0.232016019	0.58998359
mir18a	13	8	0.795945811	0.244055663	0.60335983
mir30c	13	8	0.320039106	0.263461797	0.62135423
mir652	13	8	0.383388594	0.270697965	0.62135423

mir93	10	8	0.293633071	0.276827928	0.62135423
mir494	13	8	-0.564620191	0.285000798	0.62135423
mir106a	10	8	0.436087251	0.291377879	0.62135423
mir99b	13	8	-0.317154591	0.293223345	0.62135423
mir766	10	8	-0.938252174	0.332832419	0.65119863
mir17	10	8	0.378336999	0.337545072	0.65119863
mir1228.5p	10	8	1.101835276	0.3401148	0.65119863
mir20b	10	8	0.360679188	0.341739623	0.65119863
mir29c	10	8	-0.754847539	0.350247972	0.65119863
mir1268	13	8	0.292891495	0.35120825	0.65119863
mir181c	10	8	-0.771498933	0.369498141	0.65651301
mir92b	13	8	-0.530391482	0.37553265	0.65651301
mir126	13	8	0.686413823	0.378390216	0.65651301
Let7f	10	8	0.331555741	0.383844607	0.65651301
mir1972	10	8	0.490504506	0.390957188	0.65651301
mir484	13	8	-0.125798609	0.3995046	0.65844277
mir1469	13	8	0.711272618	0.429626618	0.69521398
mir768	13	8	0.523063383	0.454734041	0.70777586
mir106b	13	8	0.380402671	0.455273868	0.70777586
mir103	13	8	0.279439065	0.461247192	0.70777586
mir423-3p	13	8	-0.140313753	0.482355731	0.72762136
mir185	13	8	-0.192688912	0.529099027	0.77471377
mir29b	10	8	0.363832095	0.530983593	0.77471377
mir345	10	8	-0.438705364	0.584076858	0.83569561
mir125a.3p	13	8	0.297247557	0.595195212	0.83569561
mir378	10	8	0.264286319	0.605821797	0.83569561
Let7b	10	8	0.239999009	0.611158227	0.83569561
mir-532-3p	10	8	0.193523783	0.619729331	0.83569561
mir27b	10	8	-0.336129367	0.633429504	0.84142128
mir99a	10	8	0.310240256	0.660935009	0.8484316
mir132	13	8	-0.13429756	0.669272763	0.8484316
mir29a	13	8	-0.184536949	0.676673175	0.8484316
mir1207.5p	10	8	0.163389492	0.685166789	0.8484316
mir574-5p	10	8	0.172937117	0.686636495	0.8484316
mir320d	13	8	0.219433152	0.695904571	0.8484316
mir263	10	8	-0.150303775	0.748890294	0.89759704
mir150	10	8	0.244716534	0.761388158	0.89759704
mir598	13	8	0.158852232	0.766487362	0.89759704
mir1977	10	8	-0.164898068	0.788942468	0.90549023
mir25	13	8	0.057780066	0.793575703	0.90549023
mir19b	10	8	-0.161841828	0.812290751	0.91511236
mir146a	10	8	-0.151828183	0.824978996	0.91778913
mir324-3p	10	8	-0.134485497	0.880188131	0.96712029

mir15b	10	8	0.082061272	0.907231512	0.97783576
mir454	13	8	-0.068747172	0.911914252	0.97783576
mir660	10	8	-0.064249668	0.934665046	0.99029987
mir22	13	8	-0.017970414	0.972566856	0.99365578
mir421	13	8	0.012717316	0.982442814	0.99365578
mir320a	10	8	0.00998913	0.983767541	0.99365578
mir342-5p	13	8	0.005124923	0.991338526	0.99365578
mir15a	13	8	-0.005142721	0.993655781	0.99365578

Supplementary Table 3. List of siRNAs used for target screening.

Gene	Specificity	Format
<i>Atxn1</i>	Mouse	siGenome SMARTpool
<i>Pten</i>	Mouse	siGenome SMARTpool
<i>Mecp2</i>	Mouse	siGenome SMARTpool
<i>Kat2b</i>	Mouse	siGenome SMARTpool
<i>Socs1</i>	Mouse	siGenome SMARTpool
<i>Prmt5</i>	Mouse	siGenome SMARTpool
<i>Bcl2l11</i>	Mouse	siGenome SMARTpool
<i>Nr4a2</i>	Mouse	siGenome SMARTpool
<i>ErbB4</i>	Mouse	siGenome SMARTpool
<i>Tgfbr2</i>	Mouse	siGenome SMARTpool
<i>Bmpr2</i>	Mouse	siGenome SMARTpool
<i>Arih2</i>	Mouse	siGenome SMARTpool
<i>Smad4</i>	Mouse	siGenome SMARTpool
<i>Kit</i>	Mouse	siGenome SMARTpool
<i>Cul5</i>	Mouse	siGenome SMARTpool
<i>Bace1</i>	Mouse	siGenome SMARTpool
<i>Hipk3</i>	Mouse	siGenome SMARTpool
<i>Arid4b</i>	Mouse	siGenome SMARTpool
<i>MyliP</i>	Mouse	siGenome SMARTpool
<i>Rora</i>	Mouse	siGenome SMARTpool
<i>Prkaal</i>	Mouse	siGenome SMARTpool
<i>Dock5</i>	Mouse	siGenome SMARTpool
<i>Ppp2r5e</i>	Mouse	siGenome SMARTpool
<i>Hif1a</i>	Mouse	siGenome SMARTpool
<i>Rc3h1</i>	Mouse	siGenome SMARTpool
<i>Runx1</i>	Mouse	siGenome SMARTpool
<i>Btla</i>	Mouse	siGenome SMARTpool
<i>Il2ra</i>	Mouse	siGenome SMARTpool
<i>CD274 (PDL1)</i>	Mouse	siGenome SMARTpool
<i>PDCD1LG2 (PDL2)</i>	Mouse	siGenome SMARTpool
<i>Tnfaip3 (A20)</i>	Mouse	siGenome SMARTpool
<i>Rnf11</i>	Mouse	siGenome SMARTpool
<i>Fbxl11/Kdm2a</i>	Mouse	siGenome SMARTpool
<i>Zbtb16</i>	Mouse	siGenome SMARTpool
<i>Itch</i>	Mouse	siGenome SMARTpool
<i>Tnip1/Abin1</i>	Mouse	siGenome SMARTpool
<i>Cyld</i>	Mouse	siGenome SMARTpool
<i>Otud7b/cezanne</i>	Mouse	siGenome SMARTpool
<i>non-targeting neg ctrl</i>	Mouse	siGenome SMARTpool

Chapter 3

Characterization of immune cell infiltration in asthma

Introduction

Current treatments for asthma focus on treating the symptoms and the severity of the disease rather than focusing on the type of disease pathogenesis experienced by the patient. In many people with asthma, but not all, type 2 inflammation plays a critical role in promoting and perpetuating airway inflammation. In other people, airway inflammation is not dependent on type 2 cytokines or Th2 cells. The distinction between asthma driven by Th2 inflammation, or “Th2-high” asthma, and asthma driven by other types of inflammation, or “Th2-low” asthma, is an important factor for developing treatment strategies that will work for individuals with asthma with a focus on precision medicine^{6,104,128}. It is also important to distinguish these two clinical subtypes of asthma for purposes of understanding disease pathogenesis. The work presented in chapter 2 grouped all asthma subjects together, regardless of the “Th2-ness” of disease. Through this work we hoped to gain an understanding of the post-transcriptional regulation of Th2 cells in asthma. This has led to further investigation into the types of inflammation we observe in human asthmatic airways. In these studies, we sought to characterize and enumerate the types of immune cells present in the airways of asthmatic subjects by flow cytometric analysis of induced sputum and bronchoalveolar lavage fluid.

In our work, we have focused on miRNA regulation of Th2 cells to understand the pathways involved in Th2-driven inflammation in asthma. However, my analysis of miRNA expression in sorted CD4 T cells from human bronchoalveolar lavage did not take into account the potential changes in frequency of each T-helper subset: Th1, Th2, and Th17. While miR-19a was upregulated in the CD4 T cells from all asthmatic subjects, other miRNAs may be differentially regulated in one or two of the subsets, and would not therefore show differential expression when we look at bulk CD4 T cell miRNA expression. Chemokine receptor expression

on CD4 t cells can be used to enrich for each of the subsets¹³⁸. The role of Th1 and Th17 cells in inflammation in asthma is less understood than that of Th2 cells¹³⁹. IL-17A increases airway hyperresponsiveness and airway smooth muscle contraction¹⁴⁰. Using chemokine receptor expression to separate Th1, Th2, and Th17 cells, we are now in the midst of a clinical study to determine frequencies of each of these cell types, as well as miRNA expression in each of these subsets in the BAL and peripheral blood of asthmatic and healthy individuals.

Type 2 innate lymphoid cells (ILC2s) were first described in 2010¹⁴¹⁻¹⁴³, which drove a lot of research into the role of these cells in allergic and metabolic diseases^{144,145}. ILC2s reside in the lungs, gut, and visceral adipose tissue, and are activated by the cytokines IL-25, IL-33, and TSLP to produce type 2 cytokines such as IL-5, IL-13, and IL-9. Some studies suggest that ILC2s are essential to the initiation of adaptive Th2 immunity¹⁴⁶, due to their production of Th2 cytokines that could polarize CD4 T cells towards a Th2 phenotype. However, their presence in tissues rather than lymph nodes suggests they have roles outside of T cell differentiation. In mouse models, ILC2s clearly promote allergic airway inflammation, but whether they are involved in initiation or perpetuation of the immune response remains unclear. In humans, a gene signature of *RORA*, *IL1R1* (*ST2*), and *IL13* that promotes asthma susceptibility implicates the involvement of ILC2s in asthma pathogenesis¹⁴⁷. With these early exciting findings, we began researching the frequency and potential activation of ILC2s in human asthma through collaboration with John Fahy at UCSF.

While recent research has focused on understanding the role of ILC2s in allergic diseases, questions remain regarding the role of other innate immune cells in asthma, such as basophils. Basophils are a key source of IL-4 and IL-13 when stimulated through the high affinity IgE receptor, FcεRI¹⁴⁸. Basophils can also make Th2 cytokines independent of FcεRI cross-linking in

response to IL-1 family members, such as IL-18 and IL-33^{148,149}. Interestingly, IL-33 increases basophil survival as a result of increased AKT activity, which together with increased Th2 cytokine production could contribute to the allergic phenotype seen in asthma¹⁴⁸. There seems to be significant overlap in function of basophils and ILC2s, and focusing future research towards understanding their individual roles will help to define therapeutic strategies towards either or both cell types in asthma.

In this chapter, I will discuss our involvement in two clinical studies at UCSF. Through collaboration with Prescott Woodruff, we are involved in the RITA (The Role of miRNAs in T cell-driven Asthma) study to quantify T-helper subsets in BAL from asthmatic and healthy subjects, as well as to determine miRNA expression in each of these subsets. Through collaboration with John Fahy, we are involved in the CASA (Characterization of Adult Subjects for Asthmatic Research Studies) study to determine the frequency and potential role of ST2-expressing cells in asthma, primarily focusing on basophils and ILC2s. My involvement in these studies was in the development of flow cytometry panels for characterization and sorting of various cell types from human biospecimens such as BAL and induced sputum. In the RITA study, I designed the flow panel and performed the sorts for the first 6 months of the study, and have continued to be involved in our interim analysis to determine the feasibility of miRNA expression analysis in such small cell numbers as those sorted from BAL. In the CASA study, I have helped design and carry out experiments to determine the function of ILC2s and basophils in asthma, have analyzed our flow cytometry data, and have generated figures for future publication.

Results

T-helper cell subsets in asthma - RITA Study

miRNA expression profiling in T-helper subsets will help to understand the pathways that are involved in differentiation of that cell type. While some elegant work has been done to analyze miRNA expression in T-helper subsets in peripheral blood of humans¹⁵⁰, we wanted to expand on this knowledge to look at miRNA expression in T-helper subsets at the site of inflammation. In the RITA study, we are sorting Th1, Th2, and Th17 enriched subsets by flow cytometry from BAL specimens from asthmatic subjects pre- and post- inhaled corticosteroid use, as well as from healthy subjects. In parallel, we are sorting the same subsets from peripheral blood to compare miRNA expression changes from circulating and tissue-resident T-helper cells.

We designed a flow panel to accurately sort Th1-, Th2-, and Th17-enriched memory populations from peripheral blood mononuclear cells (PBMCs) and BAL, while removing Tregs and NKT cells (**Table 1; Figure 1a,b**). We used literature to guide our panel development^{151,152}. To ensure we were sorting the appropriate cell types, we sorted the 8 populations created by expression of three chemokine receptors: CCR4, CCR6, and CXCR3 (**Figure 2**). We restimulated the cells with PMA and ionomycin, and performed intracellular stains for the cytokines IL-17A, IL-4, IL-13, and IFN- γ . This analysis confirmed that the IL-17A-producing T cells were in the CCR6+ gate, with an even greater enrichment in the CCR6+CXCR3- gates. The IL-4-producing T cells fell entirely within the CCR6-CCR4+ gates, with the highest enrichment in the CCR6-CCR4+CXCR3- gate. The IFN- γ -producing T cells were enriched in the CCR6-CCR4-CXCR3+ gate, with smaller numbers of IFN- γ -producers falling in the other gates. Using this analysis, we decided to sort CD3+CD4+CD45RO+CCR6+ cells as the “CCR6+” subset (Th17-enriched), CD3+CD4+CD45RO+CCR6-CCR4+ cells as the “CCR4+” subset (Th2-

enriched), and CD3+CD4+CD45RO+CCR6-CCR4- cells as the “CCR6-CCR4-“ subset (Th1-enriched). This sorting strategy optimized the number of cells we could sort while enriching for the subsets we wanted, but it does not result in a pure population of Th1, Th2, or Th17 cells. In further analysis of these samples, we are using more stringent gates:

CD3+CD4+CD45RO+CCR6+CXCR3- for Th17 cells, CD3+CD4+CD45RO+CCR6-CCR4+CXCR3- for Th2 cells, and CD3+CD4+CD45RO+CCR6-CCR4-CXCR3+ for Th1 cells.

We have observed that CXCR3 expression is very high in all subsets in BAL, suggesting the need for CXCR3 expression for T cells to migrate into the lung tissue or into the airway lumen (**Figure 1c**).

After the first 2 years of the study, we performed an interim analysis to confirm that our sorting strategy would yield enough RNA to analyze miRNA expression using the Fluidigm Biomark. In this analysis, we extracted RNA from four healthy subjects, four asthmatic subjects pre-ICS, and four sarcoidosis subjects from Laura Koth’s study. For each subject we had 4 samples from peripheral blood (Naïve, CCR6+, CCR4+, and CCR6-CCR4- subsets) and 3 samples from BAL (CCR6+, CCR4+, and CCR6-CCR4- subsets). We used a fractionation protocol to separate the large (>200 nucleotides) RNA fraction from the small (<200 nucleotides) RNA fraction containing miRNAs. In the large fraction, we used RT-qPCR to quantify the amount of RNA we obtained from the samples by qPCR for the control gene Beta-2-microglobulin (B2M) (**Figure 3**). The amount of RNA correlated well with the sorted cell numbers (**Figure 3b**). We also measured expression of the canonical transcription factors for each T-helper subset: *Rorc*, *Gata3*, and *Tbx21* (TBET) (**Figure 4**). Transcription factor expression confirmed our sorting strategy enriched for the appropriate T-helper cell types in the blood, but was more variable in the BAL probably due to lower cell numbers. Surprisingly, in

the subjects with sarcoidosis, there was a distinct signature of Th1* cells in the BAL expressing both *Tbx21* and *Rorc* (**Figure 4b**). We also measured cytokine mRNA expression in these samples, with limited success, probably due to low cell numbers and lack of restimulation.

Using the small fraction of RNA, we performed multiplex RT and preamplification to measure miRNA expression in each sample using the Fluidigm Biomark according to our previous studies^{41,92}. We altered the number of preamplification cycles for our samples by splitting them into 3 groups: Group 1 samples had at least 1ng RNA (as calculated from B2M qPCR in the large fraction for each sample) in 4ul of sample, and underwent 18 cycles of preamplification. Group 2 samples had less than 100pg RNA in 4ul of sample, and underwent 22 cycles of preamplification. Group 3 samples had at least 100pg RNA in 4ul of sample, and also underwent 22 cycles of preamplification. After RT, preamplification, and clean-up of the samples, we checked that the samples had detectable material by qPCR (**Figure 5a,b**), and then performed miRNA qPCR on the Biomark (**Figure 5c**). This analysis revealed that our Group 2 and 3 samples, which had the lower amounts of RNA, passed more of our quality control checks, and we were able to detect 21 miRNAs in at least 50% of the samples. However, many of our Group 1 samples failed quality control, and we were only able to detect 13 miRNAs in at least 50% of the samples. This suggests that something went wrong in our two different courses of RT and preamplification, or that there is a difference in efficiency of one of these steps for the samples that had higher amounts of RNA. We are continuing to test the methods of RNA extraction as well as optimizing the number of preamplification cycles to confirm whether we can use such small cell numbers for our miRNA expression analyses.

We hypothesized that ILC2s would be more prevalent in the airways or blood of people with asthma compared to healthy individuals, and that their ILC2s would be more easily activated by IL-25, IL-33, and/or TSLP. This led us to design a flow cytometry panel for characterization of induced sputum specimens from asthmatic and healthy individuals to quantify and sort ILC2s (**Table 2**). Although the panel was designed to identify and enumerate ILC2s, we were able to identify and enumerate other cell types such as CD4⁺ T cells, non-CD4 T cells, and basophils (**Figure 6**). Through this analysis, we found that there was no difference in the frequency of any of these cell types in blood between asthmatic and healthy subjects (**Figure 7a**). However, in the sputum, asthmatic subjects had increased numbers of basophils compared to healthy subjects (**Figure 7b**). ILC2s were rarely detected in the sputum, and showed no difference in prevalence between asthmatic and healthy subjects.

Expression of the type 2 cytokines IL-4, IL-5, and IL-13 in sputum cell pellets is a good marker for “Th2-ness” in subjects with asthma. The mRNA expression of these three cytokines is referred to as the “Th2 Three Gene Mean.” In our collaboration with the Fahy lab, we found that expression of ST2 in the sputum cell pellet tightly correlated with the Th2 Three Gene Mean (data not shown). This suggests that ST2-expressing cells could be responsible for the levels of Th2 cytokines present in asthmatic airways. We further interrogated our FACS data to determine the numbers of ST2-expressing cells in the blood and sputum of asthmatic subjects compared to healthy, and to characterize the types of immune cells that express ST2. We first confirmed the ST2 antibody binding to cells in blood by fluorescence minus-one stains (**Figure 8**). We found that T cells, basophils, and ILC2s all bear high expression of ST2 in the blood. Using the same gating strategy in sputum, we found that ST2 expression in the sputum is highly variable in both healthy and asthmatic subjects (**Figure 7d,e**). However, ST2⁺ basophils were significantly

enriched in sputum from asthmatic subjects compared to healthy, although there was no difference in ST2⁺ basophils in the blood (**Figure 9**). We observed no difference in ST2⁺ ILC2s in sputum.

The number of basophils in the sputum, and not the number of ILC2s, correlated with asthma severity as determined by PC20 (**Figure 10a**), suggesting a physiological role for basophils in altering airway hypersensitivity in asthma. Gene expression profiling of sputum cell pellets showed clear enrichment of Th2 cytokines in the sputum of asthmatic subjects (**Figure 10b**), which positively correlated with the number of basophils in the sputum. Basophils are capable of secreting Th2 cytokines, so we hypothesize that basophils, rather than ILC2s or CD4 T cells, could be responsible for a large fraction of the Th2 cytokine mRNA present in the cells in the sputum of asthmatic subjects. To test this hypothesis, we will use bead depletion of CD4 T cells from sputum cell pellets and compare Th2 cytokine expression in sputum cells depleted of CD4 T cells and purified CD4 T cells. We will also use bead depletion and purification of basophils from sputum cell pellets using their expression of CD123 and FcERI to determine whether basophils are responsible for the secretion of Th2 cytokines.

Discussion

With access to a specialized airway clinical research center at UCSF, it is possible to collect data from large cohorts of asthmatic and healthy subjects to gather broad data on the types of immune cells present in human airways. Because our lab focuses on the role miRNA regulation of T cells in promoting allergic asthma, we have been carefully sorting and collecting blood and BAL CD4 T cell samples for 3 years to perform miRNA expression analysis in bulk once we have all of the patients. My involvement in this project was the development of our FACS analysis panel and gating strategy, and the sorting of patient samples for the first six months of the RITA study. We hope that this study will provide us with detailed information on miRNA expression in different T-helper subsets at the site of inflammation and in circulation, as well as provide us with immunophenotyping data for individual people to help us understand the variability in T-helper subset frequencies between people.

Our interim analysis for the RITA study suggests that we can obtain enough RNA from very small sorted cell numbers in order to analyze mRNA and miRNA expression by qPCR. However, our optimization for the multiplex miRNA taqman qPCR platform (Fluidigm Biomark) has run into some problems that will need to be overcome in order to move forward with all of the clinical samples once the study is concluded. First, we will need to determine why only ~30% of our miRNA taqman assays provided data in the Biomark platform. One way to overcome this would be to further filter our two 96-miRNA panels into one panel that contains only miRNAs that have worked at least once in the Biomark platform in the past. This will also cut down on the number of Biomark chips we will have to use, and therefore will reduce the amount of material we will use up in the process. We will also need to optimize the number of preamplification cycles necessary to maintain the quality of our data such that we do not

‘jackpot’ the miRNAs that are present in the samples, and so that we do not miss miRNAs that are present at very small amounts.

Interesting data did emerge from the mRNA expression analysis in our RITA interim analysis. In subjects with sarcoidosis, sorted CCR6+ T cells, which are enriched for Th17 cells, expressed both *Rorc* and *Tbx21*, the transcription factors for Th17 and Th1 cells, respectively. This suggests that the “Th1*” or “Th1/17” subsets may be involved in the pathogenesis of sarcoidosis, and also that these cells are not involved in the pathogenesis of asthma, as the *Rorc/Tbx21* expression pattern was not observed in our four asthmatic subjects.

A broader understanding of the types of immune cells present in the airways of people with asthma will lead to better therapeutic interventions aimed at single or multiple cell types in the airways. Our work in the CASA study has been focused on quantifying ST2-expressing cells in the airways that are capable of producing Th2 cytokines. This analysis led to a surprising finding: ILC2s do not appear to be increased in frequency in asthmatic subjects compared to healthy subjects, whether we look in the peripheral blood or in induced sputum. Because genetic and functional evidence strongly suggest ILC2 involvement in asthma, our data could reflect the inability of our methods to identify differences in ILC2 frequencies due to their rare nature. It may be necessary to look for the presence of ILC2s in the lung parenchyma rather than in airway fluids.

This analysis led to another surprising finding: basophils, rather than ILC2s, were more abundant in the airways of asthmatic subjects compared to healthy subjects. Basophils also express ST2 at high levels, and are capable of producing Th2 cytokines, especially IL-4 and IL13. Our gene expression profiling in sputum cell pellets indicate a distinct Th2 cytokine signature that positively correlates with the frequency of basophils in the sputum. Our future

(and current) directions for this project are focused on tracing the Th2 cytokine signature to the CD4+ cells in the sputum cell pellet or to the FcERI-expressing cells in the sputum cell pellet. We hypothesize that the increased Th2 cytokine expression in some asthmatic subjects is due to an increase in Th2 cytokine secretion from basophils rather than ILC2s or T cells.

Materials and methods

Human subjects

RITA study: Bronchoalveolar lavage (BAL) fluid and peripheral blood were obtained from two groups of subjects: asthmatic subjects that had not been treated with inhaled corticosteroids (ICS) for 6 weeks prior to the study start date, and healthy control subjects. Asthmatic subjects were randomized to either receive ICS (budesonide) or not. BAL was obtained from steroid-naïve subjects at baseline and again after 8 weeks of ICS treatment, 200µg budesonide twice a day. This study, called the Role of microRNAs in T Cell-Driven Inflammation in Asthma (RITA), is registered on [clinicaltrials.gov](https://clinicaltrials.gov/ct2/show/study/NCT01484691): NCT01484691. Inclusion and exclusion criteria for human subjects are provided on [clinicaltrials.gov](https://clinicaltrials.gov/ct2/show/study/NCT01484691). Written informed consent was obtained from all subjects, and all studies were performed with approval from the UCSF Committee on Human Research.

CASA study: Induced sputum and peripheral blood was obtained from two groups of subjects: asthmatic subjects and healthy controls. This study, called the Characterization of Adult Subjects for Asthmatic Research Studies (CASA) is registered on [clinicaltrials.gov](https://clinicaltrials.gov/ct2/show/study/NCT01508078): NCT01508078. Inclusion and exclusion criteria for human subjects are provided on [clinicaltrials.gov](https://clinicaltrials.gov/ct2/show/study/NCT01508078). Written informed consent was obtained from all subjects, and all studies were performed with approval from the UCSF Committee on Human Research.

Flow cytometry and sorting of clinical samples

RITA study: Peripheral blood mononuclear cells (PBMCs) were isolated by Lymphoprep gradient (Accurate Chemical & Scientific Corp; cat # 1114545). BAL was collected and washed twice with PBS prior to staining with the antibody panel listed in **Table 1**. Sorting was

performed within four hours of BAL and peripheral blood collection. 250,000 cells were collected for each T-helper subset (naïve, CCR6+, CCR6-CCR4+, and CCR6-CCR4-) from PBMCs. The entire BAL was sorted and all cells were collected for each T-helper subset (CCR6+, CCR6-CCR4+, and CCR6-CCR4-). Cells were sorted into 300ul RPMI with 50% FCS at 4°C. Cells were pelleted and lysed in RLT + 1% BME, and stored at -80°C.

CASA study: Sputum biospecimens were processed by members of the Fahy lab using DTT to disrupt mucins. PBMCs were collected as described above. Cells were stained using antibodies in **Table 2** and analyzed using a FACS Aria or LSRII.

High-throughput multiplex qPCR

High-throughput multiplex qPCR was performed according to a previously described protocol²⁶. Briefly, CD4 T cells sorted by flow cytometry from clinical samples were lysed and stored in RLT buffer (Qiagen) at -80°C until all samples were collected. Frozen lysates were thawed and loaded onto QIAshredder homogenizer columns (Qiagen). Using a low concentration of ethanol (35% v/v), the large fraction of RNA (>150nt) was precipitated and captured on collection columns (RNeasy, Qiagen). The small fraction of RNA (<150nt) does not bind with low concentration of RNA, and so the flow-through from the first column was brought up to a concentration of 75% v/v ethanol and RNA was precipitated and collected on a fresh column (MinElute, Qiagen). Both RNA fractions were treated with DNase per manufacturer's recommendations (Qiagen). 2µl of RNA from each large fraction, as well as a standard curve of RNA from *in vitro*-derived T_H2 cells, were reverse transcribed using the SuperScript III kit (Invitrogen). RNA was quantified by qPCR using primers for *β2m* and comparing to the standard curve of RNA from PBMCs. qPCR was used to determine expression of transcription factors

(*Rorc*, *Tbx21*, *Gata3*). We calculated 100-1000pg RNA from the small fraction for each sample for multiplex reverse transcription using 1 mix of 96 miRNA stem loop reverse primers at a final concentration of 1nM (**Chapter 2: Supplemental table 1**). Reverse transcription and 18 or 22 cycles of preamplification were performed according to previous protocols^{41,92}. Excess primers were removed from samples using 9µl ExoSAP-IT (USB) per sample, and then 15µl of each sample was purified on Illustra AutoScreen-96 Well Plates (GE Healthcare). MiRNA qPCR data was collected on the BioMark system (Fluidigm) using a 96.96 Dynamic Array Integrated Fluidic Circuit (IFC).

Fluidigm Biomark qPCR data analysis

Data was first analyzed on Real Time PCR Analysis software (Fluidigm) with the quality threshold set at 0.5, baseline correction set to linear (derivative), and Ct threshold method set to auto (detectors). The data was further analyzed in R (version 2.14.1) through the following pipeline: Ct values < 5 or >28 were removed per Fluidigm recommendations; miRNAs that were detected in less than 60% of patient samples were removed from analysis; missing Ct values were replaced with the limit of detection (highest Ct value within the standard curve) + 0.1, and 4) the data were global mean-normalized per plate to account for inter-plate differences.

Table 1. Flow cytometry panel for sorting T-helper subsets – RITA

Antibody	Fluorophore	Clone	Company
CD3	V500	UCHT1	BD Biosciences
CD1d tetramer	AlexaFluor680	23887 (PBS-57)	NIH Tetramer core
CD127	FITC	eBioRD5	eBioscience
CD4	eFluor605NC/V605	OKT4/SK3	eBioscience
CD25	PE	BC96	eBioscience
CD45RO	PacBlue	UCHL1	eBioscience
CD45RA	APC-Cy7	HI100	Biolegend
CCR6	APC	R6H1	eBioscience
CCR4	PE-Cy7	1G1	BD Biosciences
CXCR3	PerCP-Cy5.5	G025H7	Biolegend

Table 2. Flow cytometry panel for analysis of sputum and PBMCs – CASA

Antibody	Fluorophore	Clone	Company
Anti-CD45	eFluor450	2D1	eBioscience
Lin1 mix (Anti-CD3, CD14, CD16, CD19, CD20)	FITC		BD Biosciences
Anti-CD3	V500	UCHT1	Biolegend
Anti-CD4	AlexaFluor700	OKT4	Biolegend
Anti-ST2	Biotin	B4E6	MD Bioproducts
Anti-CD25	PE	BC96	eBioscience
FcERI	PE-Cy7	AER-37 (CRA1)	Biolegend
ICOS	PerCP-Cy5.5	C398.4A	Biolegend
CCR4	A647	TG2/CCR4	Biolegend
Streptavidin	QDot605		Life Technologies

Figure 1. Gating strategy for sorting T-helper subsets from PBMCs and BAL

(a) Gating strategy for isolating Naïve CD4 T cells, CCR6+ memory CD4 T cells, CCR6-CCR4+ memory CD4 T cells, and CCR6-CCR4- memory CD4 T cells in PBMCs. Text in red indicates populations that are sorted. (b) Gating strategy for isolating CCR6+ memory CD4 T cells, CCR6-CCR4+ memory CD4 T cells, and CCR6-CCR4- memory CD4 T cells in BAL. Text in red indicates populations that are sorted. (c) CXCR3 expression in CCR6-CCR4-, CCR6-CCR4+, and CCR6+ subsets from PBMCs and BAL.

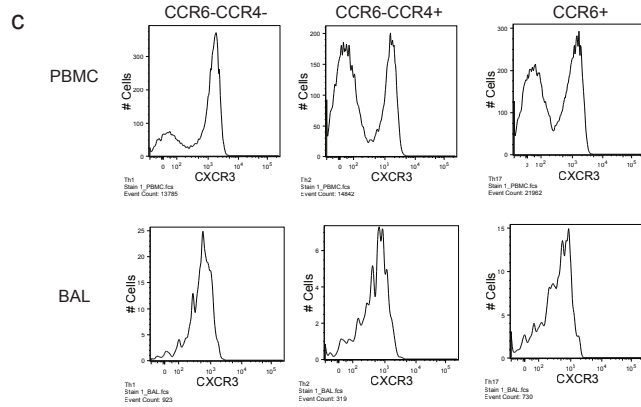
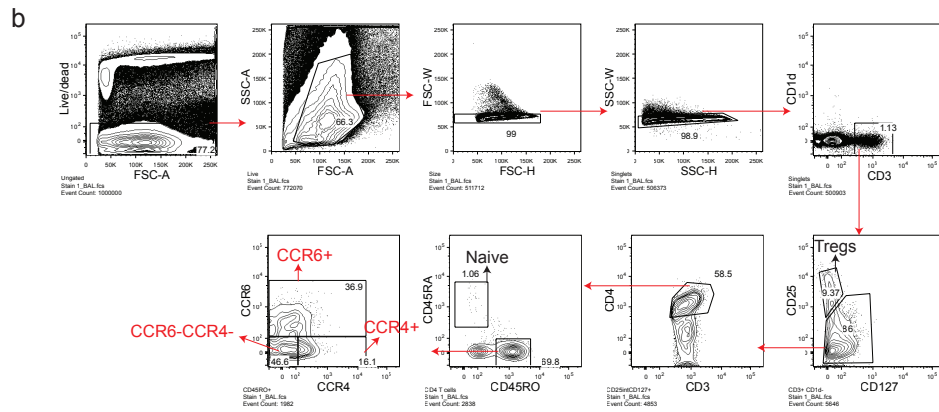
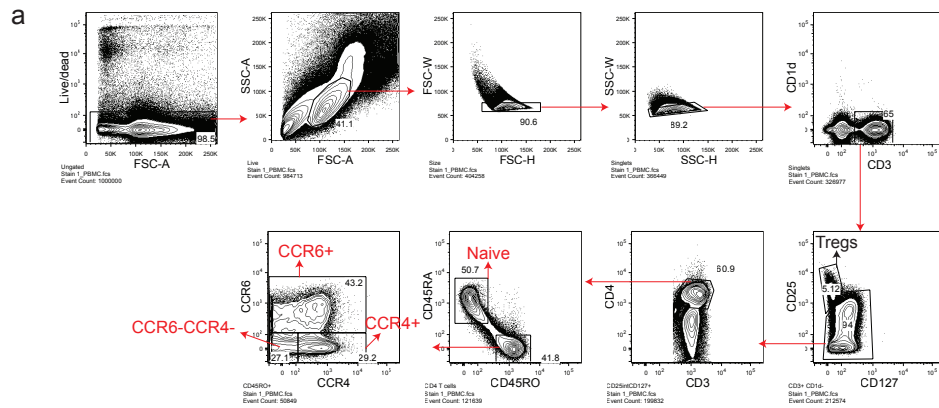


Figure 2. Cytokine production by T-helper subsets in PBMCs.

(a) Sorting strategy to obtain 8 distinct populations: 1) CCR6+CCR4-CXCR3+, 2) CCR6+CCR4+CXCR3+, 3) CCR6+CCR4+CXCR3-, 4) CCR6+CCR4-CXCR3-, 5) CCR6-CCR4-CXCR3+, 6) CCR6-CCR4+CXCR3+, 7) CCR6-CCR4+CXCR3-, 8) CCR6-CCR4-CXCR3-. Cells were stained, sorted, and restimulated with PMA and ionomycin before fixation and intracellular cytokine staining. (b) IL-17A and IFN- γ production from CCR6+ populations 1-4. (c) IL-4 and IFN- γ production from CCR6- populations 5-8.

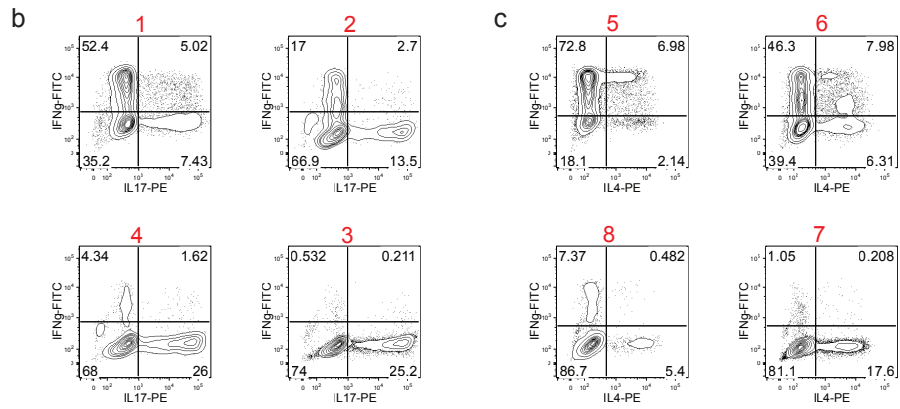
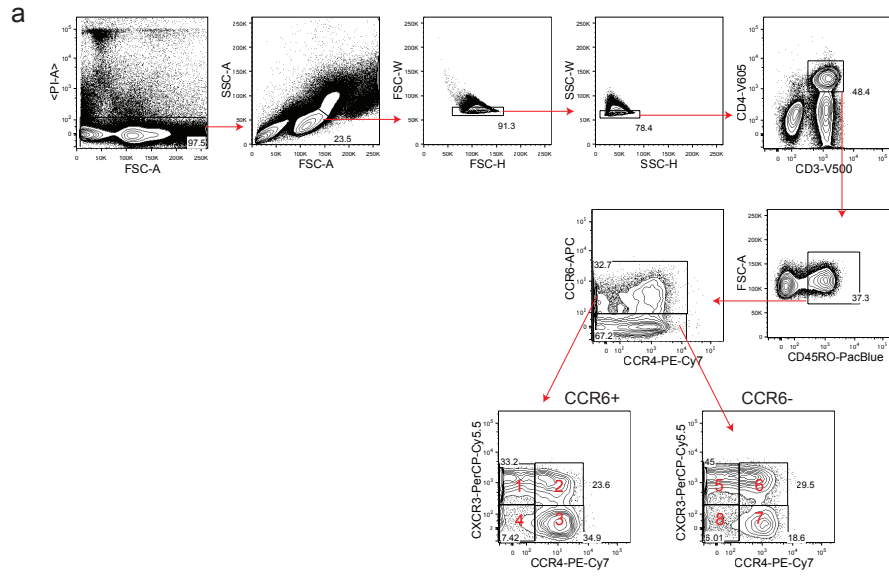


Figure 3. B2M expression analysis in RNA large fraction from RITA interim analysis

(a) Beta-2-microglobulin (B2M) expression in standard curve samples (diluted RNA extracted from human PBMCs). Equation used to quantify RNA in clinical samples: $y = 1000000e^{-0.593x}$ (b) Sorted cell count vs. calculated RNA quantity in clinical samples. (c) B2M CT for each sorted PBMC T-helper subset used to normalize all mRNA expression analyses. (d) B2M CT for each sorted BAL T-helper subset used to normalize all mRNA expression analyses.

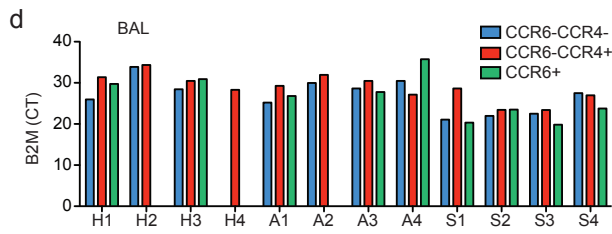
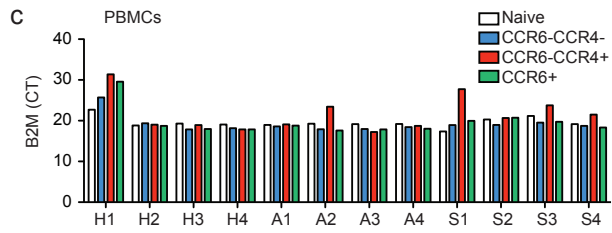
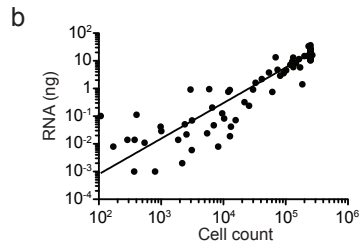
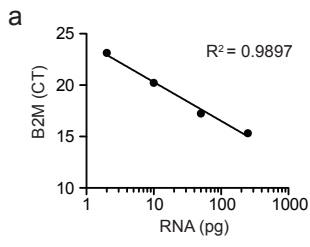


Figure 4. Transcription factor mRNA expression analysis in sorted clinical samples

(a) *Gata3*, *Rorc*, and *Tbx21* expression in sorted samples from PBMCs. Data are normalized to *B2m* expression for each sample. (b) *Gata3*, *Rorc*, and *Tbx21* expression in sorted samples from BAL. Data are normalized to *B2m* expression for each sample.

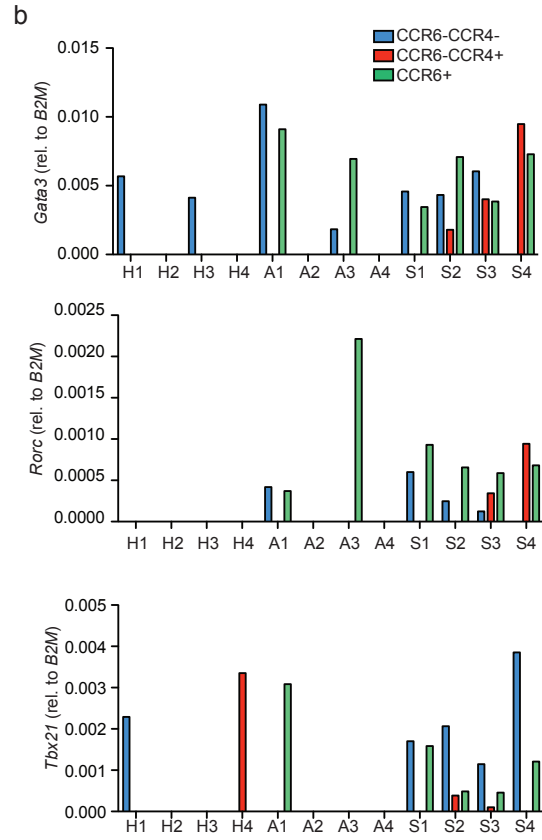
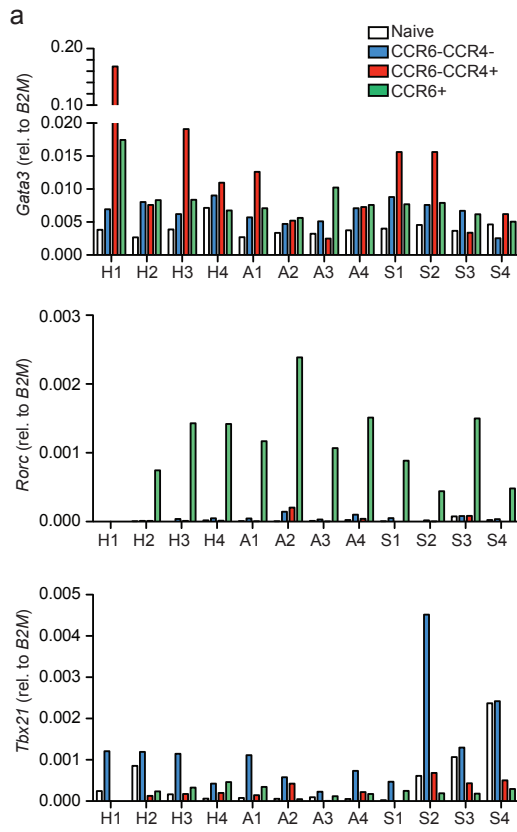


Figure 5. miRNA expression in sorted clinical samples

(a) Taqman qPCR of miR-103 and miR-191 in standard curve samples from “Group 1”. Solid line shows CT values for each input RNA amount. Dotted line shows best fit for the standard curve. (b) Taqman qPCR of miR-103 and miR-191 in standard curve samples from “Group 2 and 3”. Solid line shows CT values for each input RNA amount. Dotted line shows best fit for the standard curve. (c) Fluidigm Biomark qPCR results showing the number of miRNAs detected in 40%, 50%, or 60% of clinical samples from “Group 1” or “Group 2 and 3”.

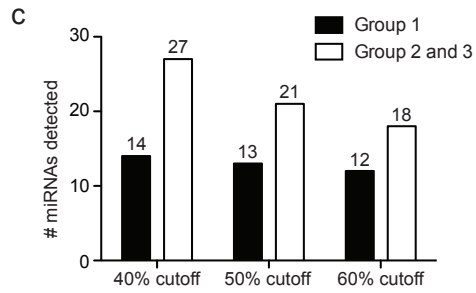
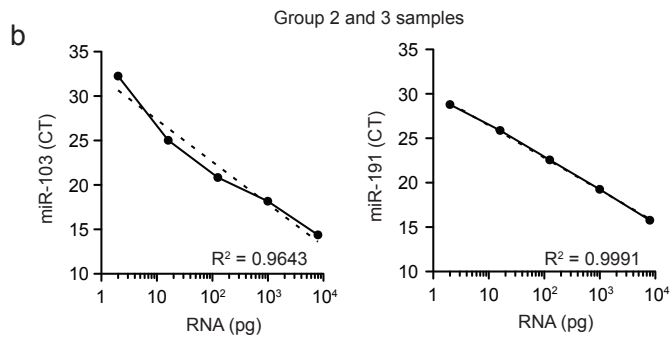
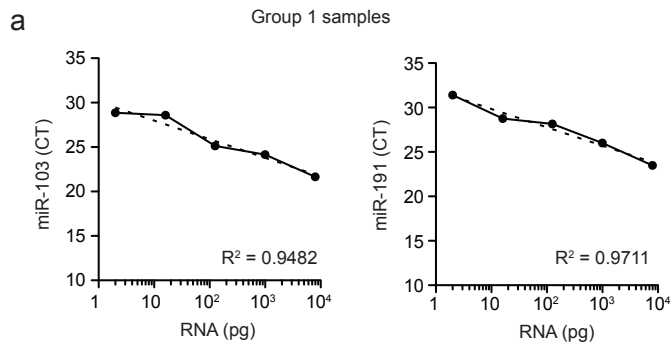


Figure 6. FACS analysis of PBMCs and sputum cells from humans with asthma (CASA study).

(a) Gating strategy used to identify basophils, CD4 T cells, non-CD4 T cells, and ILC2s in PBMCs. Data are representative of N = 33 Asthmatic and 16 Healthy individuals. (b) Gating strategy used to identify basophils, CD4 T cells, non-CD4 T cells, and ILC2s in sputum biospecimens. Data are representative of N = 33 Asthmatic and 16 Healthy individuals.

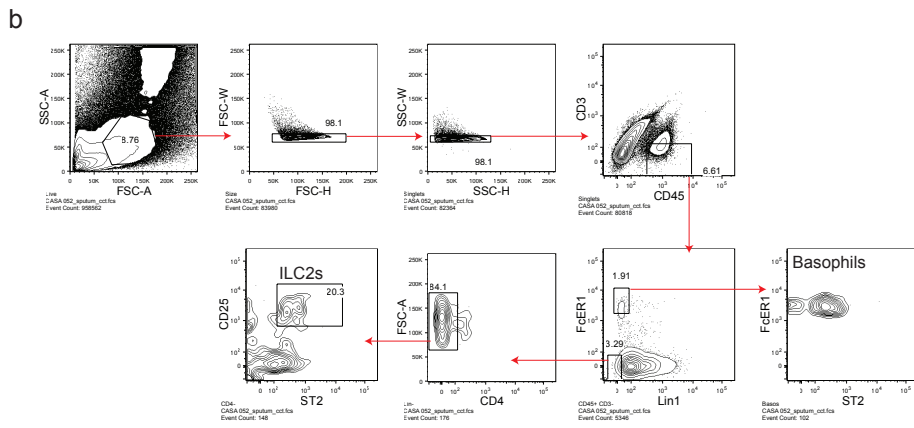
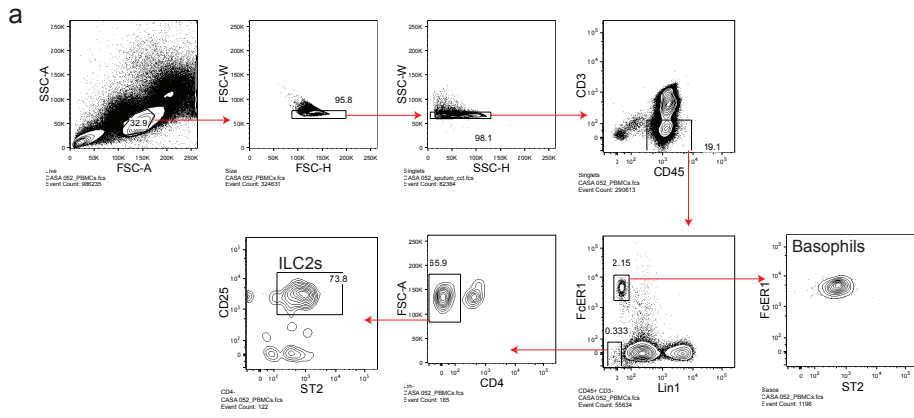


Figure 7. Distribution of cell types and total ST2 expression in PBMC and induced sputum

(a) Distribution of Lin-FcERI+ basophils, Lin-ST2+CD25+ ILC2s, CD3+CD4+ T cells, and CD3+CD4- T cells as a percentage of total CD45+ cells in PBMCs collected from healthy and asthmatic subjects. Each point represents an individual subject. Median +/- interquartile range.

(b) Distribution of Lin-FcERI+ basophils, Lin-ST2+CD25+ ILC2s, CD3+CD4+ T cells, and CD3+CD4- T cells as a percentage of total CD45+ cells in induced sputum collected from healthy and asthmatic subjects. (c) Representation of the gating of ST2+ cells from total CD45+ cells from PBMCs. (d) Percentage of all cells in PBMCs that are ST2+, using the gate in (c). (e) Percentage of all cells in induced sputum that are ST2+, using the gate in (c).

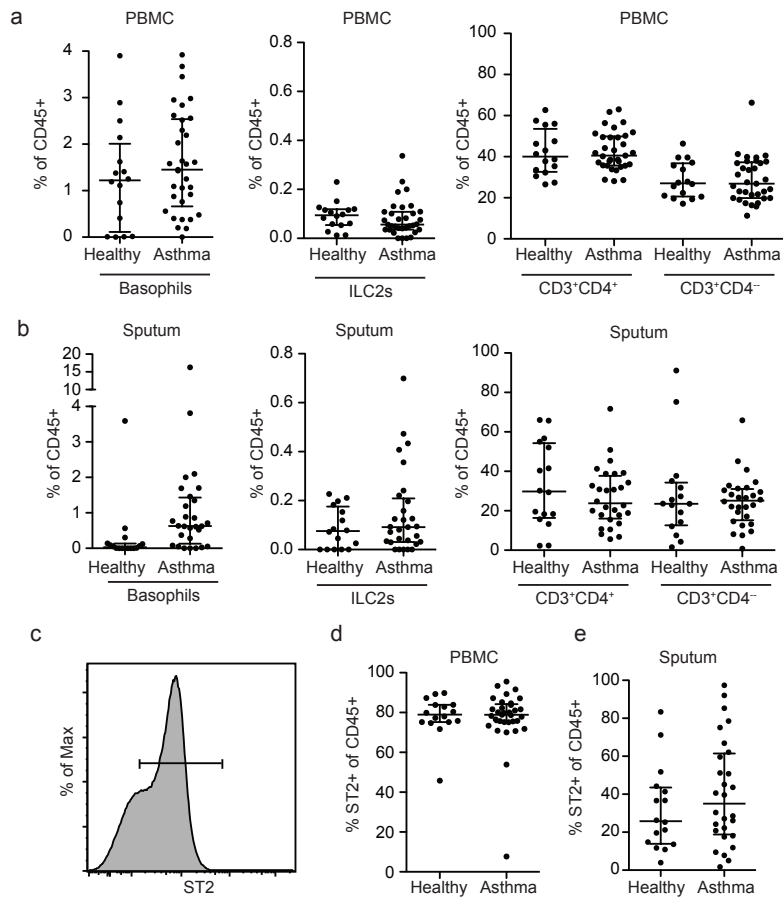


Figure 8. Fluorescence Minus-One stains for ST2 antibody specificity

(a) Representative plots showing the gating of and ST2 expression on CD3+CD4- T cells and CD3+CD4+ T cells from total Lineage+ (Lineage mix contains CD3, CD14, CD16, CD19, CD20, and CD56) CD45+ cells. Grey filled histograms represent “fluorescence minus one” controls in which the ST2 antibody was eliminated from the full antibody cocktail. Black histograms represent the full antibody cocktail including the ST2 antibody. (b) Representative plots showing the gating of and ST2 expression on FcERI+Lineage- basophils from total CD45+ cells. (c) Representative plots showing the gating of and ST2 expression on FcERI-Lineage- CD3-CD4- ILC2s from total CD45+ cells.

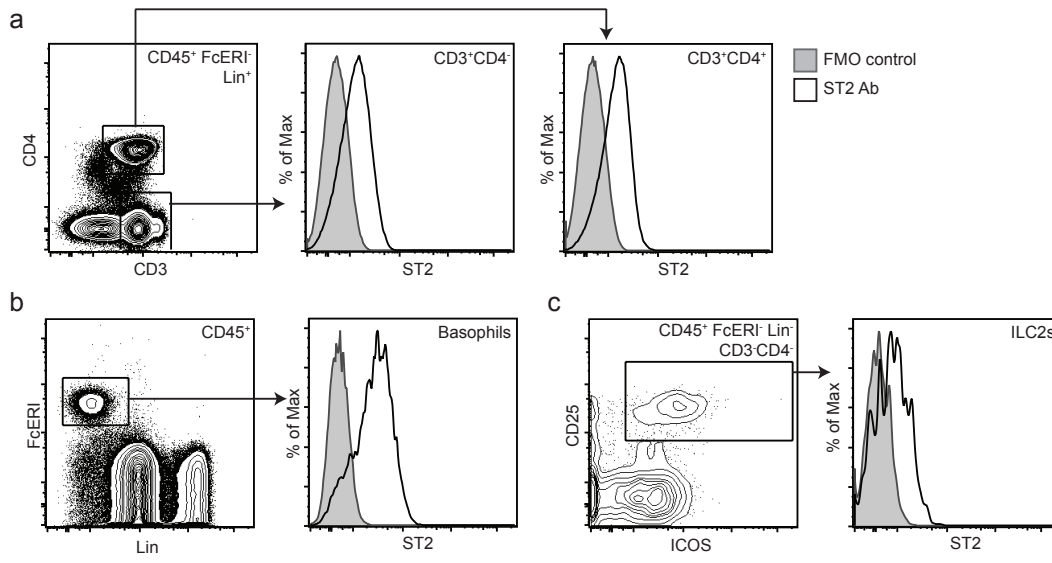


Figure 9. Distribution of ST2-expressing cell types in PBMCs and induced sputum

(a) Distribution of Lineage-FcERI+ basophils, Lin-ST2+CD25+ ILC2s, CD3+CD4+ T cells, and CD3+CD4- T cells as a percentage of total ST2+CD45+ cells in PBMCs collected from healthy and asthmatic subjects. Each point represents an individual subject. Median +/- interquartile range. (b) Distribution of Lineage-FcERI+ basophils, Lin-ST2+CD25+ ILC2s, CD3+CD4+ T cells, and CD3+CD4- T cells as a percentage of total ST2+CD45+ cells in induced sputum collected from healthy and asthmatic subjects. Each point represents an individual subject. Median +/- interquartile range.

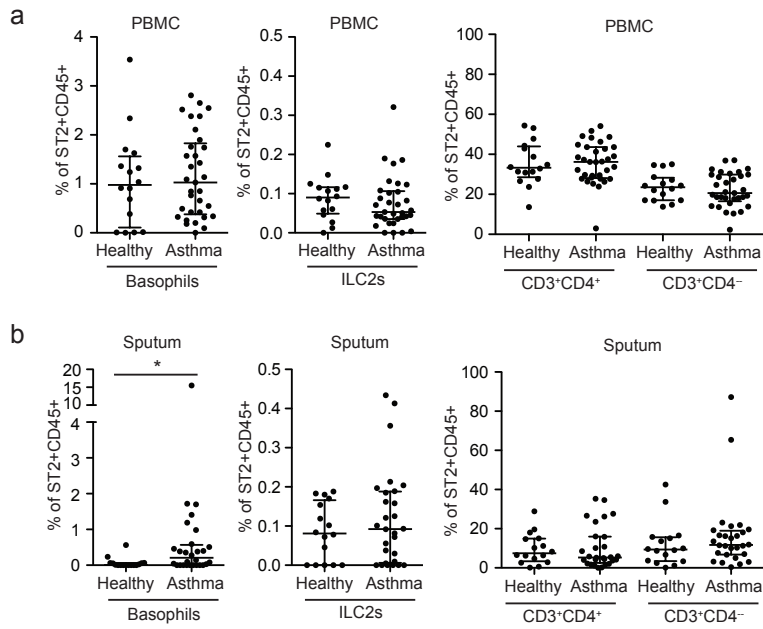
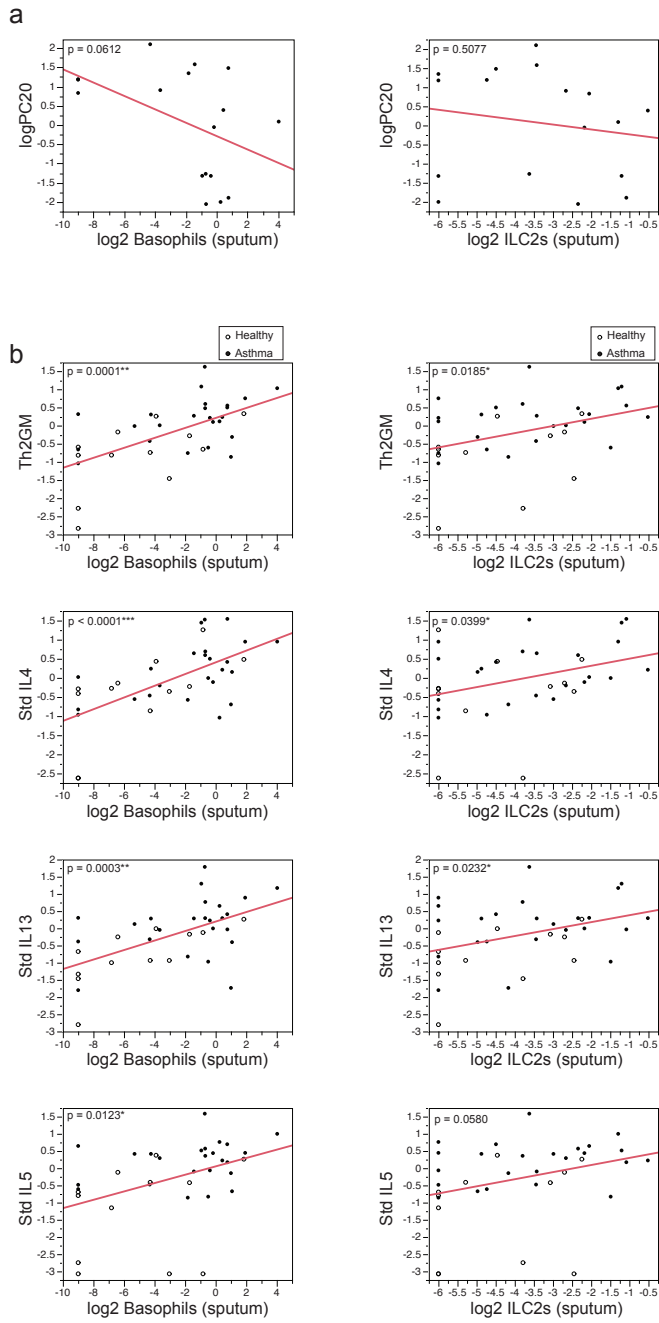


Figure 10. Sputum basophils numbers correlate with PC20 and Th2 gene expression

(a) Correlations between the frequencies of basophils (log2) and ILC2s (log2) in sputum and PC20. (b) Correlations between the frequencies of basophils (log2) and ILC2s (log2) in sputum and sputum cell pellet expression of *IL4*, *IL13*, and *IL5* as measured by standard deviation of each cytokine or the average of all three cytokines. “Th2GM” = Th2 three gene mean.



Chapter 4

Discussion, conclusions, and future directions

Summary

Our work focused on understanding miRNA regulation of Th2 cell development and function, as well as understanding miRNA regulation of T cells in asthma pathogenesis. In our published work, we identified upregulation of miR-19a in CD4 T cells from asthmatic airways. Using conditional deletion of the miR-17~92 cluster in mouse CD4 T cells, we established a role for the miR-17~92 cluster in promoting Th2 cytokine production, primarily through the activity of miR-19a and miR-19b. miR-19 targeted PTEN, SOCS1, and A20 to promote the production of IL-13 and IL-4 in Th2 polarizing cultures. Surprisingly, inhibition of SOCS1 and A20 specifically upregulated Th2 cytokines, and had no effect on Th17 or Th1 cytokines, while inhibition of PTEN promoted the production of cytokines pertaining to all T-helper subsets. We also found that the miR-17~92 cluster regulated Th2 cytokine production in vivo in a murine allergic airway inflammation model. In vitro polarized Th2 cells lacking the miR-17~92 cluster did not induce eosinophilic infiltration into the lungs, and did not induce mucus secretion by epithelial cells in the airways. Transfecting miR-19a into the cells prior to transfer promoted eosinophilic infiltration and mucus secretion in the airways, suggesting alteration of miR-19a activity in Th2 cells could alter the asthmatic phenotype.

miR-17~92 regulation of T-helper cells

The miR-17~92 cluster has well-established roles in the regulation of various T-helper cells (Th1, Th17, Tfh), as well as CD8 cytotoxic T cells and B cells. Its function in Th2 cell development and function had not previously been described. Nonetheless, this raises questions about how this cluster can specifically regulate Th2 cytokine production in some cases, when it has broad activity in different cell types, and has targets that are expressed in and affect many

different cell types. We are currently trying to decipher the expression and the role of the miR-17~92 cluster in other Th2 cytokine-producing cells, such as ILC2s and basophils, by using specific conditional deletion alleles such as *Yetcre13*, which deletes the floxed alleles of miR-17~92 in IL-13-producing cells.

Our own work showed how seemingly broad targets, such as PTEN, SOCS1, and A20, which are expressed in all lymphocytes, can have limiting roles in different contexts. PTEN affected Th1, Th2, and Th17 cell subsets, while SOCS1 and A20 affected only Th2 cells, despite their previously predicted roles in Th1 and Th17 cells. This finding highlights the importance of identifying relevant and functional miRNA targets for a specific cellular context. This will help to understand the pathways that are functional and important for a given cellular behavior, such as Th2 cytokine production and asthma pathogenesis. Our work has also given weight to the idea that NF- κ B inhibitors could be an effective treatment for asthma, because A20 is an inhibitor of the NF- κ B pathway. PI3K inhibitors may also be effective treatments for asthma; their efficacy for treatment of autoimmune disease is being tested in many clinical trials, but they have not yet been tested in allergic diseases.

Adaptive and innate immune regulation of asthma pathogenesis

We also attempted to gain a better understanding of the role of various cell types in asthma through collaboration with medical scientists at UCSF and Genentech. It has been a huge learning experience setting up these collaborations and designing flow panels for analysis of precious biospecimens. The RITA study focuses on miRNA regulation of various T-helper subsets in asthma. Our results from RITA, as well as from AsthmaNet, so far suggest that there is not a dramatic increase in Th2 cells in the lungs of asthmatic subjects, but we do not yet have the

power to determine whether individuals with “Th2-high” asthma may have a specific increase in Th2 cells relative to other T-helper subsets. It will be interesting to see the immunophenotyping results as we finish the final year of this clinical study to determine the types of lymphocytes present in the airways of asthmatic subjects and to test whether differences in immune cell infiltration correlate with differences in the Th2-ness of asthma. We also hope to determine miRNA expression in individual T-helper subsets in asthma. This will give us a better understanding of the miRNA expression changes we observed in bulk CD4 T cells from the airways of asthmatic subjects in the MAST study. Our interim analysis suggests that determining miRNA expression in the low cell numbers we are sorting from RITA subjects will be difficult, but possible. We may have to resort to combining all of the BAL T-helper subsets into one sample for each subject so that we have enough RNA to perform miRNA qPCR analysis. We are currently working to optimize the miRNA qPCR analysis so that we can maintain the ability to determine miRNA expression in different T-helper subsets present at the site of inflammation in asthma, an important analysis that has not yet been done in the context of human disease.

It is clear that T cells are not the only immune cell type that is present and functional in the airways of asthmatic subjects. Through the CASA study, we have found that innate immune cells such as basophils are more prevalent in the sputum of asthmatic subjects compared to healthy subjects, while other cell types, such as ILC2s, CD4 T cells, and non-CD4 T cells are not differentially prevalent. Sputum cell pellets from asthmatic subjects express more Th2 cytokine than healthy, and the measure of *Il4*, *Il5*, and *Il13* expression can be used to determine an individual’s “Th2-ness”. The number of basophils present in the sputum, as determined by flow cytometry, positively correlates with expression of Th2 cytokines in the sputum cell pellet, especially with IL-4. Future work in this clinical study will aim to identify the cell type

responsible for increased Th2 cytokines with a focus on basophil production of IL-4. This study has pushed the limits of our ability to perform flow cytometric immunophenotyping on a difficult biospecimen. It also has addressed the important question of whether ILC2s are the primary driving factor for asthma pathogenesis. Our results from induced sputum suggest that ILC2s are extremely rare in the airways, and their presence does not correlate with expression of Th2 cytokine or with clinical measures of asthma severity, suggesting that they are not as essential to asthma pathogenesis as previously predicted. However, mouse studies show that ILC2s are present in the lung parenchyma at branch points in the airways. This suggests that induced sputum may only capture a small fraction of the ILC2s present in the lungs of asthmatic or healthy individuals, and thus may not be the ideal biospecimen for determining the functional relevance of ILC2s in asthma. Lung biopsies or whole lung digestion for flow cytometry, or histology may be helpful in determining whether ILC2s are a driving force behind Th2 polarization of asthmatic responses. This is outside the scope of the CASA study, but will be an interesting future direction for the ILC2 field. ILC2s are the exciting new cell type in the field of allergic diseases, but basophils may have been overlooked in recent years. Our results will hopefully shed light on the importance of basophils in asthma, and may lead to therapeutics aimed at altering basophil production of Th2 cytokines.

References

1. National Asthma Education and Prevention Program. Expert Panel Report 3 (EPR-3): Guidelines for the Diagnosis and Management of Asthma-Summary Report 2007. *J. Allergy Clin. Immunol.* **120**, S94–138 (2007).
2. Wenzel, S. E. Asthma phenotypes: the evolution from clinical to molecular approaches. *Nature Medicine* **18**, 716–725 (2012).
3. Cohn, L., Elias, J. A. & Chupp, G. L. Asthma: mechanisms of disease persistence and progression. *Annu. Rev. Immunol.* **22**, 789–815 (2004).
4. Barnes, P. J. Immunology of asthma and chronic obstructive pulmonary disease. *Nat. Rev. Immunol.* **8**, 183–192 (2008).
5. Locksley, R. M. Asthma and allergic inflammation. *Cell* **140**, 777–783 (2010).
6. Fahy, J. V. Type 2 inflammation in asthma - present in most, absent in many. *Nat. Rev. Immunol.* **15**, 57–65 (2014).
7. Kuperman, D. A. *et al.* Direct effects of interleukin-13 on epithelial cells cause airway hyperreactivity and mucus overproduction in asthma. *Nature Medicine* **8**, 885–889 (2002).
8. Gould, H. J. & Sutton, B. J. IgE in allergy and asthma today. *Nat. Rev. Immunol.* **8**, 205–217 (2008).
9. Artis, D. & Spits, H. The biology of innate lymphoid cells. *Nature* **517**, 293–301 (2015).
10. Robinson, D. S. *et al.* Predominant TH2-like bronchoalveolar T-lymphocyte population in atopic asthma. *N. Engl. J. Med.* **326**, 298–304 (1992).
11. Galli, S. J., Tsai, M. & Piliponsky, A. M. The development of allergic inflammation. *Nature* **454**, 445–454 (2008).
12. Mosmann, T. R. & Coffman, R. L. Heterogeneity of cytokine secretion patterns and functions of helper T cells. *Adv. Immunol.* **46**, 111–147 (1989).
13. Ansel, K. M., Djuretic, I., Tanasa, B. & Rao, A. Regulation of Th2 differentiation and Il4 locus accessibility. *Annu. Rev. Immunol.* **24**, 607–656 (2006).
14. Ohashi, P. S. T-cell signalling and autoimmunity: molecular mechanisms of disease. *Nat. Rev. Immunol.* **2**, 427–438 (2002).
15. Hasler, P. & Zouali, M. B cell receptor signaling and autoimmunity. *FASEB J.* **15**, 2085–2098 (2001).
16. Josefowicz, S. Z., Lu, L.-F. & Rudensky, A. Y. Regulatory T Cells: Mechanisms of Differentiation and Function. *Annu. Rev. Immunol.* **30**, 531–564 (2012).
17. Kozomara, A. & Griffiths-Jones, S. miRBase: annotating high confidence microRNAs using deep sequencing data. *Nucleic Acids Research* **42**, D68–D73 (2013).
18. Ha, M. & Kim, V. N. nrm3838. *Nature Publishing Group* **15**, 509–524 (2014).
19. Bartel, D. P. MicroRNAs: target recognition and regulatory functions. *Cell* **136**, 215–233 (2009).
20. Baumjohann, D. & Ansel, K. M. MicroRNA-mediated regulation of T helper cell differentiation and plasticity. *Nat. Rev. Immunol.* **13**, 666–678 (2013).
21. O'Connell, R. M., Rao, D. S. & Baltimore, D. microRNA regulation of inflammatory responses. *Annu. Rev. Immunol.* **30**, 295–312 (2012).
22. Xiao, C. & Rajewsky, K. MicroRNA Control in the Immune System: Basic

- Principles. *Cell* **136**, 26–36 (2009).
23. Koralov, S. B. *et al.* Dicer Ablation Affects Antibody Diversity and Cell Survival in the B Lymphocyte Lineage. *Cell* **132**, 860–874 (2008).
 24. Ventura, A. *et al.* Targeted Deletion Reveals Essential and Overlapping Functions of the miR-17~92 Family of miRNA Clusters. *Cell* **132**, 875–886 (2008).
 25. Xiao, C. *et al.* Lymphoproliferative disease and autoimmunity in mice with increased miR-17-92 expression in lymphocytes. *Nat. Immunol.* **9**, 405–414 (2008).
 26. Li, Q.-J. *et al.* miR-181a is an intrinsic modulator of T cell sensitivity and selection. *Cell* **129**, 147–161 (2007).
 27. Henao-Mejia, J. *et al.* The MicroRNA miR-181 Is a Critical Cellular Metabolic Rheostat Essential for NKT Cell Ontogenesis and Lymphocyte Development and Homeostasis. *Immunity* **38**, 984–997 (2013).
 28. Ebert, P. J. R., Jiang, S., Xie, J., Li, Q.-J. & Davis, M. M. An endogenous positively selecting peptide enhances mature T cell responses and becomes an autoantigen in the absence of microRNA miR-181a. *Nat. Immunol.* **10**, 1162–1169 (2009).
 29. Papadopoulou, A. S. *et al.* The thymic epithelial microRNA network elevates the threshold for infection-associated thymic involution via miR-29a mediated suppression of the IFN- α receptor. *Nat. Immunol.* **13**, 181–187 (2012).
 30. Ucar, O., Tykocinski, L.-O., Dooley, J., Liston, A. & Kyewski, B. An evolutionarily conserved mutual interdependence between Aire and microRNAs in promiscuous gene expression. *Eur. J. Immunol.* **43**, 1769–1778 (2013).
 31. Khan, I. S., Taniguchi, R. T., Fasano, K. J., Anderson, M. S. & Jeker, L. T. Canonical microRNAs in thymic epithelial cells promote central tolerance. *Eur. J. Immunol.* **44**, 1313–1319 (2014).
 32. Carsetti, R., Rosado, M. M. & Wardmann, H. Peripheral development of B cells in mouse and man. *Immunol. Rev.* **197**, 179–191 (2004).
 33. Pillai, S. & Cariappa, A. The follicular versus marginal zone B lymphocyte cell fate decision. *Nat. Rev. Immunol.* **9**, 767–777 (2009).
 34. Belver, L., de Yébenes, V. G. & Ramiro, A. R. MicroRNAs prevent the generation of autoreactive antibodies. *Immunity* **33**, 713–722 (2010).
 35. Mraz, M. *et al.* miR-150 influences B-cell receptor signaling in chronic lymphocytic leukemia by regulating expression of GAB1 and FOXP1. *Blood* **124**, 84–95 (2014).
 36. Rao, D. S. *et al.* MicroRNA-34a Perturbs B Lymphocyte Development by Repressing the Forkhead Box Transcription Factor Foxp1. *Immunity* **33**, 48–59 (2010).
 37. Berry, G. J., Budgeon, L. R., Cooper, T. K., Christensen, N. D. & Waldner, H. The type 1 diabetes resistance locus B10 Idd9.3 mediates impaired B-cell lymphopoiesis and implicates microRNA-34a in diabetes protection. *Eur. J. Immunol.* **44**, 1716–1727 (2014).
 38. Khan, A. A., Penny, L. A., Yuzefpolskiy, Y., Sarkar, S. & Kalia, V. MicroRNA-17 92 regulates effector and memory CD8 T-cell fates by modulating proliferation in response to infections. *Blood* **121**, 4473–4483 (2013).
 39. Baumjohann, D. *et al.* The microRNA cluster miR-17~92 promotes TFH cell differentiation and represses subset-inappropriate gene expression. *Nat. Immunol.* **14**, 840–848 (2013).
 40. Kang, S. G. *et al.* MicroRNAs of the miR-17~92 family are critical regulators of

- TFH differentiation. *Nat. Immunol.* **14**, 849–857 (2013).
41. Simpson, L. J. *et al.* A microRNA upregulated in asthma airway T cells promotes TH2 cytokine production. *Nat. Immunol.* **15**, 1162–1170 (2014).
 42. Palacios, F. *et al.* Activation of the PI3K/AKT pathway by microRNA-22 results in CLL B-cell proliferation. *Leukemia* (2014). doi:10.1038/leu.2014.158
 43. Di Cristofano, A. *et al.* Impaired Fas response and autoimmunity in Pten^{+/-} mice. *Science* **285**, 2122–2125 (1999).
 44. Wu, X.-N. *et al.* Defective PTEN regulation contributes to B cell hyperresponsiveness in systemic lupus erythematosus. *Sci Transl Med* **6**, 246ra99 (2014).
 45. Wei, B. & Pei, G. microRNAs: critical regulators in Th17 cells and players in diseases. *Cell. Mol. Immunol.* **7**, 175–181 (2010).
 46. O'Connell, R. M. *et al.* MicroRNA-155 Promotes Autoimmune Inflammation by Enhancing Inflammatory T Cell Development. *Immunity* **33**, 607–619 (2010).
 47. Blüml, S. *et al.* Essential role of microRNA-155 in the pathogenesis of autoimmune arthritis in mice. *Arthritis & Rheumatism* **63**, 1281–1288 (2011).
 48. Escobar, T. M. *et al.* miR-155 Activates Cytokine Gene Expression in Th17 Cells by Regulating the DNA-Binding Protein Jarid2 to Relieve Polycomb-Mediated Repression. *Immunity* **40**, 865–879 (2014).
 49. Wang, H. *et al.* Negative regulation of Hif1a expression and TH17 differentiation by the hypoxia-regulated microRNA miR-210. *Nat. Immunol.* **15**, 393–401 (2014).
 50. Mok, Y. *et al.* MiR-210 Is Induced by Oct-2, Regulates B Cells, and Inhibits Autoantibody Production. *The Journal of Immunology* **191**, 3037–3048 (2013).
 51. Liu, S.-Q., Jiang, S., Li, C., Zhang, B. & Li, Q.-J. miR-17-92 cluster targets phosphatase and tensin homology and Ikaros Family Zinc Finger 4 to promote TH17-mediated inflammation. *J. Biol. Chem.* **289**, 12446–12456 (2014).
 52. Zhu, E. *et al.* miR-20b Suppresses Th17 Differentiation and the Pathogenesis of Experimental Autoimmune Encephalomyelitis by Targeting ROR t and STAT3. *The Journal of Immunology* **192**, 5599–5609 (2014).
 53. Zhou, X. *et al.* Selective miRNA disruption in T reg cells leads to uncontrolled autoimmunity. *J. Exp. Med.* **205**, 1983–1991 (2008).
 54. Liston, A., Lu, L.-F., O'Carroll, D., Tarakhovskiy, A. & Rudensky, A. Y. Dicer-dependent microRNA pathway safeguards regulatory T cell function. *J. Exp. Med.* **205**, 1993–2004 (2008).
 55. Chong, M. M. W., Rasmussen, J. P., Rudensky, A. Y., Rundensky, A. Y. & Littman, D. R. The RNaseIII enzyme Drosha is critical in T cells for preventing lethal inflammatory disease. *J. Exp. Med.* **205**, 2005–2017 (2008).
 56. Lu, L.-F. *et al.* Foxp3-Dependent MicroRNA155 Confers Competitive Fitness to Regulatory T Cells by Targeting SOCS1 Protein. *Immunity* **30**, 80–91 (2009).
 57. Kohlhaas, S. *et al.* Cutting edge: the Foxp3 target miR-155 contributes to the development of regulatory T cells. *The Journal of Immunology* **182**, 2578–2582 (2009).
 58. Jiang, S. *et al.* Molecular dissection of the miR-17-92 cluster's critical dual roles in promoting Th1 responses and preventing inducible Treg differentiation. *Blood* **118**, 5487–5497 (2011).
 59. de Kouchkovsky, D. *et al.* microRNA-17-92 regulates IL-10 production by

- regulatory T cells and control of experimental autoimmune encephalomyelitis. *J. Immunol.* **191**, 1594–1605 (2013).
60. Takahashi, H. *et al.* TGF- β and retinoic acid induce the microRNA miR-10a, which targets Bcl-6 and constrains the plasticity of helper T cells. *Nat. Immunol.* **13**, 587–595 (2012).
61. Jeker, L. T. *et al.* MicroRNA 10a marks regulatory T cells. *PLoS ONE* **7**, e36684 (2012).
62. Marçais, A. *et al.* microRNA-mediated regulation of mTOR complex components facilitates discrimination between activation and anergy in CD4 T cells. *J. Exp. Med.* **211**, 2281–2295 (2014).
63. Powell, J. D., Pollizzi, K. N., Heikamp, E. B. & Horton, M. R. Regulation of immune responses by mTOR. *Annu. Rev. Immunol.* **30**, 39–68 (2012).
64. Borlado, L. R. *et al.* Increased phosphoinositide 3-kinase activity induces a lymphoproliferative disorder and contributes to tumor generation in vivo. *FASEB J.* **14**, 895–903 (2000).
65. Haxhinasto, S., Mathis, D. & Benoist, C. The AKT-mTOR axis regulates de novo differentiation of CD4+Foxp3+ cells. *J. Exp. Med.* **205**, 565–574 (2008).
66. Wohlfert, E. A., Gorelik, L., Mittler, R., Flavell, R. A. & Clark, R. B. Cutting edge: deficiency in the E3 ubiquitin ligase Cbl-b results in a multifunctional defect in T cell TGF-beta sensitivity in vitro and in vivo. *J. Immunol.* **176**, 1316–1320 (2006).
67. Sauer, S. *et al.* T cell receptor signaling controls Foxp3 expression via PI3K, Akt, and mTOR. *Proc. Natl. Acad. Sci. U.S.A.* **105**, 7797–7802 (2008).
68. Merckenschlager, M. & Boehmer, von, H. PI3 kinase signalling blocks Foxp3 expression by sequestering Foxo factors. *J. Exp. Med.* **207**, 1347–1350 (2010).
69. Okoye, I. S. *et al.* MicroRNA-Containing T-Regulatory-Cell-Derived Exosomes Suppress Pathogenic T Helper 1 Cells. *Immunity* **41**, 89–103 (2014).
70. Bryniarski, K. *et al.* Antigen-specific, antibody-coated, exosome-like nanovesicles deliver suppressor T-cell microRNA-150 to effector T cells to inhibit contact sensitivity. *J. Allergy Clin. Immunol.* **132**, 170–181 (2013).
71. Singh, R. P. *et al.* The role of miRNA in inflammation and autoimmunity. *Autoimmunity Reviews* **12**, 1160–1165 (2013).
72. Lashine, Y. A., Salah, S., Aboelenein, H. R. & Abdelaziz, A. I. Correcting the expression of miRNA-155 represses PP2Ac and enhances the release of IL-2 in PBMCs of juvenile SLE patients. *Lupus* (2014). doi:10.1177/0961203314552117
73. Tang, Y. *et al.* MicroRNA-146a contributes to abnormal activation of the type I interferon pathway in human lupus by targeting the key signaling proteins. *Arthritis & Rheumatism* **60**, 1065–1075 (2009).
74. Fu, L. *et al.* Comprehensive review of genetic association studies and meta-analysis on miRNA polymorphisms and rheumatoid arthritis and systemic lupus erythematosus susceptibility. *Hum. Immunol.* (2014). doi:10.1016/j.humimm.2014.09.002
75. Luo, X. *et al.* A Functional Variant in MicroRNA-146a Promoter Modulates Its Expression and Confers Disease Risk for Systemic Lupus Erythematosus. *PLoS Genet* **7**, e1002128 (2011).
76. Otaegui, D. *et al.* Differential micro RNA expression in PBMC from multiple sclerosis patients. *PLoS ONE* **4**, e6309 (2009).

77. Fenoglio, C. *et al.* Expression and genetic analysis of miRNAs involved in CD4+ cell activation in patients with multiple sclerosis. *Neuroscience Letters* **504**, 9–12 (2011).
78. Pauley, K. M. *et al.* Upregulated miR-146a expression in peripheral blood mononuclear cells from rheumatoid arthritis patients. *Arthritis Res Ther* **10**, R101 (2008).
79. Keller, A. *et al.* Multiple sclerosis: microRNA expression profiles accurately differentiate patients with relapsing-remitting disease from healthy controls. *PLoS ONE* **4**, e7440 (2009).
80. Cox, M. B. *et al.* MicroRNAs miR-17 and miR-20a Inhibit T Cell Activation Genes and Are Under-Expressed in MS Whole Blood. *PLoS ONE* **5**, e12132 (2010).
81. Zhang, J. *et al.* MicroRNA-155 modulates Th1 and Th17 cell differentiation and is associated with multiple sclerosis and experimental autoimmune encephalomyelitis. *Journal of Neuroimmunology* **266**, 56–63 (2014).
82. Du, C. *et al.* MicroRNA miR-326 regulates TH-17 differentiation and is associated with the pathogenesis of multiple sclerosis. *Nat. Immunol.* **10**, 1252–1259 (2009).
83. Sebastiani, G. *et al.* Increased expression of microRNA miR-326 in type 1 diabetic patients with ongoing islet autoimmunity. *Diabetes Metab. Res. Rev.* **27**, 862–866 (2011).
84. Lindberg, R. L. P., Hoffmann, F., Mehling, M., Kuhle, J. & Kappos, L. Altered expression of miR-17-5p in CD4+ lymphocytes of relapsing-remitting multiple sclerosis patients. *Eur. J. Immunol.* **40**, 888–898 (2010).
85. Pan, W. *et al.* MicroRNA-21 and MicroRNA-148a Contribute to DNA Hypomethylation in Lupus CD4+ T Cells by Directly and Indirectly Targeting DNA Methyltransferase 1. *The Journal of Immunology* **184**, 6773–6781 (2010).
86. Fulci, V. *et al.* miR-223 is overexpressed in T-lymphocytes of patients affected by rheumatoid arthritis. *Hum. Immunol.* **71**, 206–211 (2010).
87. Lu, M. C. *et al.* Increased miR-223 expression in T cells from patients with rheumatoid arthritis leads to decreased insulin-like growth factor-1-mediated interleukin-10 production. *Clin Exp Immunol* **177**, 641–651 (2014).
88. Martínez-Ramos, R. *et al.* Differential expression pattern of microRNAs in CD4+ and CD19+ cells from asymptomatic patients with systemic lupus erythematosus. *Lupus* **23**, 353–359 (2014).
89. De Santis, G. *et al.* Altered miRNA expression in T regulatory cells in course of multiple sclerosis. *Journal of Neuroimmunology* **226**, 165–171 (2010).
90. Smigielska-Czepiel, K. *et al.* Comprehensive analysis of miRNA expression in T-cell subsets of rheumatoid arthritis patients reveals defined signatures of naive and memory Tregs. *Genes Immun* **15**, 115–125 (2014).
91. Hezova, R. *et al.* microRNA-342, microRNA-191 and microRNA-510 are differentially expressed in T regulatory cells of type 1 diabetic patients. *Cellular Immunology* **260**, 70–74 (2010).
92. Seumois, G. *et al.* An integrated nano-scale approach to profile miRNAs in limited clinical samples. *Am J Clin Exp Immunol* **1**, 70–89 (2012).
93. Li, J. *et al.* Altered microRNA expression profile with miR-146a upregulation in CD4+ T cells from patients with rheumatoid arthritis. *Arthritis Res Ther* **12**, R81 (2010).

94. Guo, Q. *et al.* Forced miR-146a expression causes autoimmune lymphoproliferative syndrome in mice via downregulation of Fas in germinal center B cells. *Blood* **121**, 4875–4883 (2013).
95. Solberg, O. D. *et al.* Airway epithelial miRNA expression is altered in asthma. *Am. J. Respir. Crit. Care Med.* **186**, 965–974 (2012).
96. Kurowska-Stolarska, M. *et al.* MicroRNA-155 as a proinflammatory regulator in clinical and experimental arthritis. *Proc. Natl. Acad. Sci. U.S.A.* **108**, 11193–11198 (2011).
97. Ceribelli, A., Satoh, M. & Chan, E. K. MicroRNAs and autoimmunity. *Current Opinion in Immunology* **24**, 686–691 (2012).
98. Janssen, H. L. A. *et al.* Treatment of HCV Infection by Targeting MicroRNA. *N. Engl. J. Med.* **368**, 1685–1694 (2013).
99. Murugaiyan, G. *et al.* MicroRNA-21 promotes Th17 differentiation and mediates experimental autoimmune encephalomyelitis. *J. Clin. Invest.* (2015). doi:10.1172/JCI74347DS1
100. Mattes, J., Collison, A., Plank, M., Phipps, S. & Foster, P. S. Antagonism of microRNA-126 suppresses the effector function of TH2 cells and the development of allergic airways disease. *Proc. Natl. Acad. Sci. U.S.A.* **106**, 18704–18709 (2009).
101. Murugaiyan, G., Beynon, V., Mittal, A., Joller, N. & Weiner, H. L. Silencing MicroRNA-155 Ameliorates Experimental Autoimmune Encephalomyelitis. *The Journal of Immunology* **187**, 2213–2221 (2011).
102. Olive, V., Li, Q. & He, L. mir-17-92: a polycistronic oncomir with pleiotropic functions. *Immunol. Rev.* **253**, 158–166 (2013).
103. Banham-Hall, E., Clatworthy, M. R. & Okkenhaug, K. The Therapeutic Potential for PI3K Inhibitors in Autoimmune Rheumatic Diseases. *Open Rheumatol J* **6**, 245–258 (2012).
104. Woodruff, P. G. *et al.* T-helper Type 2–driven Inflammation Defines Major Subphenotypes of Asthma. *Am. J. Respir. Crit. Care Med.* **180**, 388–395 (2009).
105. Wynn, T. A. IL-13 effector functions. *Annu. Rev. Immunol.* **21**, 425–456 (2003).
106. Corren, J. *et al.* Lebrikizumab treatment in adults with asthma. *N. Engl. J. Med.* **365**, 1088–1098 (2011).
107. Wenzel, S. *et al.* Dupilumab in persistent asthma with elevated eosinophil levels. *N. Engl. J. Med.* **368**, 2455–2466 (2013).
108. Liu, Y., Li, H., Xiao, T. & Lu, Q. Epigenetics in Immune-Mediated Pulmonary Diseases. *Clinic Rev Allerg Immunol* **45**, 314–330 (2013).
109. Polikepahad, S. *et al.* Proinflammatory role for let-7 microRNAs in experimental asthma. *J. Biol. Chem.* **285**, 30139–30149 (2010).
110. Bronevetsky, Y. & Ansel, K. M. Regulation of miRNA biogenesis and turnover in the immune system. *Immunol. Rev.* **253**, 304–316 (2013).
111. Steiner, D. F. *et al.* MicroRNA-29 regulates T-box transcription factors and interferon- γ production in helper T cells. *Immunity* **35**, 169–181 (2011).
112. Moltzahn, F. *et al.* Microfluidic-based multiplex qRT-PCR identifies diagnostic and prognostic microRNA signatures in the sera of prostate cancer patients. *Cancer Res.* **71**, 550–560 (2011).
113. Bronevetsky, Y. *et al.* T cell activation induces proteasomal degradation of Argonaute and rapid remodeling of the microRNA repertoire. *J. Exp. Med.* **210**,

- 417–432 (2013).
114. Hsu, S. D. *et al.* miRTarBase: a database curates experimentally validated microRNA-target interactions. *Nucleic Acids Research* **39**, D163–D169 (2010).
115. Mavrakis, K. J. *et al.* Genome-wide RNA-mediated interference screen identifies miR-19 targets in Notch-induced T-cell acute lymphoblastic leukaemia. *Nat. Cell Biol.* **12**, 372–379 (2010).
116. Gantier, M. P. *et al.* A miR-19 regulon that controls NF- κ B signaling. *Nucleic Acids Research* **40**, 8048–8058 (2012).
117. Mingueneau, M. *et al.* The transcriptional landscape of $\alpha\beta$ T cell differentiation. *Nat. Immunol.* **14**, 619–632 (2013).
118. Olive, V. *et al.* A component of the mir-17-92 polycistronic oncomir promotes oncogene-dependent apoptosis. *Elife* **2**, e00822 (2013).
119. Srivastava, N., Sudan, R. & Kerr, W. G. Role of Inositol Poly-Phosphatases and Their Targets in T Cell Biology. *Front Immunol* **4**, 288 (2013).
120. Palmer, D. C. & Restifo, N. P. Suppressors of cytokine signaling (SOCS) in T cell differentiation, maturation, and function. *Trends Immunol.* **30**, 592–602 (2009).
121. Tanaka, K. *et al.* Loss of suppressor of cytokine signaling 1 in helper T cells leads to defective Th17 differentiation by enhancing antagonistic effects of IFN- γ on STAT3 and Smads. *J. Immunol.* **180**, 3746–3756 (2008).
122. Egwuagu, C. E. *et al.* Suppressors of cytokine signaling proteins are differentially expressed in Th1 and Th2 cells: implications for Th cell lineage commitment and maintenance. *J. Immunol.* **168**, 3181–3187 (2002).
123. Fujimoto, M. *et al.* A regulatory role for suppressor of cytokine signaling-1 in T(h) polarization in vivo. *Int. Immunol.* **14**, 1343–1350 (2002).
124. Dickensheets, H. *et al.* Suppressor of cytokine signaling-1 is an IL-4-inducible gene in macrophages and feedback inhibits IL-4 signaling. *Genes Immun* **8**, 21–27 (2006).
125. Tamiya, T., Kashiwagi, I., Takahashi, R., Yasukawa, H. & Yoshimura, A. Suppressors of Cytokine Signaling (SOCS) Proteins and JAK/STAT Pathways: Regulation of T-Cell Inflammation by SOCS1 and SOCS3. *Arteriosclerosis, Thrombosis, and Vascular Biology* **31**, 980–985 (2011).
126. Coornaert, B. *et al.* T cell antigen receptor stimulation induces MALT1 paracaspase-mediated cleavage of the NF- κ B inhibitor A20. *Nat. Immunol.* **9**, 263–271 (2008).
127. Liu, F., Qin, H.-B., Xu, B., Zhou, H. & Zhao, D.-Y. Profiling of miRNAs in pediatric asthma: upregulation of miRNA-221 and miRNA-485-3p. *Mol Med Rep* **6**, 1178–1182 (2012).
128. Bhakta, N. R. & Woodruff, P. G. Human asthma phenotypes: from the clinic, to cytokines, and back again. *Immunol. Rev.* **242**, 220–232 (2011).
129. Rodriguez, A. *et al.* Requirement of bic/microRNA-155 for normal immune function. *Science* **316**, 608–611 (2007).
130. Thai, T.-H. *et al.* Regulation of the germinal center response by microRNA-155. *Science* **316**, 604–608 (2007).
131. Malmhäll, C. *et al.* MicroRNA-155 is essential for TH2-mediated allergen-induced eosinophilic inflammation in the lung. *J. Allergy Clin. Immunol.* (2013). doi:10.1016/j.jaci.2013.11.008
132. Collison, A., Mattes, J., Plank, M. & Foster, P. S. Inhibition of house dust mite-

- induced allergic airways disease by antagonism of microRNA-145 is comparable to glucocorticoid treatment. *J. Allergy Clin. Immunol.* **128**, 160–167.e4 (2011).
133. Kumar, M. *et al.* Let-7 microRNA-mediated regulation of IL-13 and allergic airway inflammation. *J. Allergy Clin. Immunol.* **128**, 1077–85.e1–10 (2011).
134. Sharma, A. *et al.* Antagonism of mmu-mir-106a attenuates asthma features in allergic murine model. *J. Appl. Physiol.* **113**, 459–464 (2012).
135. Edwards, M. R. *et al.* Targeting the NF- κ B pathway in asthma and chronic obstructive pulmonary disease. *Pharmacology and Therapeutics* **121**, 1–13 (2009).
136. Suzuki, A. *et al.* T cell-specific loss of Pten leads to defects in central and peripheral tolerance. *Immunity* **14**, 523–534 (2001).
137. Chen, C. *et al.* Integrin α 9 β 1 in airway smooth muscle suppresses exaggerated airway narrowing. *J. Clin. Invest.* **122**, 2916–2927 (2012).
138. Becattini, S. *et al.* T cell immunity. Functional heterogeneity of human memory CD4⁺ T cell clones primed by pathogens or vaccines. *Science* **347**, 400–406 (2015).
139. Lloyd, C. M. & Hessel, E. M. Functions of T cells in asthma: more than just T(H)2 cells. *Nat. Rev. Immunol.* **10**, 838–848 (2010).
140. Kudo, M. *et al.* IL-17A produced by α β T cells drives airway hyper-responsiveness in mice and enhances mouse and human airway smooth muscle contraction. *Nature Medicine* **18**, 547–554 (2012).
141. Moro, K. *et al.* Innate production of T(H)2 cytokines by adipose tissue-associated c-Kit(+)/Sca-1(+) lymphoid cells. *Nature* **463**, 540–544 (2010).
142. Saenz, S. A. *et al.* IL25 elicits a multipotent progenitor cell population that promotes T(H)2 cytokine responses. *Nature* **464**, 1362–1366 (2010).
143. Price, A. E. *et al.* Systemically dispersed innate IL-13-expressing cells in type 2 immunity. *Proc. Natl. Acad. Sci. U.S.A.* **107**, 11489–11494 (2010).
144. McKenzie, A. N. J., Spits, H. & Eberl, G. Innate lymphoid cells in inflammation and immunity. *Immunity* **41**, 366–374 (2014).
145. Molofsky, A. B. *et al.* Innate lymphoid type 2 cells sustain visceral adipose tissue eosinophils and alternatively activated macrophages. *J. Exp. Med.* **210**, 535–549 (2013).
146. Halim, T. Y. F. *et al.* Group 2 Innate Lymphoid Cells Are Critical for the Initiation of Adaptive T Helper 2 Cell-Mediated Allergic Lung Inflammation. *Immunity* **40**, 425–435 (2014).
147. Moffatt, M. F. *et al.* A large-scale, consortium-based genomewide association study of asthma. *N. Engl. J. Med.* **363**, 1211–1221 (2010).
148. Kroeger, K. M., Sullivan, B. M. & Locksley, R. M. IL-18 and IL-33 elicit Th2 cytokines from basophils via a MyD88- and p38 -dependent pathway. *Journal of Leukocyte Biology* **86**, 769–778 (2009).
149. Yoshimoto, T. *et al.* IL-18, although antiallergic when administered with IL-12, stimulates IL-4 and histamine release by basophils. *Proc. Natl. Acad. Sci. U.S.A.* **96**, 13962–13966 (1999).
150. Rossi, R. L. *et al.* Distinct microRNA signatures in human lymphocyte subsets and enforcement of the naive state in CD4⁺ T cells by the microRNA miR-125b. *Nat. Immunol.* **12**, 796–803 (2011).
151. Acosta-Rodriguez, E. V. *et al.* Surface phenotype and antigenic specificity of human interleukin 17-producing T helper memory cells. *Nat. Immunol.* **8**, 639–646 (2007).

152. Banham, A. H. Cell-surface IL-7 receptor expression facilitates the purification of FOXP3(+) regulatory T cells. *Trends Immunol.* **27**, 541–544 (2006).

Appendix 1

Interleukin-4 production by follicular helper T cells requires the conserved Il4 enhancer hypersensitivity site V

Pandurangan Vijayanand, Grégory Seumois, Laura J Simpson, Sarah Abdul-Wajid, Dirk Baumjohann, Marisella Panduro, Xiaozhu Huang, Jeneen Interlandi, Ivana M Djuretic, Daniel R Brown, Arlene H Sharpe, Anjana Rao, and K Mark Ansel. *Immunity*. 2012. 36(2); 175-187.

Interleukin-4 Production by Follicular Helper T Cells Requires the Conserved *Il4* Enhancer Hypersensitivity Site V

Pandurangan Vijayanand,^{1,3,4,8} Grégory Seumois,^{1,3,4,8} Laura J. Simpson,² Sarah Abdul-Wajid,² Dirk Baumjohann,² Marisella Panduro,² Xiaozhu Huang,¹ Jeneen Interlandi,⁵ Ivana M. Djuretic,⁵ Daniel R. Brown,^{6,7} Arlene H. Sharpe,⁷ Anjana Rao,^{3,5} and K. Mark Ansel^{2,*}

¹Pulmonary and Critical Care Division, Department of Medicine

²Department of Microbiology & Immunology, Sandler Asthma Basic Research Center University of California, San Francisco, San Francisco, CA 94143, USA

³Division of Signaling and Gene Expression, La Jolla Institute for Allergy & Immunology, La Jolla, CA 92037, USA

⁴Division of Infection, Inflammation and Immunity, School of Medicine, Southampton NIHR Respiratory Biomedical Research Unit, Sir Henry Wellcome Laboratories, Southampton General Hospital and University of Southampton, Southampton, Hampshire, SO16 6YD, UK

⁵Department of Pathology, Immune Disease Institute and Program in Cellular and Molecular Medicine, Harvard Medical School, Boston, MA 02115, USA

⁶Department of Pediatrics, Massachusetts General Hospital, Boston, MA 02114, USA

⁷Department of Pathology, Harvard Medical School and Brigham and Women's Hospital, Boston, MA 02115, USA

*These authors contributed equally to this work

*Correspondence: mark.ansel@ucsf.edu

DOI 10.1016/j.immuni.2011.12.014

SUMMARY

Follicular helper T cells (T_{fh} cells) are the major producers of interleukin-4 (IL-4) in secondary lymphoid organs where humoral immune responses develop. *Il4* regulation in T_{fh} cells appears distinct from the classical T helper 2 (Th2) cell pathway, but the underlying molecular mechanisms remain largely unknown. We found that hypersensitivity site V (HS V; also known as CNS2), a 3' enhancer in the *Il4* locus, is essential for IL-4 production by T_{fh} cells. Mice lacking HS V display marked defects in type 2 humoral immune responses, as evidenced by abrogated IgE and sharply reduced IgG1 production *in vivo*. In contrast, effector Th2 cells that are involved in tissue responses were far less dependent on HS V. HS V facilitated removal of repressive chromatin marks during Th2 and T_{fh} cell differentiation and increased accessibility of the *Il4* promoter. Thus, T_{fh} and Th2 cells utilize distinct but overlapping molecular mechanisms to regulate *Il4*, a finding with important implications for understanding the molecular basis of allergic diseases.

INTRODUCTION

Type 2 immune responses entail a humoral response characterized by interleukin-4 (IL-4)-dependent IgE and IgG1 production, and cellular responses in peripheral tissues that are coordinated by T helper 2 (Th2) cells and innate immune cells that produce the signature Th2 cell-type cytokines IL-4, IL-5, and IL-13 (Voehringer et al., 2004). Type 2 immune responses have an important

role in protective immunity against parasitic infections (Else et al., 1994), but when inappropriately exaggerated and misdirected to harmless antigens, cause allergic diseases such as asthma (Kay, 2001a, 2001b; Kim et al., 2010). Finding biological modifiers of the Th2 cell-type cytokines has emerged as a rational approach in developing new treatments for asthma (Levine and Wenzel, 2010). A complete mechanistic understanding of the molecular details of Th2 cell-type cytokine gene regulation may facilitate the development of novel approaches for therapeutic gene silencing in allergic diseases.

Elegant studies with cytokine gene reporter mice identified T cell subsets and innate immune cells that produce Th2 cell-type cytokines during type 2 immune responses *in vivo* (King and Mohrs, 2009; Neill et al., 2010; Price et al., 2010; Reese et al., 2007; Reinhardt et al., 2009; Saenz et al., 2010; Voehringer et al., 2004, 2006; Zaretsky et al., 2009). Follicular helper T (T_{fh}) cells have emerged as the major class of IL-4-producing T cells in the lymph node, and the IL-4 produced by these cells is critically required for shaping type 2 humoral immunity (King and Mohrs, 2009; Reinhardt et al., 2009; Zaretsky et al., 2009). The *trans*-acting factors required for IL-4 production by T_{fh} cells are distinctly different (GATA3- and STAT6-independent) from conventional Th2 cells, and the *cis*-regulatory requirements remain unknown (Reinhardt et al., 2009).

Gene expression in eukaryotes is tightly regulated by the chromatin structure of the underlying gene locus, which in turn influences the accessibility of *trans*-acting factors and the core transcriptional machinery to their binding sites in proximal gene promoters as well as distal *cis*-regulatory DNA elements (Berger, 2007; Li et al., 2007). Under physiological conditions, cell type specificity of gene expression is primarily conferred by distal *cis*-regulatory elements (Heintzman et al., 2009; Visel et al., 2009a, 2009b). A number of such elements were identified in the extended (~200 kb) murine Th2 cell-type cytokine locus spanning the *Il4*, *Il5*, and *Il13* genes and the constitutively

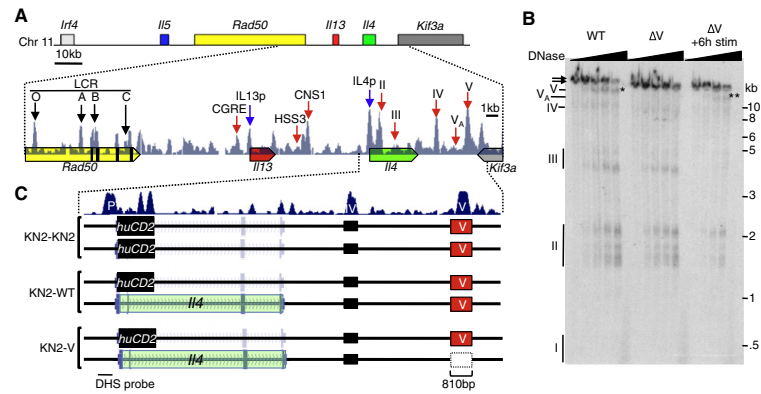


Figure 1. cis-Regulatory Regions in the Mouse Th2 Cell Locus and Chromatin Analysis of HS V-Deficient T Cells
 (A) Diagram represents the murine Th2 cell-type cytokine locus showing locations of the DNase I hypersensitivity sites (HS) and conserved noncoding sequences (red arrows), locus control region (LCR, black arrows), *Il13* and *Il4* promoter (blue arrows), and species conservation tracks.
 (B) DNase I HS analysis of unstimulated wild-type (WT) and ΔV Th2 cells either left unstimulated or stimulated for 6 hr with PMA and ionomycin (+6h stim) to induce HS V_A . Southern blot with a 5' IL-4 probe revealed the indicated HS sites. Double arrow shows parent BamHI fragment. Note the HS V deletion decreases the size of this band, but not HS fragments in ΔV T cells. HS V and HS V_A fragments are indicated by the * and ** symbols, respectively. See also Figure S1.
 (C) Schematic representation of the two *Il4* alleles in KN2-KN2, KN2-WT, and KN2-V allelic reporter mice.

expressed gene *Rad50* (Figure 1A; Agarwal and Rao, 1998; Ansel et al., 2006; Wilson et al., 2009). Targeted deletion of selected *cis*-regulatory elements in mice demonstrated their nonredundant functions in regulating Th2 cell-type cytokine gene expression (Ansel et al., 2004; Koh et al., 2010; Lee et al., 2003; Loots et al., 2000; Mohrs et al., 2001; Solymar et al., 2002; Tanaka et al., 2006, 2011; Yagi et al., 2007).

We previously identified two putative distal enhancers located 3' of the *Il4* gene, marked by cell type-specific DNase I hypersensitivity (hypersensitivity site V: HS V and HS V_A) (Figure 1A; Figure S1A available online). HS V is not accessible in naive T cells or differentiated Th1 cells, but becomes constitutively accessible in resting Th2 cells; it overlaps a highly conserved noncoding sequence (CNS2) in the *Il4* locus (Ansel et al., 2006). HS V_A becomes accessible only upon activation of Th2 cells, and the corresponding sequence binds GATA3, STAT6, and NFAT (Agarwal et al., 2000). Combined deletion of a 3.7 kb region spanning both HS V and HS V_A resulted in impaired IL-4 and IL-13 production in both Th2 cells and mast cells (Solymar et al., 2002). Confirming these findings, a similar strain of CNS2-deficient mice (Yagi et al., 2007), which bear a smaller deletion that disrupts HS V but also deletes about half of the sequence corresponding to HS V_A (Figure S1A), including NFAT and GATA3 binding sequences (Agarwal et al., 2000), also showed impaired IL-4 production in NK T cells and T-CD4 T cells (Sofi et al., 2011; Yagi et al., 2007). Unfortunately, the functional impairment in cytokine production observed in HS V and V_A -deficient and in CNS2-deficient mice could not be unambiguously attributed to one or the other region, because the integrity of both putative regulatory regions was compromised.

There are compelling reasons to examine the function of the HS V (CNS2) region in isolation. The interesting features of this region include (1) constitutive accessibility in Th2 cells (Agarwal and

Rao, 1998); (2) DNA hypomethylation in naive T cells (Lee et al., 2002); (3) maintained DNA hypomethylation during Th2 cell differentiation but increased DNA methylation during Th1 cell differentiation (Lee et al., 2002); and (4) binding of a number of important transcriptional regulators—including STAT6, STAT5, GATA3, Notch, RBP-J κ , ATP-dependent chromatin remodeler BRG-1, chromatin looping factor SATB1, and histone methyl transferase MLL—to the HS V region in a Th2 cell-preferential manner (Cai et al., 2006; Liao et al., 2008; Tanaka et al., 2006, 2011; Wei et al., 2010; Wurster and Pazin, 2008; Yamashita et al., 2006).

To address these issues, we generated mice bearing a precise deletion of the HS V (CNS2) region. An unexpected finding in the HS V-deficient (ΔV) mice was the complete abrogation of IgE production despite only mild reduction in type 2 cellular responses in affected tissues. To determine whether this dichotomous response was due to the differential requirement for HS V by the cell types that produce IL-4, we made use of allelic IL-4 reporter mice, which allowed us to track IL-4-producing cells in vivo. We show that Tfh cells critically depend on HS V for IL-4 production. In contrast, effector Th2 cells, basophils, and eosinophils were far less dependent on HS V.

RESULTS

Deletion of HS V Impairs *Il4* Transcription

To examine the function of HS V in regulation of Th2 cell-type cytokine genes, we generated mice with a specific deletion of HS V that did not disrupt the adjacent enhancer, HS V_A (Figures 1A and S1). DNase I hypersensitivity analysis of in-vitro-polarized HS V-deficient (ΔV) Th2 cells confirmed selective loss of HS V; importantly, other hypersensitivity sites that mark *cis*-regulatory elements remained intact, including the activation-inducible site HS V_A (Figure 1B). Unlike Th2 cells from mice

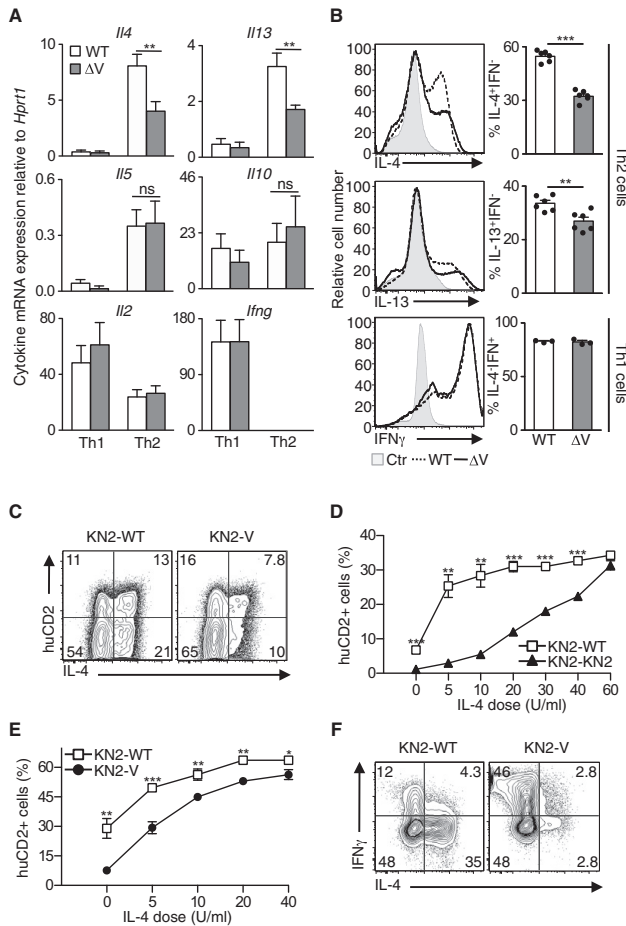


Figure 2. Cytokine Gene Expression Profile of HS V-Deficient CD4⁺ T Cells

(A) *Hprt1*-normalized cytokine mRNA abundance in CD4⁺ T cells differentiated in vitro under Th2 and Th1 cell polarizing conditions for 1 week and stimulated with PMA and ionomycin for 4 hr. Bars display average and error bars indicate standard error of mean.

(B) Histograms show intracellular cytokine staining of cells described in (A).

(C) Contour plots show IL-4 and huCD2 staining in Th2 cells generated in vitro (A).

(D and E) CD4⁺ T cells from the indicated mice were differentiated in vitro under submaximal Th2 cell polarizing conditions. Graphs show the percentage huCD2⁺ cells in relation to the concentration of exogenous IL-4 added to the culture. See also Figure S2A.

(F) Contour plot shows intracellular cytokine staining of restimulated CD4⁺ T cells from KN2-WT and KN2-V mice cultured with 11 U/ml of IL-4. See also Figure S2B.

n.s., no statistically significant difference ($p > 0.05$), ** $p < 0.01$, *** $p < 0.001$ with Student's *t* test. See also Table S2.

KN2 reporter mice (Mohrs et al., 2005) and the second is wild-type or bears the HS V deletion (designated KN2-WT and KN2-V respectively; Figure 1C). In the KN2 allele, a *CD2* gene cassette replaces the first two exons of *Il4*; thus, IL-4 protein is not produced but *Il4* transcription is faithfully reported as surface expression of human CD2 (huCD2) (Mohrs et al., 2005). Th2 cell cultures from both allelic reporter mice contained equal numbers of huCD2⁺ cells, indicating comparable Th2 cell polarization; among these huCD2⁺ IL4-competent cells, however, the frequency of IL-4 production was reduced in KN2-V T cells compared to KN2-WT cells, confirming a direct *cis*-regulatory role for HS V in the control of *Il4* activity in Th2 cells (Figure 2C).

To assess the magnitude of positive feedback through IL-4, we compared huCD2 expression in KN2-WT and KN2-KN2 T cells, which do and do not produce IL-4, respectively. As expected, endogenous IL-4 produced from the

functional IL-4 allele in KN2-WT T cells strongly potentiated Th2 cell polarization when the cells were differentiated under suboptimal Th2 cell conditions, with limiting amounts of exogenous IL-4 provided in culture (Figures 2D and S2A). Similarly, a 2- to 3-fold lower dose of exogenous IL-4 was necessary to induce huCD2 expression in KN2-WT T cells (which produce their own endogenous IL-4), compared to KN2-V T cells (which lack HS V in the functional IL-4 allele) (Figures 2E and S2A). At a low concentration of exogenous IL-4 (11 U/ml), the cytokine profile indicated a very strong dependence for HS V in Th2 cell polarization (Figures 2F and S2B). These results suggested that the deletion of HS V was likely to have pronounced effects on in vivo responses in which IL-4 feedback is important.

with the combined HS V and *V_A* deletion, which show diminished transcription of all the linked Th2 cell-type cytokine genes (*Il4*, *Il13*, and *Il5*) (Solymer et al., 2002), restimulated ΔV Th2 cells showed a nearly 50% reduction in the expression of *Il4* and *Il13* mRNA, but no significant change ($p > 0.05$) in *Il5* and *Il10* (Figure 2A). Compared to wild-type (WT) Th2 cells, the frequency of restimulated ΔV Th2 cells producing IL-4 (mean \pm SEM, 55% \pm 1.3% versus 32% \pm 1.3%) and IL-13 (mean \pm SEM, 34% \pm 1.2% versus 27% \pm 1.5%) protein was also reduced by 40% and 20%, respectively, (Figure 2B). As expected, the cytokine profile of ΔV Th1 cells was similar to that of WT Th1 cells (Figures 2A and 2B).

As a major product of Th2 cells that is also a potent inducer of Th2 cell differentiation, IL-4 is the key element of a positive-feedback mechanism that polarizes Th2 cell responses both in vitro and in vivo. To assess the requirement for HS V under conditions where this positive feedback was minimal, we generated heterozygous allelic reporter mice in which one *Il4* allele derives from

In Vivo Type 2 Responses in HS V-Deficient Mice

To determine the consequences of HS V deficiency in vivo, we used a mouse model of allergic airway disease. Airway

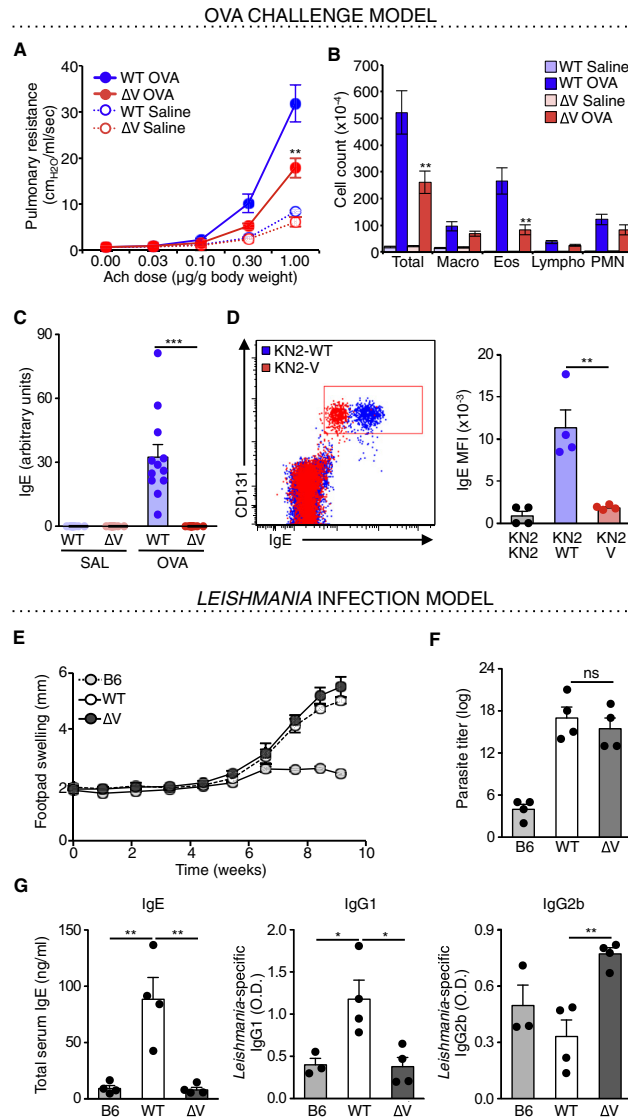


Figure 3. In Vivo Type 2 Responses in HS V-Deficient Mice

Cohorts of wild-type (WT) and HS V-deficient (ΔV) BALB/c mice were subjected to the ovalbumin (OVA) model of allergic airway disease.

(A) Airway hyperresponsiveness after saline ($n = 10$) and OVA challenge ($n = 12$) was measured as increasing pulmonary resistance in response to acetylcholine (ACh). Data are shown as mean \pm standard error mean (SEM). (B) Total number and cellular composition of the leukocytes in bronchoalveolar lavage fluid (mean \pm SEM); macrophages (Macro), eosinophils (Eos), lymphocytes (Lympho), and polymorphonuclear neutrophils (PMN). (C) Serum OVA-specific IgE abundance measured by ELISA ($n = 12$). Average (bars) of data from individual mice (filled circles) are shown; error bars are SEM.

(D) Overlay of dot plots showing IgE and CD131 staining of live, singlet-gated, CD45⁺ cells infiltrating the lungs of OVA-challenged KN2-WT and KN2-V mice. Graph at right shows mean fluorescence intensity (MFI) of IgE staining on basophils.

(E–G) Cohorts of four wild-type C57BL/6 (B6), wild-type BALB/c (WT), and HS V-deficient BALB/c (ΔV) mice were infected with *Leishmania major* promastigotes in the hind footpad.

(E) Footpad swelling over the course of infection. (F) Footpad parasite burden (log titer) 64 days after infection.

(G) ELISA measurement of total serum IgE and *Leishmania* freeze-thaw antigen-specific IgG1 and IgG2b.

n.s., no statistically significant difference ($p > 0.05$), * $p < 0.05$, ** $p < 0.01$, *** $p < 0.001$ with Student's t test.

Immunoglobulin (Ig) isotype switching to IgE, a hallmark of type 2 humoral immunity, is known to be critically dependent on IL-4 production (Finkelman et al., 1988; Reinhardt et al., 2009). Strikingly, the IgE response was completely abolished in ΔV mice (Figure 3C). Flow cytometric measurement of IgE bound to lung-infiltrating basophils confirmed an almost log-scale reduction in the amount of IgE present in ΔV mice (Figure 3D). Because basophil IgE staining in KN2-V mice was very similar to that seen in IL-4-deficient KN2-KN2 mice (Figure 3D), we conclude that HS V is critically required for IL-4 production by the cells that direct IgE responses in vivo.

To corroborate our findings on the effects of HS V deficiency in the asthma model in vivo, we utilized *Leishmania* infection. The magnitude of type 2 responses in this model inversely correlates with the capacity to clear parasites and resolve tissue inflammation (Mohrs et al., 2001). Thus, control C57BL/6 mice that primarily mount a type 1 response with abundant IFN- γ -producing Th1 cells effectively cleared the parasite. BALB/c mice, which mount a sustained type 2 response, showed a significant increase in the size of footpad lesions and parasite burden up to 10 weeks after infection (Figures 3E and 3F). We observed no difference between ΔV and WT BALB/c mice, suggesting that in this experimental

hyperresponsiveness (AHR) was reduced in OVA-challenged ΔV mice compared to WT controls (Figure 3A). Peribronchial and perivascular inflammatory infiltrates and mucus hypersecretion typical of allergic inflammation were preserved in ΔV mice (data not shown), but reduced numbers of eosinophils and lymphocytes were found in the bronchoalveolar lavage fluid (Figure 3B). Overall, therefore, the pathological type 2 cellular response in the lungs was partially diminished in ΔV mice.

system, there was no diminution in type 2 tissue responses in the absence of HS V (Figures 3E and 3F). Nevertheless, the type 2 humoral response was again significantly affected in the ΔV mice as reflected by the complete absence of IgE and a reduction of *Leishmania*-specific IgG1, which is also partly dependent on IL-4 (Kopf et al., 1993); *Leishmania*-specific IgG2b production, which is IL-4 independent, was unaffected (Figure 3G).

Together these results support an important role for HS V in type 2 humoral immunity in vivo. However, the dichotomous effects of HS V deficiency on the different arms of type 2 immune responses, namely the complete absence of the IL-4-dependent humoral response with at most a partial reduction in type 2 tissue responses, indicated that the cell types driving these responses were differentially affected by HS V deficiency.

HS V-Deficient Tfh Cells Develop Normally but Fail to Produce IL-4

Previous studies with KN2 mice showed that the vast majority of huCD2⁺ IL-4-competent cells in the lymph nodes are CXCR5⁺ PD-1^{hi} Tfh cells that reside in germinal centers and the follicular mantle zone (King and Mohrs, 2009; Reinhardt et al., 2009; Zaretsky et al., 2009). These Tfh cells, or their precursors generated early in immune responses, are the source of IL-4 and other signals that act on B cells to induce IgE and IgG1 production (King and Mohrs, 2009; Reinhardt et al., 2009; Zaretsky et al., 2009). The KN2 allele does not encode IL-4 protein but marks cells that are competent to make IL-4. Therefore, the allelic reporter mice allowed us to ask whether Tfh cells and other in-vivo-generated huCD2⁺ IL-4-competent cells require the HS V *cis*-regulatory region for IL-4 production from the other allele.

In the asthma model, we observed a significant induction (3%–4%) of huCD2⁺ T cells in the draining parathymic lymph nodes, but not in the nondraining inguinal nodes (0.1%–0.3%), 25 days after OVA immunization (Figure 4A, compare top and second panels). Consistent with previous reports (King and Mohrs, 2009; Reinhardt et al., 2009), equal numbers of huCD2⁺ IL-4-competent cells and CXCR5⁺PD-1^{hi} Tfh cells were observed in the parathymic lymph nodes of KN2-WT, KN2-V, and KN2-KN2 mice (Figure 4A, second and third panels; quantified in the bar graphs to the right), indicating that IL-4 (lacking in KN2-KN2 mice) and the enhancer activity of HS V (lacking in KN2-V compared to KN2-WT mice) are both dispensable for the generation of Tfh cells in vivo. CXCR5⁺PD-1^{hi} Tfh cells were predominantly huCD2⁺ (Figure 4A, third panel, inset histograms), implying that the majority of Tfh cells transcribed the KN2 reporter allele in vivo. Conversely, essentially all huCD2⁺ cells in the draining lymph nodes also expressed CXCR5 and PD-1 (Figure 4A, bottom panel), confirming that the vast majority of IL-4-competent T cells in this location are indeed Tfh cells under these experimental conditions.

The ability of these huCD2⁺ cells to produce cytokines from the wild-type or HS V-deficient *Il4* allele was assessed ex vivo by intracellular staining and flow cytometric analysis of IL-4 production after stimulation with PMA and ionomycin for 4 hr. We prevented surface expression of any new huCD2 by inhibiting protein transport with brefeldin A during the entire time of in vitro stimulation, allowing us to focus on cells that were already expressing huCD2 in vivo. As expected of Tfh cells (Reinhardt

et al., 2009), the huCD2⁺CD4⁺ cells from KN2-WT mice predominantly made IL-4 and not IL-13; strikingly, however, huCD2⁺CD4⁺ cells from KN2-V mice almost completely failed to make any IL-4 even under these supraphysiological stimulation conditions (Figure 4B, top panel). As expected, similar results were observed when we restricted our analysis to CXCR5⁺PD-1^{hi} Tfh cells (Figure 4B, bottom panel). Thus, in Tfh cells exhibiting normal expression of huCD2 from the KN2 *Il4* reporter allele, the HS V-deficient allele is completely unable to support IL-4 production, again indicating a critical *cis*-acting requirement for HS V for *Il4* expression in Tfh cells.

These findings were confirmed in *Leishmania* infection. When CD4⁺ T cells taken from the draining popliteal lymph nodes 10 weeks after infection were restimulated in vitro, we observed a significant reduction in the number of IL-4-producing cells in ΔV mice compared to WT BALB/c mice (Figure 4C). IL-4 production was also affected in vivo, as evidenced by the near absence of *Il4* mRNA in freshly isolated lymph node cells from ΔV mice (Figure 4D).

We next utilized an acute LCMV (lymphocytic choriomeningitis virus) infection model that allowed us to generate relatively larger numbers of IL-4-producing Tfh cells for undertaking detailed mRNA and chromatin analyses (Yusuf et al., 2010). Consistent with our findings in the OVA model, comparable numbers of CXCR5⁺PD-1^{hi} Tfh cells and germinal center B cells were observed in the lymph nodes and spleen of both WT and ΔV mice (Figures 4E and 4F). Expression of *Bcl6*, *Blimp1*, *ICOS*, SLAM-associated protein (SAP, encoded by *Sh2d1a*), and *Il21* mRNA in FACS-sorted CXCR5⁺PD-1^{hi} Tfh cells freshly isolated from lymph nodes and spleen were not significantly different between WT and ΔV mice (Figure 4G), further confirming that the enhancer activity of HS V is dispensable for the generation of Tfh cells in vivo. However, IL-4 production was significantly reduced in vivo, as evidenced by the near absence of *Il4* mRNA in the FACS-sorted CXCR5⁺PD-1^{hi} Tfh cells from ΔV mice (Figure 4H). We conclude that ΔV Tfh cells are phenotypically normal but have an isolated defect in *Il4* transcription.

Early IL-4 Production by Lymph Node T Cells Is Dependent on HS V

Because IgE is produced at early times after sensitization with OVA, we measured OVA-specific IgE, IgG1, and IgG2b at days 9 and 14 after primary immunization with OVA (Figure 5A). Comparison of KN2-WT and KN2-KN2 mice (which produce and lack IL-4, respectively) emphasized the requirement for IL-4 in IgE and IgG1 responses (Figure 5A, left and middle panels). KN2-V mice resembled KN2-KN2 mice in that they failed to generate an IgE response and produced markedly reduced quantities of OVA-specific IgG1 (Figure 5A, left and middle panels). The IL-4-independent IgG2b response was comparable in the three groups of mice (Figure 5A, right panel).

We also assessed cytokine production by huCD2⁺CD4⁺ Tfh cells after ex vivo stimulation on days 4 and 7 after intraperitoneal OVA-alum immunization. As before (Figure 4B), huCD2⁺ IL-4-competent parathymic lymph node T cells from KN2-V mice failed to produce IL-4 (Figure 5B). We obtained similar results when T cells in the lung-draining mediastinal nodes were analyzed after inhaled OVA challenge in the asthma model (Figure 5C). Together, these findings support a key *cis*-regulatory

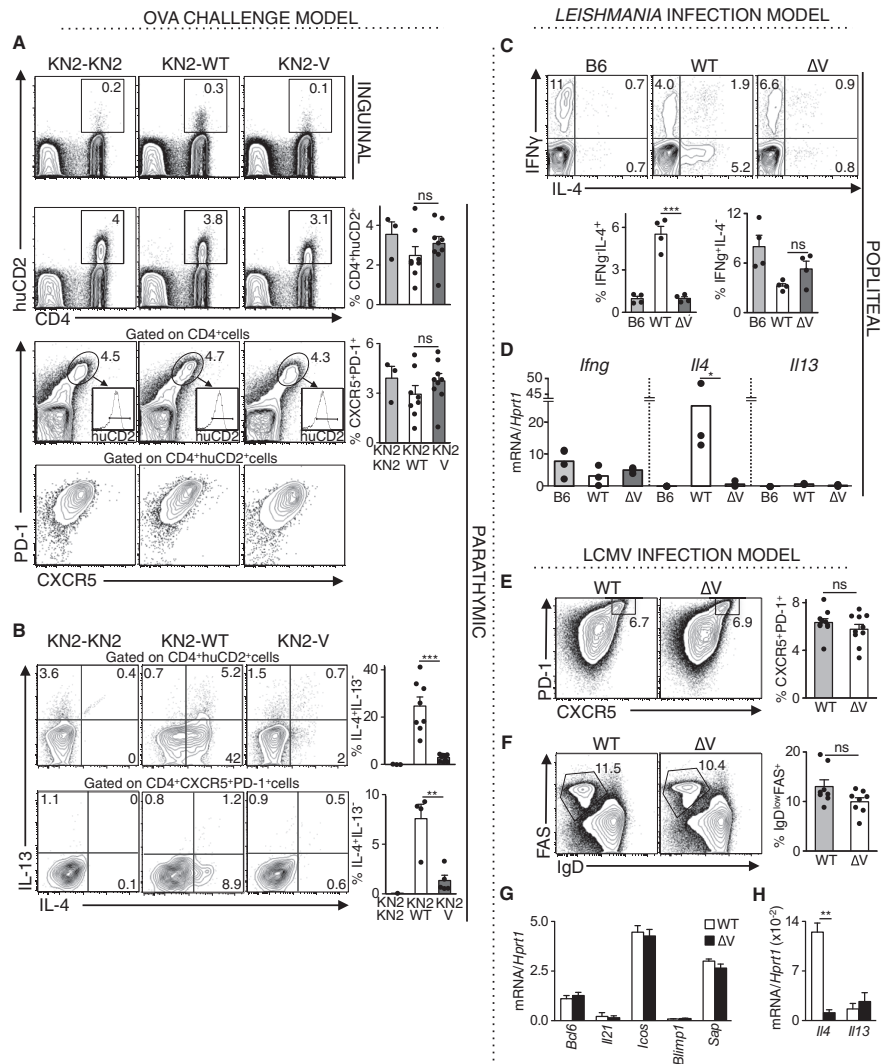


Figure 4. HS V-Deficient Tfh Cells Fail to Produce IL-4

(A) Cohorts of KN2-KN2, KN2-WT, and KN2-V BALB/c mice were subjected to the ovalbumin (OVA) model of allergic airway disease. Contour plots for CD4 and huCD2 show all live and singlet-gated lymph node cells. Numbers indicate percentage of cells that are huCD2⁺CD4⁺. Contour plots for CXCR5 and PD-1 show all CD4⁺CD8⁻B220⁻ cells (third row) or only huCD2⁺CD4⁺CD8⁻B220⁻ cells (fourth row). Numbers indicate percentage of CXCR5⁺PD-1⁺ cells; inset histograms show huCD2 staining of these cells. Bars represent the average and filled circles represent data from individual mice; error bars are standard error mean (SEM). (B) Contour plots show intracellular staining of cytokines in restimulated huCD2⁺CD4⁺ (top) and CXCR5⁺PD-1⁺ (bottom) lymph node cells described in (A). (C) Cohorts of wild-type C57BL/6 (B6), wild-type BALB/c (WT), and HS V-deficient BALB/c mice (ΔV) were infected with *L. major*. Ten weeks later, restimulated T cells in the draining popliteal lymph nodes were analyzed by flow cytometry. Contour plots show intracellular staining of cytokines in size-gated CD4⁺CD8⁻B220⁻ cells. Data are summarized in graphs shown below. (D) *Hprt1*-normalized *Ifng*, *Il4*, and *Il13* mRNA abundance in unstimulated popliteal lymph node cells from *L. major*-infected mice. (E and F) Cohorts of WT and HS V-deficient C57BL/6 mice ($n = 4-10$ per experiment) were infected with LCMV. Two weeks later, CD4⁺ T cells and B cells isolated from lymph nodes and spleen were analyzed by flow cytometry.

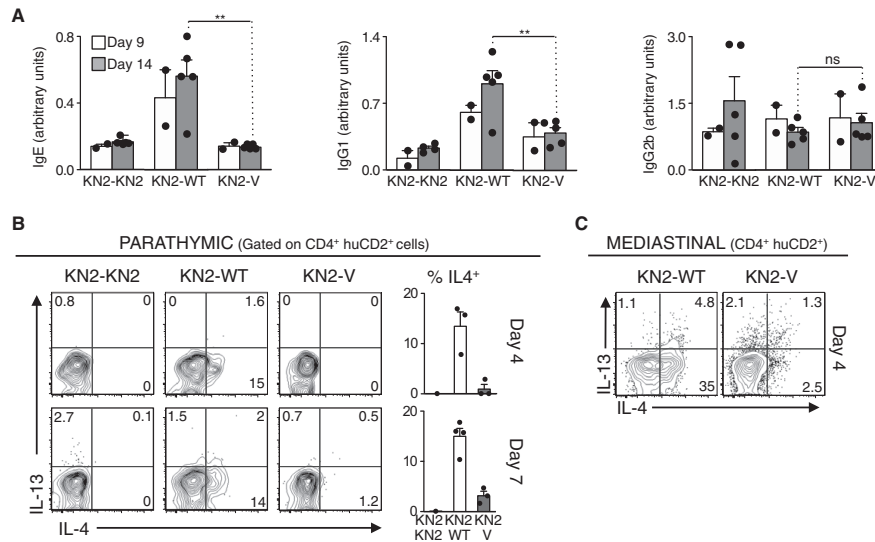


Figure 5. HS V-Deficient Lymph Node T Cells Fail to Produce IL-4 Early in the Primary Immune Response

Cohorts of KN2-KN2, KN2-WT, and KN2-V BALB/c mice were sensitized to ovalbumin by intraperitoneal immunization.

(A) ELISA measurement of ovalbumin-specific IgE, IgG1, and IgG2b levels in serum. Bars represent the average; error bars are SEM; circles represent data from each mouse.

(B) On days 4 and 7, the draining parathymic lymph node cells were stimulated *in vitro* with PMA, ionomycin, and brefeldin A for 4 hr and analyzed by flow cytometry. Contour plots show intracellular staining of cytokines in size-gated huCD2⁺CD4⁺CD8⁻B220⁻ cells. Data are summarized in the bar graphs to the right.

(C) Three weeks after sensitization, mice were intranasally challenged with ovalbumin for 3 consecutive days, and T cells in the lung-draining mediastinal lymph nodes were analyzed as described in (B).

function for HS V in T cells producing IL-4 very early in the immune response and suggest that Tfh cells and their early precursors share similar requirements for *Ii4* regulation.

Type 2 Tissue Responses in the Lungs of HS V-Deficient Mice

Given that tissue inflammation and AHR were less severely affected than humoral immune responses in ΔV mice, we hypothesized that the cell types and cytokines that drive type 2 tissue responses are less dependent than Tfh cells on HS V. To test this hypothesis, we again employed *Ii4* allelic reporter mice, in this case focusing on CD4⁺ T cells, basophils, and eosinophils as the three major IL-4-producing cell types in allergic lung inflammation (Mohrs et al., 2005; Voehringer et al., 2006).

In contrast to Tfh cells, lung-infiltrating Th2 cells produced IL-13 when restimulated *ex vivo* (Figure 6A, top left panel). Comparing KN2-KN2, KN2-WT, and KN2-V mice, a similar proportion of CD4⁺ T cells expressed huCD2 from the *Ii4* KN2

reporter allele, which has an intact HS V (Figure 6A, right top panel). Thus IL-4, which is absent in KN2-KN2 mice, is dispensable for the generation of CD4⁺ Th2 cells in this experimental system. However, the fraction of T cells able to express IL-4 protein from the other allele upon restimulation was reduced in KN2-V mice compared to KN2-WT mice (Figure 6A, top panels). This effect could not be explained by feedback from reduced IL-4 production *in vivo*, because it was apparent even when we restricted our analysis to huCD2⁺ T cells or to cells that produced IL-13 upon restimulation (Figure 6B, top panel). Thus, HS V enhances *Ii4* expression *in cis* in Th2 cells *in vivo*, consistent with our *in vitro* findings.

In contrast to Th2 cells, lung-infiltrating basophils produced IL-4 in an entirely HS V-independent fashion upon *in vitro* stimulation with PMA and ionomycin (Figure 6A, bottom panels). Moreover, *in vitro*, all huCD2⁺ basophils produced IL-4 and IL-13, confirming that HS V is not essential for IL-4 production by basophils (Figure 6B, bottom panel). We were unable to measure IL-4 protein production by eosinophils, but FACS-sorted eosinophils

(E) Contour plots for CXCR5 and PD-1 show size-gated CD4⁺CD44^{hi}CD62L⁻CD8⁻B220⁻ cells. Numbers indicate percentage of CXCR5⁺PD-1⁺ cells.

(F) Contour plots for IgD and FAS show size-gated CD19⁺CD4⁻CD8⁻ cells. Numbers indicate percentage of IgD⁺FAS⁺ cells. Summary of data from four independent experiments are shown in graphs at right.

(G and H) *Hprt1*-normalized *Bcl6*, *Blimp1*, ICOS, SLAM-associated protein (SAP, encoded by *Sh2d1a*), *Ii21*, *Ii4*, and *Ii13* mRNA in FACS-sorted pure populations of CXCR5⁺PD-1^{hi} Tfh cells, freshly isolated from lymph node cells and spleen of mice described in (E).

n.s., no statistically significant difference ($p > 0.05$), * $p < 0.05$, ** $p < 0.01$, *** $p < 0.001$ with Student's t test.

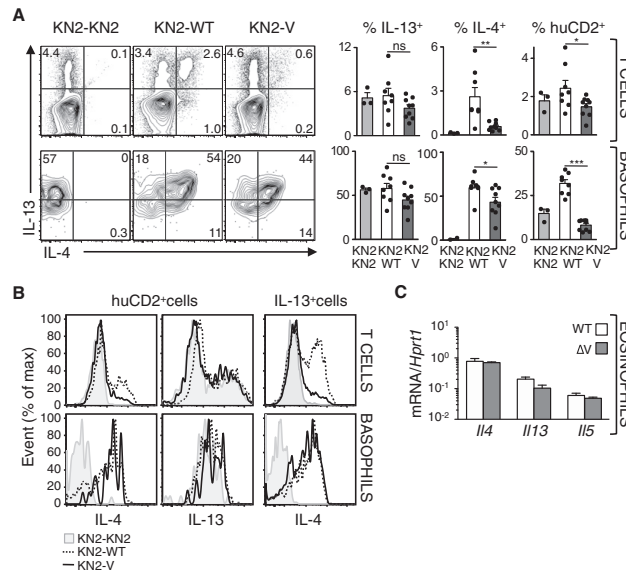


Figure 6. HS V Function in IL-4-Producing Cells Infiltrating the Lungs in a Murine Model of Asthma
Cohorts of KN2-KN2, KN2-WT, and KN2-V BALB/c mice were sensitized and challenged with ovalbumin to induce allergic airway inflammation. Lung-infiltrating cells were analyzed by flow cytometry after *in vitro* stimulation with PMA and ionomycin. See also Table S1.

(A) Contour plots show intracellular staining of cytokines in CD4⁺CD3⁺CD8⁻ B220⁻ cells (T cells) and CD45⁺IgE⁺CD49b⁺CD3⁻MHCII⁻ cells (basophils). See also Figure S4. Graphs at right show compiled data for IL-4, IL-13, and huCD2 expression. Bars represent the average; error bars are SEM; filled circles represent data from each mouse.

(B) Histograms of IL-4 and IL-13 staining in huCD2⁺ T cells and basophils, and IL-4 staining in IL-13⁺ cells as indicated.

(C) *Hprt1*-normalized cytokine mRNA abundance in FACS-sorted CD45⁺CD3⁻CD11b⁺MHCII⁻CD11c⁻Siglec F⁺ cells (eosinophils). See also Figure S4.

n.s., no statistically significant difference ($p > 0.05$), * $p < 0.05$, ** $p < 0.01$, *** $p < 0.001$ with Student's *t* test.

from the lungs of OVA-challenged WT and ΔV mice expressed *Ii4* mRNA at comparable levels (Figure 6C).

Notably, the proportion of basophils expressing huCD2 *in vivo* was reduced in KN2-KN2 mice compared with KN2-WT mice (Figure 6A, bottom right panel), indicating that IL-4 is important for basophil expression of *Ii4* *in vivo*. A similar reduction in huCD2⁺ basophils was also observed in KN2-V mice (Figure 6A, bottom right panel), suggesting that the source of IL-4 that affects basophil numbers *in vivo* is strongly HS V dependent. We speculate that because Tfh cells in KN2-KN2 and KN2-V mice cannot produce IL-4 (Figure 4B), the consequent drastic decrease in IgE (Figures 3 and 5) deprives basophils of their ability to use antigen-specific IgE to respond to OVA challenge *in vivo*.

In summary, unlike the Tfh cells that direct type 2 humoral responses and are strongly dependent on HS V, the cells and cytokines involved in type 2 tissue responses are less dependent, or only indirectly dependent, on HS V for IL-4 production.

HS V Affects Chromatin Accessibility and NFAT Binding to the *Ii4* Promoter

To investigate the mechanism by which HS V deficiency affected *Ii4* transcription in T cells, we first tested whether loss of HS V affected early transcription of the *Ii4* gene by naive T cells. Remarkably, naive T cells lacking the HS V (CNS2) region were completely unable to produce *Ii4* transcripts after *ex vivo* stimulation (Figure 7A). These findings are reminiscent of our observations in Tfh cells and their early precursors (Figures 4B, 4F, 5B, and 5C) and suggest that all of these cells share similar *cis*-regulatory requirements for *Ii4* transcription. In a similar time course assay, *in vitro*-differentiated Th2 cells showed only a 50% reduction in *Ii4* transcription (Figure 7B).

Ii4 transcription by naive T cells is strongly dependent on the NFAT-calcineurin pathway, as judged by sensitivity to the calcineurin inhibitor cyclosporin A (CsA) (Ansel et al., 2004) and by the binding of NFAT proteins to the *Ii4* promoter (Ansel et al., 2004). Chromatin immunoprecipitation (ChIP) assays performed after brief (45 min) stimulation showed that binding of the transcription factor NFAT1, the predominant NFAT family member in naive T cells (Macián et al., 2002), was severely reduced in ΔV naive T cells as well as polarized Th2 cell populations (Figures 7B, S3A, and S3B). Together, these results suggest an important role for a distal *cis*-regulatory region, HS V (CNS2), in facilitating NFAT1 binding to the *Ii4* promoter upon T cell activation.

The diminished binding of NFAT1 to the *Ii4* promoter in ΔV T cells prompted us to examine the effect of HS V deficiency on chromatin structure in the *Ii4* locus in naive T cells and differentiated Th2 cells (Figures 7C and 7D). Because *Ii4* transcription was selectively affected in T cells, with minimal or no effect on *Ii13* and *Ii5* expression, respectively, we focused on known *cis*-regulatory elements near the *Ii4* gene: the *Ii4* promoter; the 3' *Ii4* silencer, HS IV (Ansel et al., 2004); HS V_A (Agarwal et al., 2000; Agarwal and Rao, 1998); and HS V (CNS2) itself. We limited our analysis to two histone modifications whose association with gene expression has been thoroughly documented: histone-3 lysine-4 dimethylation (H3K4me2), a "permissive" modification found at enhancers and promoters whose presence correlates with increased chromatin accessibility to *trans*-factors (Birney et al., 2007); and H3K27me3, a "repressive" mark (Bernstein et al., 2006; Wei et al., 2009).

Of the four regions tested, HS V (CNS2) displayed by far the highest enrichment for H3K4me2 in naive T cells and Tfh cells (Figure 7C, black bars; Baguet and Bix, 2004). H3K4me2 was retained at HS V during Th2 cell differentiation and increased at the *Ii4* promoter and HS V_A (Figure 7C, black bars). HS V deficiency did not influence H3K4me2 levels in naive T cells and Tfh cells (Figure 7C, compare black and gray bars). In differentiated

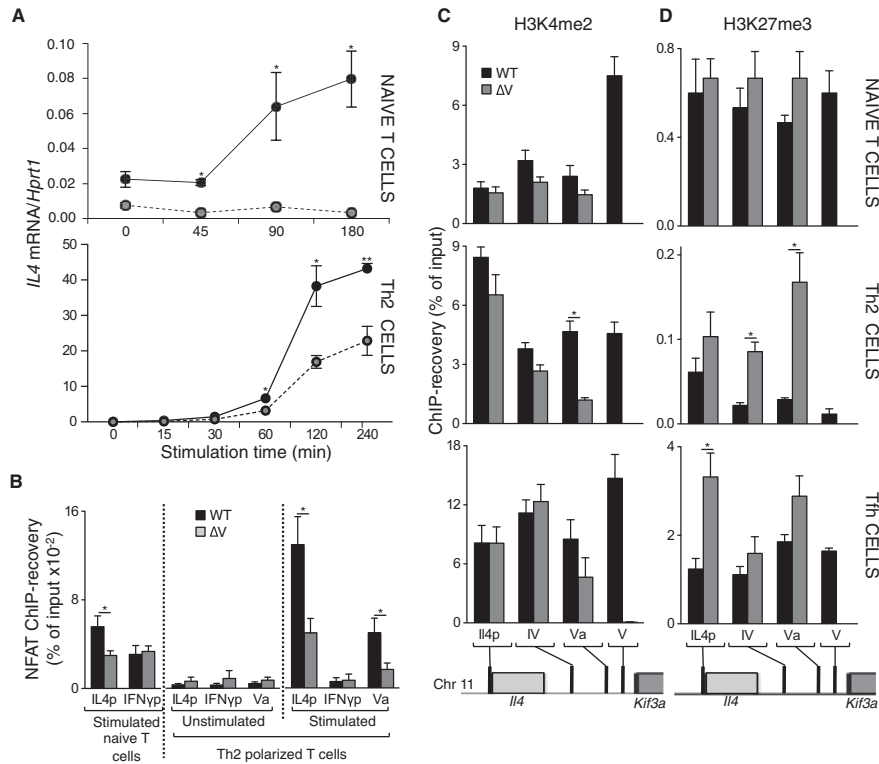


Figure 7. Chromatin Accessibility and NFAT Binding in the Th2 Cell Locus of HS V-Deficient T Cells

(A) *Hprt1*-normalized *Il4* mRNA abundance in wild-type (WT) and HS V-deficient (ΔV) naive T cells and Th2 cells (derived in vitro) stimulated with CD3 and CD28 antibodies and PMA and ionomycin, respectively, for the indicated times. Dots display average and error bars indicate standard error of mean (SEM).

(B) ChIP-PCR analysis: real-time PCR quantification of *Il4* promoter (IL-4p), HS V_A, and *Irfg* promoter (IFN γ p) sequences after ChIP with antibody to NFAT in WT and ΔV Th2 cells and naive T cells, either left unstimulated or stimulated for 45 min with PMA and ionomycin. Data are expressed as the normalized percentage of input DNA recovered and represent mean and SEM of at least three independent ChIP experiments. Data were normalized to the mean ChIP recovery of all experiments. Raw data from independent experiments are shown in Figures S3A and S3B.

(C and D) Real-time PCR quantification of *Il4* promoter (IL-4p), HS IV, HS V_A, and HS V sequences after anti-H3K4me2 (C) and anti-H3K27me3 (D) ChIP of chromatin extracts obtained from resting CD4⁺ naive T cells, Th2 cells derived in vitro, and Tfh cells derived in vivo from wild-type (WT) and HS V-deficient (ΔV) mice. Data are expressed as the percentage of input DNA recovered and represent mean and SEM of at least three independent ChIP experiments. Data from anti-H3K27me3 ChIP of Tfh cells were normalized and raw data from independent experiments are shown in Figure S3C. Real-time PCR quantification of control sequences is shown in Figure S3E. See also Figure S3D and Table S2.

ΔV Th2 cells, H3K4me2 levels remained lower than WT at HS V_A (Figure 7C).

In naive T cells, the *Il4* promoter and *cis*-regulatory regions were also substantially enriched for H3K27me3 (Figure 7D, top panel). Notably, however, Th2 cell differentiation led to a striking loss of the “repressive” H3K27me3 modification at all four tested regions of the *Il4* gene (Koyanagi et al., 2005) (Figure 7D, compare black bars in top and middle panels), and Th2 cells from ΔV mice incompletely erased the repressive H3K27me3 mark, especially at HS V_A (Figure 7D, middle panel, compare black and gray bars). Defective erasure of repressive H3K27me3 marks was also observed in ΔV Tfh cells, especially at the *Il4*

promoter (Figure 7D, bottom panel and Figure S3C). Together, these data indicate that HS V (CNS2) is an important player in the chromatin-remodeling events that normally establish an accessible conformation across the *Il4* locus in Th2 cells and Tfh cells.

DISCUSSION

We have performed a detailed analysis of mice bearing a precise deletion of HS V (CNS2). Our results show unambiguously that this conserved *cis*-regulatory element has an important and nonredundant function in enhancing *Il4* transcription. In

two *in vivo* models, HS V-deficient mice exhibited cell type-specific defects in *Ii4* expression that manifested in surprisingly dichotomous effects on type 2 immune responses *in vivo*—a profound reduction of type 2 humoral immunity with total abrogation of IgE production, in the face of only mildly attenuated or unaffected type 2 tissue inflammatory responses.

We used allelic IL-4 reporter mice to uncover differential requirements for HS V among the cell types that drive these responses. We show that Tfh cells, lymph node T cells that make IL-4 early in the primary immune response, and even naive T cells stimulated *ex vivo* are strikingly dependent on HS V for *Ii4* expression. These findings suggest that similar signals and transcription factors are responsible for *Ii4* expression in all of these lymph node-resident T cells and probably explain the total abrogation of IgE production and sharply reduced IgG1 responses observed in HS V-deficient mice.

In contrast, Th2 cells derived *in vivo* or *in vitro* were only partially dependent on HS V for *Ii4* expression. IL-4 signaling induces nuclear translocation of STAT6, which is a direct transactivator of both *Ii4* and *Gata3*. GATA3, in turn, binds to its own promoter and several *cis*-regulatory sites in the Th2 cell-type cytokine locus, forming a feedforward positive-feedback loop that drives Th2 cell differentiation and the production of IL-13 and IL-5 (Zhu et al., 2010). Notably, HS V deficiency had minimal or no effect on IL-13 or IL-5 production by Th2 cells *in vitro* or *in vivo*. Thus, Th2 cells access an HS V-independent IL-4-driven positive-feedback loop to drive powerful inflammatory responses in tissues. HS V continues to function as a local enhancer of *Ii4* in these cells but has only modest effects on their ability to marshal inflammatory responses.

Allergic inflammation in peripheral tissues also involves innate immune cells. A previous study detected HS V reporter transgenic activity in mast cells and basophils but found reduced IL-4 expression only in mast cells from mice lacking HS V and part of HS V_A (Yagi et al., 2007). Our findings indicate that HS V affects basophil production of IL-4 *in vivo* but probably through an indirect mechanism. Given the importance of IgE receptor signaling in basophil activation, it is quite likely that their reduced IL-4 production in HS V-deficient mice reflects the lack of allergen-specific IgE. This effect may also contribute to the mild reduction in lung inflammation and AHR in HS V-deficient mice.

Notch intracellular domain and its binding partner RBP-J κ bind to HS V and influence transcription of *Ii4* in transgenic reporter assays (Amsen et al., 2004; Fang et al., 2007; Tanaka et al., 2006). Disruption of the Notch signaling pathway in mice leads to impaired humoral responses, as evidenced by sharply reduced IgE and IgG1 production and a significant reduction in IL-4 production by T cells in the draining lymph nodes and spleen, which presumably were Tfh cells (Amsen et al., 2007; Tanaka et al., 2006; Tu et al., 2005). The similarity of these findings with our observations in ΔV mice suggest that Notch may mediate its effects on *Ii4* expression by Tfh cells more directly through HS V and implicates the Notch pathway as a critical regulator of Tfh cell function and humoral immunity. Further research is needed to determine the relative contribution of Notch and other *trans*-acting factors in HS V-dependent *Ii4* expression in Tfh cells and how these factors mediate their effects on *Ii4* locus chromatin structure and gene transcription.

To address the molecular mechanism by which HS V selectively affects *Ii4* gene transcription, we examined the chromatin structure and remodeling events in the *Ii4* locus during differentiation of naive cells into Th1, Th2 (*in vitro*), and Tfh (*in vivo*) cells. In naive T cells and Tfh cells, HS V displayed by far the highest enrichment for H3K4me2, suggesting increased chromatin accessibility at this site compared with other *cis*-regulatory elements in the locus (Baguet and Bix, 2004). HS V is also the only site of DNA demethylation between the *Ii4* promoter and the distal *Kif3a* gene in naive T cells, suggesting a high degree of accessibility to *trans*-acting factors during early stages of T cell differentiation when other *cis*-elements in the locus may be relatively inaccessible (Lee et al., 2002). This feature, and the ability of the HS V (CNS2) region to enhance *Ii4* transcription in a GATA3- and STAT6-independent manner, likely make HS V particularly critical for *Ii4* transcription in naive T cells, Tfh cells, as well as in T cells that produce IL-4 early in the *in vivo* immune response.

H3K27me3, a repressive chromatin modification extensively present in the Th2 cell-type cytokine locus of naive T cells, is removed during Th2 cell differentiation, but maintained during Th1 cell differentiation (Figures 7D and S3A; Koyanagi et al., 2005). In ΔV Th2 cells, erasure of the H3K27me3 mark was incomplete across the locus, especially at HS V_A, where the mark was not erased at all. The failure to erase these marks was particularly pronounced in ΔV Tfh cells, correlating with the stringent requirement for HS V for *Ii4* transcription in these cells. Further investigation is needed to determine whether HS V recruits histone demethylases to the locus and to probe the connection between removal of H3K27me3 marks and *Ii4* promoter and enhancer accessibility for NFAT and other transcription factors that mediate *Ii4* transcription.

In summary, our experiments have revealed a critical role for the distal *Ii4* enhancer HS V in Tfh cell function and consequently type 2 humoral immunity. Mechanistically, HS V (CNS2) has an important role in shaping chromatin structure in differentiating T cells, as well as facilitating access of *trans*-acting factors such as NFAT to the *Ii4* locus. Our data imply that Tfh cells and Th2 cells utilize distinct but overlapping molecular mechanisms to support *Ii4* locus activity and may provide insight for more targeted strategies to block pathology in allergic diseases.

EXPERIMENTAL PROCEDURES

Mice

Mice were used in accordance with protocols approved by the animal care and use committees of the CBR Institute for Biomedical Research, Harvard Medical School, UCSF, and LIAI. ΔV mice were generated with standard gene-targeting techniques (details in Supplemental Information).

T Cell Differentiation, FACS Analysis, and Quantification of Cytokine Messenger RNA Expression

Purification of CD4⁺ T cells from spleen and lymph nodes, *in vitro* induction of Th1 and Th2 cell differentiation, and restimulation for flow cytometric analysis of intracellular cytokine staining and messenger RNA expression levels were performed as described previously (Ansel et al., 2004) (details in Supplemental Information). In brief, purified CD4⁺ T cells were stimulated with hamster anti-mouse CD3 (clone 2C11, 0.25 μ g/ml) and hamster anti-mouse CD28 (clone 37.51, 1 μ g/ml) on plates coated with goat anti-hamster IgG (MP Biomedicals) for 48–60 hr under Th1 (IL-12 and anti-IL-4) and Th2 (IL-4, anti-IFN- γ , and anti-IL-12) cell or nonpolarizing conditions. After 2–3 days, cells were removed

from the plates and expanded in media with 20 U/ml of recombinant human IL-2 (National Cancer Institute) and analyzed on day 6. For short-term stimulation, 5×10^6 naive T cells were resuspended in media containing 0.5 $\mu\text{g/ml}$ anti-CD3 and 1 $\mu\text{g/ml}$ anti-CD28 and mixed with 2.5×10^7 latex beads (5 μm diameter; Interfacial Dynamics Corporation) coated with goat anti-hamster IgG. Unstimulated controls were cultured with beads but without anti-CD3 and anti-CD28 and were similar to cells held on ice.

Experimental Allergic Lung Disease Model and Antibody Production

Mice were immunized on days 1, 7, and 14 by intraperitoneal (i.p.) injection of 50 μg OVA (Grade V; Sigma Aldrich)/1 mg alum (Thermo Scientific) emulsion, followed by intranasal challenge with saline (control) or 100 μg OVA on days 21, 22, and 23 as described (Kuperman et al., 2002). On day 24, measurement of airway resistance and BAL fluid total and differential cell counts were performed as described (Kuperman et al., 2002). Primary immune response was induced by a single i.p. injection of 50 μg OVA/1 mg alum emulsion, and serum samples were obtained at different time points for measuring OVA-specific IgE, IgG1, and IgG2b antibodies by ELISA. Isolation and flow cytometric analysis of immune cells present in lungs and lymph nodes are described in the Supplemental Information.

Leishmania Infection Model

Amastigotes were serially passaged in the footpads of BALB/c mice to maintain *Leishmania major* LV39. Four mice per group were infected in the right hind footpad with 1×10^6 stationary-phase promastigotes. Lesion size was measured with a dial-gauge micrometer (Mitutoyo) biweekly beginning 1 week after infection. To evaluate footpad swelling, we determined the difference in measurement between the right hind footpad and the uninfected left hind footpad. Parasite burdens were counted by limiting dilution assays in which parasites were extracted from ground footpad tissue collected from individual mice. Serum was obtained 9 weeks after infection and total IgE and *Leishmania* freeze/thaw antigen-specific IgG1 and IgG2b levels were measured by ELISA. Cytokine mRNA from unstimulated popliteal lymph node cells (1×10^5) was measured by real-time quantitative PCR.

LCMV Infection Model

LCMV stocks were prepared and quantified as described (McCausland et al., 2007). All infections were done by i.p. injection of $1\text{--}2 \times 10^5$ PFU LCMV Armstrong per mouse. Two weeks after infection, CD4⁺ T cells were isolated from lymph nodes and spleen with a CD4-positive isolation kit (Dyna). Staining for flow cytometry was performed with fluorophore-conjugated antibodies against B220, CD8, PD-1, CD-44, CD62L, and CD4 (Ebioscience). CXCR5 staining was performed as described in the earlier section. CXCR5⁺PD-1^{hi} CD4⁺CD44^{hi}CD62L⁺CD8[−]B220[−] cells were sorted with a FACS Aria (Becton Dickinson). Three-quarters of the sorted Tfh cells were fixed (as described below) for chromatin analysis and one-quarter stored in Trizol for mRNA quantification by real-time PCR. For flow cytometric analysis of germinal center B cells, lymph node and spleen cells were stained with antibodies against CD19, CD4, CD8, PNA, FAS, GL7, and IgD and analyzed on a FACS Canto (Becton Dickinson).

Chromatin Immunoprecipitation

The detailed protocol is described in the Supplemental Information.

Statistical Analysis

A two-tailed Student's t test was used for statistical analysis. Differences with a p value of less than 0.05 were considered significant.

SUPPLEMENTAL INFORMATION

Supplemental Information includes Supplemental Experimental Procedures, four figures, and two tables and can be found with this article online at doi:10.1016/j.immuni.2011.12.014.

ACKNOWLEDGMENTS

The authors thank L. Du, L. Smith, E. Yanni, Z. Yang, Y. Soo Choi, and J. Yang for expert technical assistance and M. Kubo and S. Crotty for advice and

critical reading of the manuscript. This project was funded by the Burroughs Wellcome Fund (to K.M.A.), GSK National Clinician Scientist Fellowship Award and Peel Travel Fellowship Award in United Kingdom (to P.V.), NIH grants AI40127 and AI44432, and an award from the American Asthma Foundation (to A.R.). L.J.S. is a National Science Foundation Graduate Research Fellow. D.B. is the recipient of a Swiss National Science Foundation Postdoctoral Fellowship. P.V., G.S., K.M.A., and A.R. conceived the work, designed, performed and analyzed experiments, and wrote the paper; L.J.S., S.A.-W., J.J., I.M.D., and D.R.B. assisted in some of the experiments under the supervision of P.V., G.S., K.M.A., A.R., and A.H.S.; and X.H. performed some of the experiments with the model of allergic airway disease.

Received: June 1, 2011

Revised: November 18, 2011

Accepted: December 6, 2011

Published online: February 9, 2012

REFERENCES

- Agarwal, S., and Rao, A. (1998). Modulation of chromatin structure regulates cytokine gene expression during T cell differentiation. *Immunity* 9, 765–775.
- Agarwal, S., Avni, O., and Rao, A. (2000). Cell-type-restricted binding of the transcription factor NFAT to a distal IL-4 enhancer in vivo. *Immunity* 12, 643–652.
- Amson, D., Blander, J.M., Lee, G.R., Tanigaki, K., Honjo, T., and Flavell, R.A. (2004). Instruction of distinct CD4 T helper cell fates by different notch ligands on antigen-presenting cells. *Cell* 117, 515–526.
- Amson, D., Antov, A., Jankovic, D., Sher, A., Radtke, F., Souabni, A., Busslinger, M., McCright, B., Gridley, T., and Flavell, R.A. (2007). Direct regulation of Gata3 expression determines the T helper differentiation potential of Notch. *Immunity* 27, 89–99.
- Ansel, K.M., Greenwald, R.J., Agarwal, S., Bassing, C.H., Monticelli, S., Interlandi, J., Djuretic, I.M., Lee, D.U., Sharpe, A.H., Alt, F.W., and Rao, A. (2004). Deletion of a conserved I4 silencer impairs T helper type 1-mediated immunity. *Nat. Immunol.* 5, 1251–1259.
- Ansel, K.M., Djuretic, I., Tanasa, B., and Rao, A. (2006). Regulation of Th2 differentiation and I4 locus accessibility. *Annu. Rev. Immunol.* 24, 607–656.
- Baguette, A., and Bix, M. (2004). Chromatin landscape dynamics of the I4-I13 locus during T helper 1 and 2 development. *Proc. Natl. Acad. Sci. USA* 101, 11410–11415.
- Berger, S.L. (2007). The complex language of chromatin regulation during transcription. *Nature* 447, 407–412.
- Bernstein, B.E., Mikkelsen, T.S., Xie, X., Kamal, M., Huebert, D.J., Cuff, J., Fry, B., Meissner, A., Wernig, M., Plath, K., et al. (2006). A bivalent chromatin structure marks key developmental genes in embryonic stem cells. *Cell* 125, 315–326.
- Birney, E., Stamatoyannopoulos, J.A., Dutta, A., Guigó, R., Gingeras, T.R., Margulies, E.H., Weng, Z., Snyder, M., Dermitzakis, E.T., Thurman, R.E., et al. ENCODE Project Consortium; NISC Comparative Sequencing Program; Baylor College of Medicine Human Genome Sequencing Center; Washington University Genome Sequencing Center; Broad Institute; Children's Hospital Oakland Research Institute. (2007). Identification and analysis of functional elements in 1% of the human genome by the ENCODE pilot project. *Nature* 447, 799–816.
- Cai, S., Lee, C.C., and Kohwi-Shigematsu, T. (2006). SATB1 packages densely looped, transcriptionally active chromatin for coordinated expression of cytokine genes. *Nat. Genet.* 38, 1278–1288.
- Eise, K.J., Finkelman, F.D., Maliszewski, C.R., and Grencis, R.K. (1994). Cytokine-mediated regulation of chronic intestinal helminth infection. *J. Exp. Med.* 179, 347–351.
- Fang, T.C., Yashiro-Ohtani, Y., Del Bianco, C., Knoblock, D.M., Blacklow, S.C., and Pear, W.S. (2007). Notch directly regulates Gata3 expression during T helper 2 cell differentiation. *Immunity* 27, 100–110.

- Finkelman, F.D., Katona, I.M., Urban, J.F., Jr., Holmes, J., Ohara, J., Tung, A.S., Sample, J.V., and Paul, W.E. (1988). IL-4 is required to generate and sustain in vivo IgE responses. *J. Immunol.* **141**, 2335–2341.
- Heintzman, N.D., Hon, G.C., Hawkins, R.D., Kheradpour, P., Stark, A., Harp, L.F., Ye, Z., Lee, L.K., Stuart, R.K., Ching, C.W., et al. (2009). Histone modifications at human enhancers reflect global cell-type-specific gene expression. *Nature* **459**, 108–112.
- Kay, A.B. (2001a). Allergy and allergic diseases. First of two parts. *N. Engl. J. Med.* **344**, 30–37.
- Kay, A.B. (2001b). Allergy and allergic diseases. Second of two parts. *N. Engl. J. Med.* **344**, 109–113.
- Kim, H.Y., DeKruyff, R.H., and Umetsu, D.T. (2010). The many paths to asthma: phenotype shaped by innate and adaptive immunity. *Nat. Immunol.* **11**, 577–584.
- King, I.L., and Mohrs, M. (2009). IL-4-producing CD4⁺ T cells in reactive lymph nodes during helminth infection are T follicular helper cells. *J. Exp. Med.* **206**, 1001–1007.
- Koh, B.H., Hwang, S.S., Kim, J.Y., Lee, W., Kang, M.J., Lee, C.G., Park, J.W., Flavell, R.A., and Lee, G.R. (2010). Th2 LCR is essential for regulation of Th2 cytokine genes and for pathogenesis of allergic asthma. *Proc. Natl. Acad. Sci. USA* **107**, 10614–10619.
- Kopf, M., Le Gros, G., Bachmann, M., Lamers, M.C., Bluethmann, H., and Köhler, G. (1993). Disruption of the murine IL-4 gene blocks Th2 cytokine responses. *Nature* **362**, 245–248.
- Koyanagi, M., Baguet, A., Martens, J., Margueron, R., Jenuwein, T., and Bix, M. (2005). EZH2 and histone 3 trimethyl lysine 27 associated with Ii4 and Ii3 gene silencing in Th1 cells. *J. Biol. Chem.* **280**, 31470–31477.
- Kuperman, D.A., Huang, X., Koth, L.L., Chang, G.H., Dolganov, G.M., Zhu, Z., Elias, J.A., Sheppard, D., and Erle, D.J. (2002). Direct effects of interleukin-13 on epithelial cells cause airway hyperreactivity and mucus overproduction in asthma. *Nat. Med.* **8**, 885–889.
- Lee, D.U., Agarwal, S., and Rao, A. (2002). Th2 lineage commitment and efficient IL-4 production involves extended demethylation of the IL-4 gene. *Immunity* **16**, 649–660.
- Lee, G.R., Fields, P.E., Griffin, T.J., and Flavell, R.A. (2003). Regulation of the Th2 cytokine locus by a locus control region. *Immunity* **19**, 145–153.
- Levine, S.J., and Wenzel, S.E. (2010). Narrative review: the role of Th2 immune pathway modulation in the treatment of severe asthma and its phenotypes. *Ann. Intern. Med.* **152**, 232–237.
- Li, B., Carey, M., and Workman, J.L. (2007). The role of chromatin during transcription. *Cell* **128**, 707–719.
- Liao, W., Schones, D.E., Oh, J., Cui, Y., Cui, K., Roh, T.Y., Zhao, K., and Leonard, W.J. (2008). Priming for T helper type 2 differentiation by interleukin 2-mediated induction of interleukin 4 receptor alpha-chain expression. *Nat. Immunol.* **9**, 1288–1296.
- Loots, G.G., Locksley, R.M., Blankespoor, C.M., Wang, Z.E., Miller, W., Rubin, E.M., and Frazer, K.A. (2000). Identification of a coordinate regulator of interleukins 4, 13, and 5 by cross-species sequence comparisons. *Science* **288**, 136–140.
- Macián, F., García-Cózar, F., Im, S.H., Horton, H.F., Byrne, M.C., and Rao, A. (2002). Transcriptional mechanisms underlying lymphocyte tolerance. *Cell* **109**, 719–731.
- McCausland, M.M., Yusuf, I., Tran, H., Ono, N., Yanagi, Y., and Crotty, S. (2007). SAP regulation of follicular helper CD4 T cell development and humoral immunity is independent of SLAM and Fyn kinase. *J. Immunol.* **178**, 817–828.
- Mohrs, M., Blankespoor, C.M., Wang, Z.E., Loots, G.G., Afzal, V., Hadeiba, H., Shinkai, K., Rubin, E.M., and Locksley, R.M. (2001). Deletion of a coordinate regulator of type 2 cytokine expression in mice. *Nat. Immunol.* **2**, 842–847.
- Mohrs, K., Wakil, A.E., Killeen, N., Locksley, R.M., and Mohrs, M. (2005). A two-step process for cytokine production revealed by IL-4 dual-reporter mice. *Immunity* **23**, 419–429.
- Neill, D.R., Wong, S.H., Bellosi, A., Flynn, R.J., Daly, M., Langford, T.K., Bucks, C., Kane, C.M., Fallon, P.G., Pannell, R., et al. (2010). Nuocytes represent a new innate effector leukocyte that mediates type-2 immunity. *Nature* **464**, 1367–1370.
- Price, A.E., Liang, H.E., Sullivan, B.M., Reinhardt, R.L., Eisle, C.J., Erle, D.J., and Locksley, R.M. (2010). Systemically dispersed innate IL-13-expressing cells in type 2 immunity. *Proc. Natl. Acad. Sci. USA* **107**, 11489–11494.
- Reese, T.A., Liang, H.E., Tager, A.M., Luster, A.D., Van Rooijen, N., Voehringer, D., and Locksley, R.M. (2007). Chitin induces accumulation in tissue of innate immune cells associated with allergy. *Nature* **447**, 92–96.
- Reinhardt, R.L., Liang, H.E., and Locksley, R.M. (2009). Cytokine-secreting follicular T cells shape the antibody repertoire. *Nat. Immunol.* **10**, 385–393.
- Saenz, S.A., Siracusa, M.C., Perrigoue, J.G., Spencer, S.P., Urban, J.F., Jr., Tocker, J.E., Budelsky, A.L., Kleinschek, M.A., Kastelein, R.A., Kambayashi, T., et al. (2010). IL25 elicits a multipotent progenitor cell population that promotes T(H)2 cytokine responses. *Nature* **464**, 1362–1366.
- Sofi, M.H., Qiao, Y., Ansel, K.M., Kubo, M., and Chang, C.H. (2011). Induction and maintenance of IL-4 expression are regulated differently by the 3' enhancer in CD4 T cells. *J. Immunol.* **186**, 2792–2799.
- Solymer, D.C., Agarwal, S., Bassing, C.H., Alt, F.W., and Rao, A. (2002). A 3' enhancer in the IL-4 gene regulates cytokine production by Th2 cells and mast cells. *Immunity* **17**, 41–50.
- Tanaka, S., Tsukada, J., Suzuki, W., Hayashi, K., Tanigaki, K., Tsuji, M., Inoue, H., Honjo, T., and Kubo, M. (2006). The interleukin-4 enhancer CNS-2 is regulated by Notch signals and controls initial expression in NKT cells and memory-type CD4 T cells. *Immunity* **24**, 689–701.
- Tanaka, S., Motomura, Y., Suzuki, Y., Yagi, R., Inoue, H., Miyatake, S., and Kubo, M. (2011). The enhancer HS2 critically regulates GATA-3-mediated Ii4 transcription in T(H)2 cells. *Nat. Immunol.* **12**, 77–85.
- Tu, L., Fang, T.C., Artis, D., Shestova, O., Pross, S.E., Maillard, I., and Pear, W.S. (2005). Notch signaling is an important regulator of type 2 immunity. *J. Exp. Med.* **202**, 1037–1042.
- Visel, A., Blow, M.J., Li, Z., Zhang, T., Akiyama, J.A., Holt, A., Plajzer-Frick, I., Shoukry, M., Wright, C., Chen, F., et al. (2009a). CHIP-seq accurately predicts tissue-specific activity of enhancers. *Nature* **457**, 854–858.
- Visel, A., Rubin, E.M., and Pennacchio, L.A. (2009b). Genomic views of distant-acting enhancers. *Nature* **461**, 199–205.
- Voehringer, D., Shinkai, K., and Locksley, R.M. (2004). Type 2 immunity reflects orchestrated recruitment of cells committed to IL-4 production. *Immunity* **20**, 267–277.
- Voehringer, D., Reese, T.A., Huang, X., Shinkai, K., and Locksley, R.M. (2006). Type 2 immunity is controlled by IL-4/IL-13 expression in hematopoietic non-eosinophil cells of the innate immune system. *J. Exp. Med.* **203**, 1435–1446.
- Wei, G., Wei, L., Zhu, J., Zang, C., Hu-Li, J., Yao, Z., Cui, K., Kanno, Y., Roh, T.Y., Watford, W.T., et al. (2009). Global mapping of H3K4me3 and H3K27me3 reveals specificity and plasticity in lineage fate determination of differentiating CD4⁺ T cells. *Immunity* **30**, 155–167.
- Wei, L., Vahedi, G., Sun, H.W., Watford, W.T., Takatori, H., Ramos, H.L., Takahashi, H., Liang, J., Gutierrez-Cruz, G., Zang, C., et al. (2010). Discrete roles of STAT4 and STAT6 transcription factors in tuning epigenetic modifications and transcription during T helper cell differentiation. *Immunity* **32**, 840–851.
- Wilson, C.B., Rowell, E., and Sekimata, M. (2009). Epigenetic control of T-helper-cell differentiation. *Nat. Rev. Immunol.* **9**, 91–105.
- Wurster, A.L., and Pazin, M.J. (2008). BRG1-mediated chromatin remodeling regulates differentiation and gene expression of T helper cells. *Mol. Cell. Biol.* **28**, 7274–7285.
- Yagi, R., Tanaka, S., Motomura, Y., and Kubo, M. (2007). Regulation of the Ii4 gene is independently controlled by proximal and distal 3' enhancers in mast cells and basophils. *Mol. Cell. Biol.* **27**, 8087–8097.
- Yamashita, M., Hirahara, K., Shinakasu, R., Hosokawa, H., Norikane, S., Kimura, M.Y., Hasegawa, A., and Nakayama, T. (2006). Crucial role of MLL



for the maintenance of memory T helper type 2 cell responses. *Immunity* 24, 611–622.

Yusuf, I., Kageyama, R., Monticelli, L., Johnston, R.J., Ditoro, D., Hansen, K., Barnett, B., and Crotty, S. (2010). Germinal center T follicular helper cell IL-4 production is dependent on signaling lymphocytic activation molecule receptor (CD150). *J. Immunol.* 185, 190–202.

Zaretsky, A.G., Taylor, J.J., King, I.L., Marshall, F.A., Mohrs, M., and Pearce, E.J. (2009). T follicular helper cells differentiate from Th2 cells in response to helminth antigens. *J. Exp. Med.* 206, 991–999.

Zhu, J., Yamane, H., and Paul, W.E. (2010). Differentiation of effector CD4 T cell populations (*). *Annu. Rev. Immunol.* 28, 445–489.

Appendix 2

An integrated nano-scale approach to profile miRNAs in limited clinical samples

Grégory Seumois, Pandurangan Vijayanand, Christopher J Easley, Nada Omran, Lukas Kalinke, Mal North, Asha P Ganesan, Laura J Simpson, Nathan Hunkapiller, Felix Moltzahn, Prescott G Woodruff, John V Fahy, David J Erle, Ratko Djukanovic, Robert Blelloch, and K Mark Ansel.
Am J Clin Exp Immunology. 2012. 1(2); 70-89.

Original Article

An integrated nano-scale approach to profile miRNAs in limited clinical samples

Grégory Seumois^{1,2,3,8*}, Pandurangan Vijayanand^{1,2,3,8*}, Christopher J Easley⁴, Nada Omran², Lukas Kalinke², Mal North², Asha P Ganesan², Laura J Simpson^{1,7}, Nathan Hunkapiller⁵, Felix Moltzahn⁶, Prescott G Woodruff³, John V Fahy³, David J Erle^{3,4}, Ratko Djukanovic², Robert Blelloch⁶, K Mark Ansel^{1,7}

¹Sandler Asthma Basic Research Center, University of California San Francisco, San Francisco, CA, USA; ²Division of Infection, Inflammation and Immunity, University of Southampton, School of Medicine, Southampton NIHR Respiratory Biomedical Research Unit, Sir Henry Wellcome Laboratories, Southampton General Hospital, Southampton, UK; ³Pulmonary and Critical Care Division, Department of Medicine, University of California San Francisco; ⁴Lung Biology Center, University of California San Francisco; ⁵Center for Reproductive Sciences, Department of Obstetrics, Gynecology & Reproductive Sciences, University of California San Francisco; ⁶The Eli and Edythe Broad Center of Regeneration Medicine and Stem Cell Research, Center for Reproductive Sciences, and Department of Urology, University of California San Francisco; ⁷Department of Microbiology & Immunology, University of California San Francisco; ⁸Current address: Division of Cell Signaling and Gene Expression, La Jolla Institute for Allergy and Immunology, San Diego, USA. *These authors contributed equally to this work.

Received September 19, 2012; Accepted September 26, 2012; Epub September 27, 2012; Published November 30, 2012

Abstract: Profiling miRNA expression in cells that directly contribute to human disease pathogenesis is likely to aid the discovery of novel drug targets and biomarkers. However, tissue heterogeneity and the limited amount of human diseased tissue available for research purposes present fundamental difficulties that often constrain the scope and potential of such studies. We established a flow cytometry-based method for isolating pure populations of pathogenic T cells from bronchial biopsy samples of asthma patients, and optimized a high-throughput nano-scale qRT-PCR method capable of accurately measuring 96 miRNAs in as little as 100 cells. Comparison of circulating and airway T cells from healthy and asthmatic subjects revealed asthma-associated and tissue-specific miRNA expression patterns. These results establish the feasibility and utility of investigating miRNA expression in small populations of cells involved in asthma pathogenesis, and set a precedent for application of our nano-scale approach in other human diseases. The microarray data from this study (Figure 7) has been submitted to the NCBI Gene Expression Omnibus (GEO; <http://ncbi.nlm.nih.gov/geo>) under accession no. GSE31030.

Keywords: microRNA (miRNA), asthma, helper T cell, microfluidic, qPCR arrays

Introduction

MicroRNAs (miRNAs) have emerged as highly promising diagnostic and prognostic biomarkers of disease, and disease-associated miRNAs may also be attractive targets for therapy [1-5]. miRNA expression profiling in healthy and diseased tissue is an important first step for investigating the role of miRNAs in human diseases. However, these studies are often constrained by the limited quantity of tissue that can be obtained from diseased subjects for research purposes. In addition, the heterogeneous cellular composition of tissue samples can confound analyses by increasing the bio-

logical noise and masking subtle but biologically important changes in miRNA expression. In some studies, rare cell populations derived from human tissue samples have been expanded *ex vivo* to yield larger quantities of more homogenous cell populations [6, 7]. However, the information derived from these cells may not reflect the disease-specific changes that occur *in vivo* because of changes in cell biology that likely occur during *in vitro* culture. The use of blood samples as surrogates for diseased tissue may have utility for diseases caused by immune cells that recirculate through the bloodstream, yet even in this case isolating particular cell subsets may be necessary, and

Nano-scale miRNA profiling in asthma

this approach may still fail to capture disease-specific changes that occur only in affected tissues.

In this report, we present an integrated approach for miRNA expression profiling in clinical samples that overcomes the problems arising from tissue paucity and heterogeneity. We demonstrate the utility of this approach in an investigation of the role of miRNAs in human asthma, a common allergic airway disease that affects over 300 million people worldwide. miRNA expression profiling in pure populations of pathogenic T cells, isolated from well phenotyped patients with mild or moderately severe allergic asthma and healthy control volunteers, revealed miRNAs that were differentially expressed in T cells of asthma patients, including some miRNAs that exhibited airway tissue-specific changes in asthma. We further show that this technique has great potential for biomarker discovery by profiling miRNAs in biological fluids relevant to lung diseases, including sputum and bronchoalveolar lavage (BAL) supernatants. The nano-scale approach reported here will be useful to investigate the role of miRNAs in various other human diseases and in other experimental settings where it is desirable to profile expression in low abundance cell populations.

Materials and methods

Study subjects

The Ethics Committees of the Southampton University Hospitals Trust approved the study, and written informed consent was obtained from all subjects. Twelve subjects with asthma (6 with mild asthma never treated with corticosteroids and 6 subjects with moderate asthma treated with inhaled corticosteroids) [8], meeting established diagnostic criteria [9], and 10 healthy subjects were studied.

Sample acquisition, processing and cell sorting

Bronchial biopsy and BAL samples were acquired from 3 healthy and 12 asthmatic subjects (6 mild and 6 moderate) as described previously [10]. Biopsy samples were immediately dispersed by treating with collagenase I (Sigma, Poole, UK), reconstituted in RPMI 1640 at 1 mg per milliliter, for a 1-hour period at 37°C.

Nonspecific binding of antibodies to Fc receptors was blocked by pre-treating cells with 2 mg per milliliter of polyclonal human IgG (Sigma). Cells were then stained with fluorescently conjugated antibodies (Lin1 cocktail (includes CD3, CD14, CD16, CD19, CD20, and CD56) FITC-conjugated, anti-EpCAM PerCP-Cy5.5-conjugated, anti-CD8 APC-conjugated, anti-CD3 PE-Cy7-conjugated, anti-HLA-DR APC-Cy7-conjugated, all from BD Biosciences, Oxford, UK) and propidium iodide prior to analysis and sorting on the FACS Aria™ (BD Biosciences, Oxford, UK). T cells were identified following a serial gating strategy as previously described by us [10]. BAL cells were separated from the fluid phase and cells sorted as described for the biopsy samples.

For isolating T cell subtypes from blood samples, PBMCs were first separated into a CD4⁺ memory cells fraction and non-CD4⁺ memory cell fraction by use of the memory CD4⁺ T cell isolation kit (Miltenyi Biotec, Surrey, UK). The CD4⁺ memory cells were then stained with fluorescently conjugated antibodies (anti-CD45RA FITC-conjugated, anti-CD4 APC-Cy7-conjugated, anti-CCR4 PE-conjugated, and anti-CD25 APC-conjugated) and sorted on the FACS Aria™ to obtain two cell populations: CD4⁺CD45RA⁻CCR4⁻ and CD4⁺CD45RA⁺CCR4⁺CD25⁻. Naive T cells were sorted from the non-CD4⁺ memory cells following staining with anti-CD45RA FITC-conjugated, anti-CD4 PerCP-Cy5.5-conjugated, anti-CD62L APC-Cy7-conjugated antibodies and anti-CD45RO PE-conjugated.

Microarray

Fifty nanograms of total RNA was labeled and then hybridized onto custom-designed human miRNA arrays (Agilent, Palo Alto, US) following the manufacturer's instructions.

Nano-scale PCR

FACS sorted cells were stored in Trizol LS (Invitrogen, Cambridge, UK). Total RNA was extracted using the miRNeasy kit (Qiagen, Valencia, US) as per the manufacturer's instruction. The optional DNase treatment was included in our procedure. The amount of RNA in each clinical sample was quantified by using a highly sensitive real-time PCR-based assay that is based on detecting mRNA levels of a house-keeping gene (beta-2-microglobulin (B2M):

Nano-scale miRNA profiling in asthma

Fwd-5'-ctgccgtgtgaacca-tgtgacttt-3'; Rev-5'-tcggcactcttcaaacctccatga-3'; Taqman probe-5'-/56-FAM/agtgggatcgaga-catgtaagcagca/-3IABLK_FQ/-3'). A standard curve, which was generated using serial dilutions of known quantities of RNA, showed that the assay could linearly detect RNA concentrations ranging from 5ng to 1pg.

We adapted a previously described multiplex qRT-PCR [11]. Reverse transcription (RT) was performed in multiplex using 96 stem-loop primers at a final concentration of 1nM. Briefly, in a 4µl reaction volume, 1ng RNA was incubated with primers and RNase inhibitor (0.325U/µl) (Applied Biosystems Inc (ABI), Carlsbad, US) for 5 minutes at 65°C and then cooled down in ice for at least 2 minutes before adding 3µl of freshly prepared RT mix [8.75mM dNTPs, 25U multiscribe RTase, RTase 10X buffer, 0.43U/µl RNase inhibitor, all from ABI]. RT reaction was carried out in 7µl volume in the following sequence: 16°C for 30 minutes, 42°C for 30 minutes, 80°C for 5 minutes and, finally, 4°C prior to the next step. cDNA from the RT step was pre-amplified in a multiplex PCR reaction by adding 18µl of a pre-amp mix [96-plex forward primers 50nM, universal reverse primer 5mM, dNTPs 4mM, MgCl₂ 2mM, 2X Taqman Universal PCR master mix without AmpErase UNG, and 6.25U of AmpliTaq Gold DNA Polymerase II (ABI)]. The PCR pre-amplification reaction was carried out in a 25µl volume in the following sequence: 95°C for 10 minutes, 55°C for 1 minute, 12 to 24 cycles of (95°C for 1 second + 65°C for 1 minute) and, finally, 4°C prior to the next step. Excessive amounts of residual primers from the pre-amplification step were removed by treating the samples with 10ul of ExoSAP-IT™ (USB, Cleveland, US) for 15 minutes at 37°C, then at 85°C for a further 15 minutes and, finally, cool down to 4°C. Subsequently, the samples were run through a size-exclusion gel filtration column (Illustra Microspin G-50 column, GE Healthcare Biosciences, US). Two out of 40µl of cleaned-up pre-amplified samples was used for the nanoliter qPCR reactions performed on the Biomark high-throughput qPCR platform (Fluidigm, South San Francisco, USA). qPCR was carried out as per the manufacturer's instruction except that the annealing temperature during the PCR reaction was set at 55°C instead of 65°C. The data was analyzed using Biomark system software that incorpo-

rates an automatic noiseband threshold setting for each qPCR assay, and qPCR curve quality scoring and flagging to eliminate false positive signals. We use no RNA and no RT samples to establish the background signal for each miRNA assay, and eliminate all higher Ct values by redefining them as background + 0.1. The list of miRNAs that can be detected by each 96-plex mix (1 to 4) are available online: ansel.ucsf.edu/AJCEI2012.

Size-fractionation of RNA for parallel profiling of miRNA and mR5NA

Cell lysate stored in Trizol was mixed with chloroform (1 in 6 dilution), centrifuged for 20 minutes at 8000g and the aqueous phase containing the RNA was collected. Using a low concentration of ethanol (35% v/v) the large RNAs (>150nt) were first precipitated and captured in a collection column (RNeasy, Qiagen), whereas the small RNAs (<150nt) fraction, which do not precipitate in the low ethanol concentrations, are effectively separated and present in the flow through. The small RNAs can then be precipitated from the flow-through using a higher concentration of ethanol (75% v/v) and collected on a fresh column (MinElute, Qiagen). Samples that were stored in chaotropic buffer (RLT) were run through a Qiasredder column (Qiagen) and the eluate collected before the differential ethanol precipitation steps. RNA fractions were treated with DNase as per manufacturer's instructions (Qiagen).

Primer sequences

List of primers used for qPCR analysis: Eri-1 mRNA: Fwd-5'-cggctcagcagactcaaaca-3'; Rev-5'-ggcgtccatcataatccat-3'; Ctl-4 mRNA: Fwd-5'-actc-atgtaccaccgccata-3'; Rev-5'-ggg-catg-gttctggatcaat-3'; IL4 mRNA: Fwd-5'-agat-catc-ggcatt-tttgaacg-3'; Rev-5'-tttgccatccatcctc-cg-3'; 28S rRNA: Fwd-5'-ctcgtctgatctcggagctaa-3'; Rev-5'-actgagggaatcctggttagttct-3'; 5S rRNA: Fwd-5'-ctcgtctgatctcggagctaa-3'; Rev-5'-gtctccatc-caagtactaaccag-3'; 5.8S rRNA: Fwd-5'-atcgtaggcaccgctacgctgtctg-3'; Sno202 RNA: Fwd-5'-cgtctactgactgatgaaagtactt-3'; miRNA-146a: Fwd-5'-tgagaactgaattccatgggtt-3'; miRNA-15a: Fwd-5'-tagcagcacataatggtttgtg-3'; miRNA-21: Fwd-5'-tagcttatcagactgatgttg-3';

Nano-scale miRNA profiling in asthma

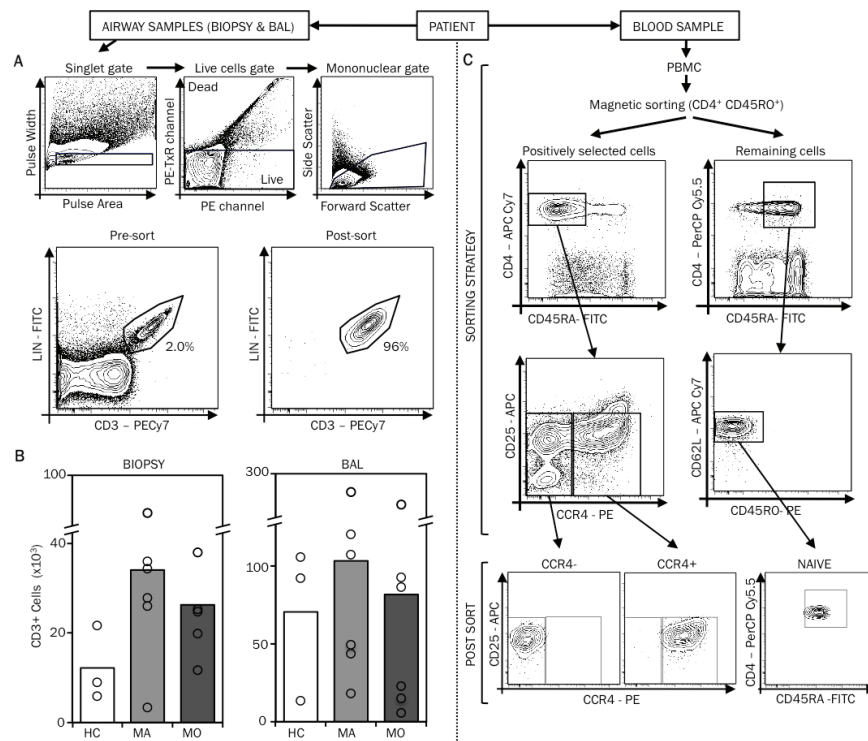


Figure 1. Isolation of T cells from bronchial biopsy specimens. **A.** Human bronchial biopsy specimens were enzymatically dispersed and cells stained with fluorescently conjugated antibodies (Lin1 cocktail includes CD3, CD14, CD16, CD19, CD20, and CD56) FITC-conjugated, anti-EpCAM PerCP-Cy5.5-conjugated, anti-CD8 APC-conjugated, anti-CD3 PE-Cy7-conjugated, anti-HLA-DR APC-Cy7-conjugated) and propidium iodide for analysis on the FACSARIA™. FACS plots illustrate the gating strategy used to identify T cells in these bronchial biopsy specimens. Utilizing this gating strategy, T cells populations were sorted by FACS. The FACS plots of the post-sort samples are also displayed. **B.** The mean and range of the numbers of T cells obtained from bronchial biopsy specimens and BAL of healthy controls (HC), mild (MA) and moderate (MO) asthmatic patients are displayed. **C.** From 100ml of blood, using the memory CD4⁺ T cell isolation kit, PBMC-CD4⁺ memory cell were first selected and were subsequently stained with fluorescently conjugated antibodies (anti-CD3 PE-Cy7-conjugated, anti-CD45RA FITC-conjugated, anti-CD4 APC-Cy7-conjugated, anti-CCR4 PE-conjugated, and anti-CD25 APC-conjugated) and sorted on the FACSARIA™ to obtain two cell populations: CD4⁺CD45RA⁺CCR4⁻ and CD4⁺CD45RA⁺CCR4⁺CD25⁻. Naive T cells were sorted from the non-CD4⁺ memory cells following staining with anti-CD3 PE-Cy7-conjugated, anti-CD45RA FITC-conjugated, anti-CD4 PerCP-Cy5.5-conjugated, anti-CD62L APC-Cy7-conjugated and anti-CD45RO PE-conjugated antibodies. The FACS plots illustrating the gating strategy and the post-sort cell populations are displayed.

Rev-Universal primer (NCode™ qRT-PCR Kit, Invitrogen).

Statistical analysis

qPCR data was normalized using the standard delta-Ct (Δ Ct) method by calculating the difference between the Ct value of the miRNA and

the mean Ct value of the housekeeping miRNAs, miR-103 and miR-191, in that sample. Quantile normalization and Δ Ct methods yielded very similar results (data not shown). Housekeeping miRNAs were repeated in each separate 96-plex mix. A two-way ANOVA linear model was fit to the normalized Δ Ct values for all miRNA to calculate t-statistic and the "nomi-

Nano-scale miRNA profiling in asthma

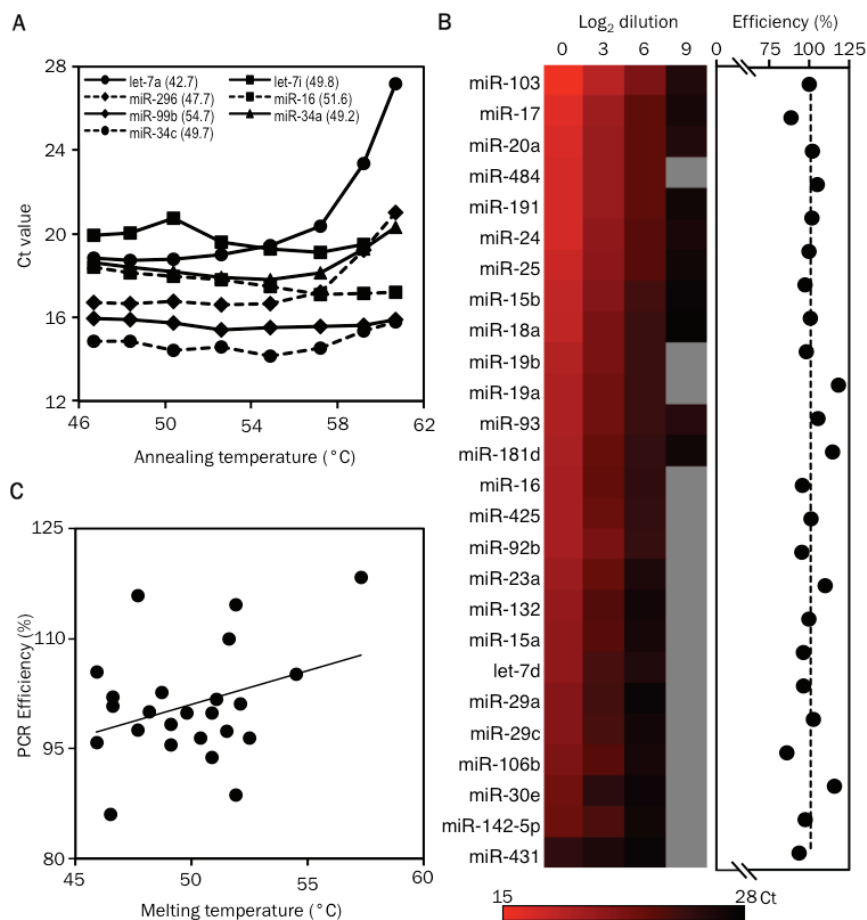


Figure 2. Validation of primer and probe sets for detecting human miRNAs. Validation of primer and probe sets for detecting human miRNAs. A. Gradient quantitative PCR showing the relationship between annealing temperature and threshold cycle of detection (Ct) for Let-7a, miR-292, miR-99b, miR-34c, Let-7i, miR-16 and miR-34. The melting temperatures of the Taqman probes used for detecting these miRNAs are shown in parenthesis. B. The heat map displays the Ct values for miRNAs measured in samples containing serial 8-fold dilutions of starting RNA material using the nanoscale PCR platform (mix 1). miRNAs that were not detected are shown in grey. The PCR efficiency for each miRNA is displayed as dots in the next graph. C. The graph displays the correlation between the PCR efficiency and the melting temperature of the Taqman probes used for detecting miRNAs.

nal p-value" for each miRNA for the comparisons of interest. A 3x3 model using both disease group and sample source as factors was made using the airway T cell data, and a 3x3 model using disease group and cell type was made for the blood T cells. All procedures were carried out using functions in the R package *limma* in *Bioconductor* [12]

Results

Isolation of pure populations of T cells from small bronchial biopsy specimens

Allergic airway inflammation and airway hyper-reactivity, the hallmarks of asthma, are orchestrated by Th2 cytokine-producing T cells (Th2

Nano-scale miRNA profiling in asthma

cells) that infiltrate the lung [13]. Based on the reasoning that the cells that drive asthma pathogenesis are most likely to bear functionally relevant disease-associated perturbations in miRNA expression, we analyzed *ex vivo* the T cells that infiltrate the diseased tissue, as well as circulating T cells capable of making Th2 cytokines.

To enable this analysis, we first established procedures to isolate pure populations of T cells from the airways and peripheral blood of patients with asthma. Using fiber-optic bronchoscopy, we obtained up to 8 small (2-3 mm) bronchial biopsies from patients with mild asthma (treated with bronchodilators alone, n=6), moderate asthma (treated with bronchodilators and inhaled corticosteroids, n=6), and healthy control subjects (n=3). The biopsy samples were enzymatically dispersed into single cell suspensions, labelled with fluorescently conjugated antibodies, and FACS sorted to obtain pure populations of T cells (**Figure 1A**) [14]. Using this approach, we isolated pure (>95%) populations of airway tissue-infiltrating T cells (mean±s.d.) (24200 ± 6300 cells) (**Figure 1B**). We also isolated airway-luminal T cells from bronchoalveolar lavage (BAL) fluid (mean±s.d.) (85200 ± 35900 cells), recognizing the possibility of functional differences between these two lung compartments (**Figure 1B**).

We recently showed that human Th2 cells reside in the CCR4⁺ memory CD4⁺ T cell fraction of blood T cells and that the proportion of CCR4⁺ cells in the blood increases with asthma severity [15]. To avoid mistaking differences in the relative abundance of Th2 cells for disease-specific changes in miRNA expression, and to capture changes that occur in a cell type-specific manner, we analyzed three purified populations of blood T cells (mean±s.d.): Th2-enriched CD4⁺CCR4⁺ memory T cells ($3.7 \pm 0.5 \times 10^6$); Th2-depleted CD4⁺CCR4⁻ memory T cells ($1.9 \pm 0.4 \times 10^6$); and uncommitted naïve CD4⁺ T cells ($1.5 \pm 0.3 \times 10^6$) (**Figure 1C**). The entire procedure for isolating airway and circulating T cell subtypes from each study subject was completed in less than 6 hours.

Validation of a high-throughput quantitative PCR method for miRNA detection

The small numbers of T cells obtained from bronchial biopsies provided insufficient materi-

al for miRNA profiling with microarrays or deep sequencing. Therefore, we optimized and validated an economical high-throughput quantitative RT-PCR method to permit measurement of miRNA abundance in a large number of small quantity clinical samples on the Fluidigm Biomark platform. Biomark dynamic arrays employ integrated fluid circuits for automated mixing of 96 template samples with 96 qPCR assays in preformed 7 nanoliter reaction chambers [16]. This method provided a high degree of reproducibility in replicate measurements, significant sample and reagent sparing, and the ability to perform 9216 simultaneous miRNA measurements.

For assay design, we adopted the previously described and broadly applied method of miRNA-specific reverse transcription with stem-loop primers, followed by quantitative PCR (qPCR) with a universal reverse primer and miRNA-specific forward primers and dual-labeled probes [17]. The short length of miRNAs (~22 nt) restricts assay design, resulting in a broad range of probe melting temperatures (42-60 °C). Temperature gradient qPCR on a conventional real-time thermocycler showed that assays with the lowest probe melting temperatures performed poorly at higher annealing temperatures, but all assays yielded optimal signals at 55°C (**Figure 2A**). We observed a mean PCR efficiency of $101 \pm 2\%$ for a larger panel of custom assays on the Biomark platform, with linear performance across as much as a 32,000-fold range of starting RNA concentrations (**Figure 2B**; data not shown). Importantly, we did not observe a correlation between PCR efficiency and probe melting temperature (**Figure 2C**).

Pre-amplification is an essential step for profiling miRNAs in limiting RNA samples

To minimize sample requirements, miRNAs in each sample were first reverse transcribed (RT) in multiplex using 96 miRNA-specific stem loop primers that correspond with the qPCR assays to be performed. PCR pre-amplification with corresponding forward primers is necessary to ensure adequate starting template concentration in nanoliter qPCR reactions, and this is especially true for limiting RNA samples [11]. Pre-amplification conditions and the number of amplification cycles must be optimized to

Nano-scale miRNA profiling in asthma

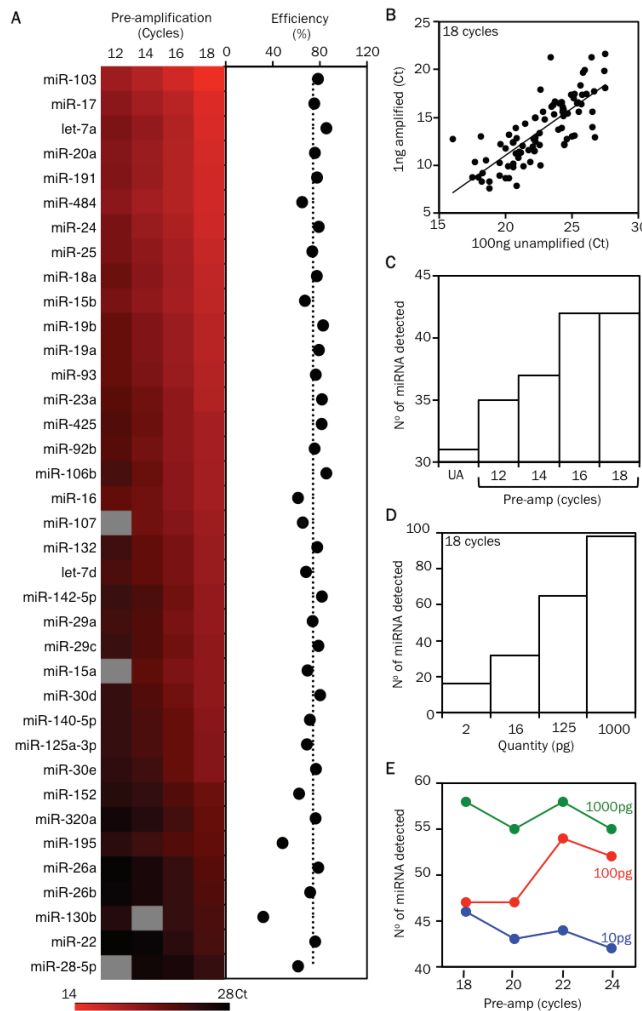


Figure 3. Optimizing the pre-amplification step for detecting miRNAs in samples with small cell numbers. A. Heat map displays the threshold cycle of detection (Ct) values of miRNAs detected in samples containing 1 ng of RNA that were pre-amplified by a 12, 14, 16 or 18 cycle 96-plex PCR reaction (mix 1). The PCR efficiency during the pre-amplification step for each miRNA is displayed as dots in the next graph. B. Comparison of the miRNA profile of unamplified cDNA (UA) from 100 ng (~100,000 cell equivalent) of RNA with cDNA from 1 ng (~1000 cell equivalent) of RNA after 18 cycles of 96-plex pre-amplification (mix 2-3). C. Bar graph displays the number of miRNAs detected in relation to the extent of pre-amplification (12, 14, 16 or 18 cycles) of cDNA from a 1 ng RNA sample (mix 1). D. Bar graph displays the number of miRNAs detected in relation to the starting amount of RNA (serial 8-fold dilutions of a 1 ng RNA sample) that was used for the 18 cycle pre-amplification step (mix 2-3). E. Displays the number of miRNAs detected in relation to the extent of pre-amplification (18, 20, 22 or 24 cycles) of cDNA from a 1 ng RNA sample (green line). Comparative data from 100 and 10 pg of starting RNA material are displayed in the red and blue lines, respectively (mix 4). The list of miRNAs that can be detected by each 96-plex mix (1 to 4) are available online: ansel.ucsf.edu/AJCEI2012.

obtain sufficient material for qPCR while avoiding PCR saturation or selective amplification of one or a few templates (“jackpotting”). To address these issues, we compared miRNA measurements for cDNA from 1 ng (~1000 cell equivalent) of RNA after 12, 14, 16, and 18 cycles of 96-plex pre-amplification. Linear pre-amplification was observed between 12 and 18 cycles at a PCR efficiency of $73 \pm 2\%$ for 37 miRNAs that yielded a product in at least three amplified samples (Figure 3A, 4). Measurements

for amplified samples correlated closely with measurements for unamplified cDNA from 100 ng (~100,000 cell equivalent) of the same RNA, indicating uniform miRNA pre-amplification (Figure 3A). Six poorly amplified outliers in early analyses were mostly eliminated by separating miRNAs with close sequence homology into separate groups to avoid primer competition. The one remaining outlier (miR-16) was still detected in a highly linear manner across pre-amplified samples with starting RNA quantities

Nano-scale miRNA profiling in asthma

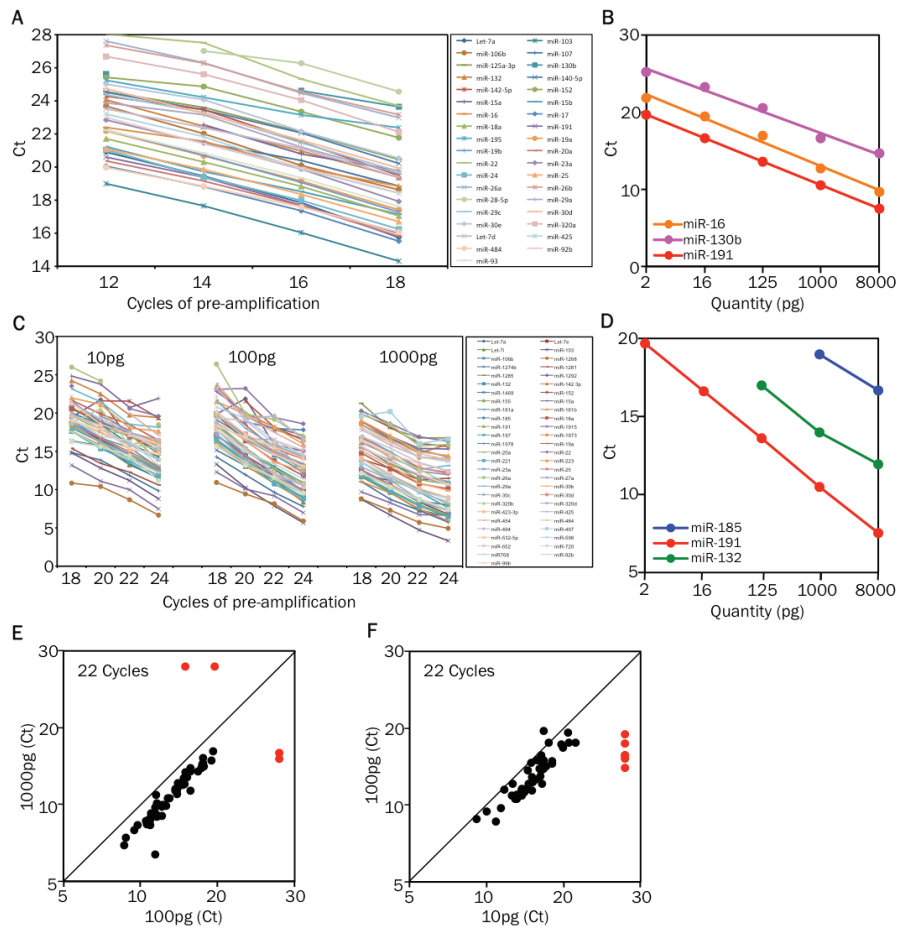


Figure 4. Optimizing the pre-amplification step for detecting miRNAs in samples with small cell numbers. A. Comparison of Ct values of multiple miRNAs in cDNA samples from 1 ng RNA after 12, 14, 16, and 18 cycles of 96-plex PCR pre-amplification (mix 1). B. The graph displays the threshold cycle of detection (Ct) values for miR-16, miR-130b and miR-191 in samples with starting RNA quantities ranging from 8 nanograms down to 2 picograms (pg) (mix 2). RNA from all samples were first reverse transcribed (RT) in multiplex using 96 miRNA-specific stem loop primers and the cDNA was pre-amplified by an 18 cycle 96-plex PCR reaction. C. Comparison of Ct values of multiple miRNAs in cDNA samples from 10 pg, 100pg, and 1000pg of RNA after 18, 20, 22, and 24 cycles of 96-plex PCR pre-amplification (mix4). D. The graph displays the Ct values for miR-191 (highly expressed), miR-132 (medium expression levels) and miR-185 (low abundance) in samples with starting RNA quantities ranging from 8 nanograms down to 2 picograms (pg) (mix 3). E. Comparison of the miRNA profile of cDNA from 10 pg (~10 cell equivalent) and 100 pg (~100 cell equivalent) of RNA after 22 cycles of 96-plex pre-amplification (mix 4). Threshold cycle of detection (Ct) values for miRNAs from the 10 pg and 100 pg samples are plotted on the x-axis and y-axis, respectively. The red dots indicate the miRNAs that were not detected in the 10 pg sample. F. Comparison of the miRNA profile of cDNA from 100 pg (~100 cell equivalent) and 1000 pg (~1000 cell equivalent) of RNA after 22 cycles of 96-plex pre-amplification (mix 4). Threshold cycle of detection (Ct) values for miRNAs from the 100 pg and 1000 pg samples are plotted on the y-axis and x-axis, respectively. The red dots indicate the miRNAs that were not detected in one or the other sample.

Nano-scale miRNA profiling in asthma

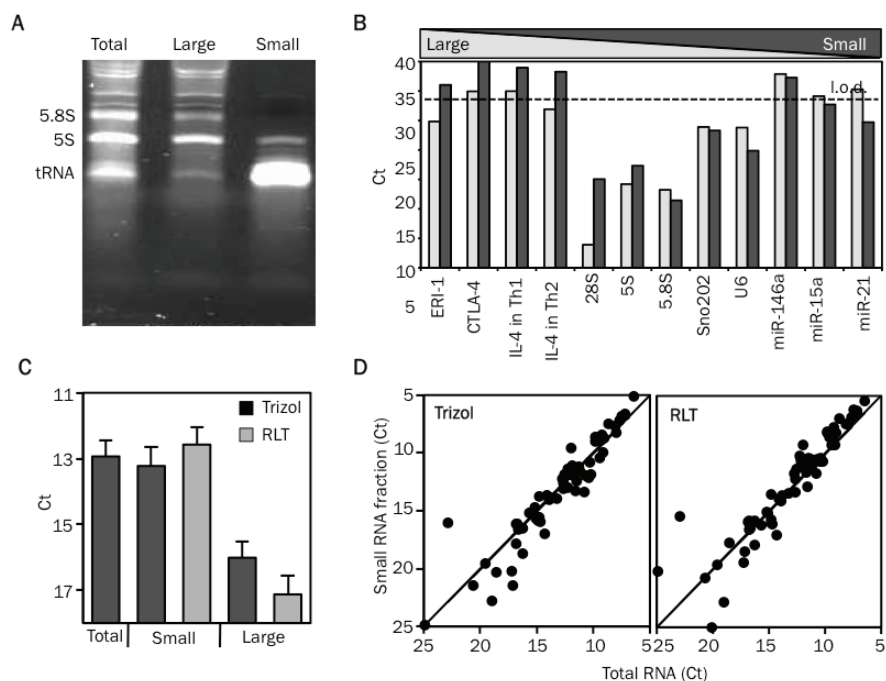


Figure 5. Size-fractionation of RNA enables parallel profiling of miRNA and mRNA. A. A 8% PAGE (polyacrylamide gel electrophoresis) gel illustrating the size profile of total RNA, large RNA fraction (Large) and small RNA fraction (Small). The major bands on the gel correspond to the 5.8S (158nt) and 5S (121nt) rRNA and to tRNAs. B. Bar graph illustrates the comparison of the different RNA populations present in large and small RNA fractions. It displays the threshold cycle of detection (Ct) values, for messenger RNAs (Eri-1, CTLA-4, IL-4), ribosomal RNAs (28S, 5.8S, 5S), small nuclear RNAs (Sno202, U6) and miRNAs (miR-146, miR-15b, miR-21) from large and small RNA fractions derived from mouse Th1 and Th2 cells. C. Displays the mean (+SEM) Ct values for all the miRNAs detected from total RNA, small RNA fraction prepared from samples stored in Trizol or RLT and large RNA fraction prepared from samples stored in Trizol or RLT. D. Comparison of the miRNA profile of a total RNA preparation with small RNA fraction prepared from cellular samples stored in RLT or Trizol. Threshold cycle of detection (Ct) values for miRNAs from the total RNA and small RNA fractionated samples are plotted on the x-axis and y-axis, respectively.

ranging from 8 ng down to 2 pg (~2 cell equivalent; **Figure 4B**). Therefore, we expect quantitative comparisons of miRNA expression between study subjects and cell types to be robust for all miRNAs, though quantitative comparison with other miRNAs within a sample may be skewed for a few poorly pre-amplified miRNAs.

We next determined the extent of pre-amplification that was required to reliably detect miRNAs present in limiting RNA samples. Eighteen cycles of pre-amplification gave the maximum yield of detectable miRNAs in 1 ng RNA samples (**Figure 3C**), and pre-amplification

remained unsaturated up to 22 cycles (**Figure 4C**). However, starting with smaller amounts of the same RNA progressively reduced the number of detectable miRNAs (**Figure 3D, 4D**). Increasing the extent of pre-amplification from 18 to 22 cycles for 100 pg RNA samples succeeded in recovering low abundance miRNAs without skewing the results (**Figure 3E, 4E**). miRNA measurements remained accurate even in 10 pg RNA samples (**Figure 4F**), though 24 cycles of pre-amplification were still insufficient to allow reliable detection of the least abundant miRNAs in these samples (**Figure 3E**).

Nano-scale miRNA profiling in asthma

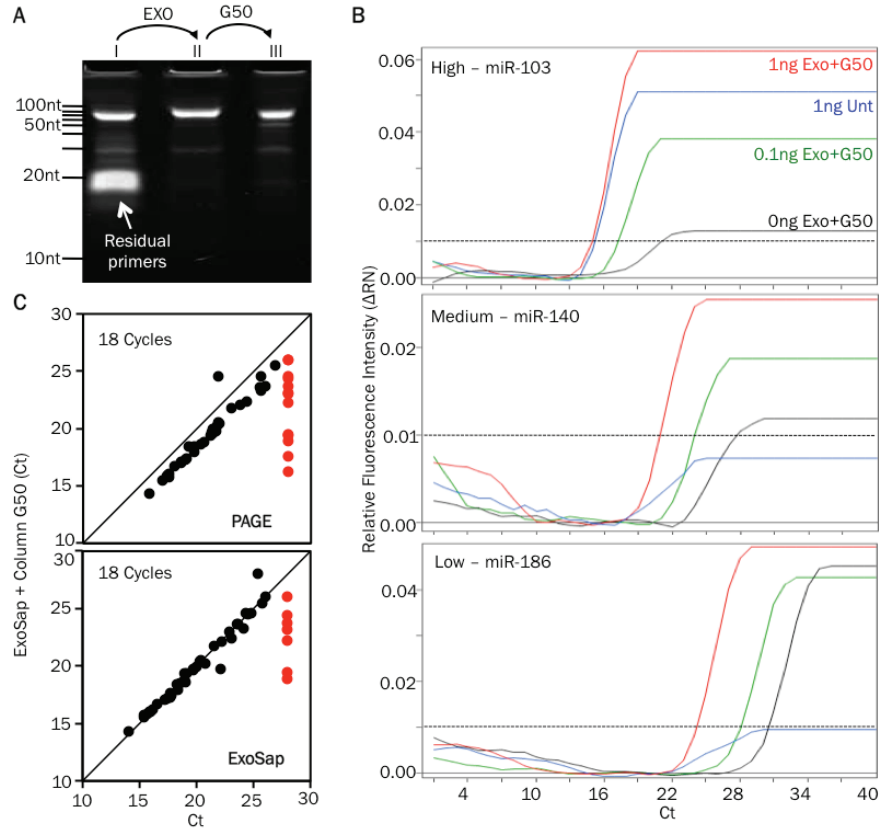


Figure 6. Clean-up of pre-amplified samples improves qPCR sensitivity. **A.** 11% PAGE (polyacrylamide gel electrophoresis) gel showing the PCR product (≈ 80 bp) and residual primers in untreated sample (lane I) (≈ 20 bp). Excess primers are eliminated following ExoSAP treatment (lane II) and gel filtration using G50 column (lane III). **B.** qPCR curves of 3 different miRNAs (miR103, -140, -186, which have high, medium and low expression levels in Th2 cells, respectively) before (blue line) and following purification with ExoSAP and G50 column (red line) of a 1ng pre-amplified RNA sample. Purified 0.1ng (green line) and 0ng (black line) RNA samples are shown (the black dotted line indicate the threshold of detection). **C.** Comparison of the miRNA profile of the ExoSAP + G50 column purified sample versus PAGE (upper plot) or ExoSAP only purified sample. Threshold cycle of detection (Ct) values for miRNAs the different methods compared are plotted. The red open dots indicate the miRNAs that were not detected by PAGE or ExoSAP only methods.

To further maximize the amount of biological information that can be obtained from limited quantities of human samples, we used RNA isolation strategies that fractionate large (>150 nt) and small (<150 nt) RNA into separate pools for mRNA and miRNA profiling, respectively (**Figure 5A, 5B**). Clinical samples stored in either phenol-based (i.e. Trizol) or chaotropic (i.e. RLT, QIAGEN) lysis solutions are compatible with this

strategy, and RNA fractionation did not skew or reduce the sensitivity of miRNA measurements (**Figure 5C, 5D**).

Optimized clean-up of pre-amplified templates improves qPCR sensitivity and specificity

For the higher PCR efficiency required for real-time detection in a Taqman assay, we and oth-

Nano-scale miRNA profiling in asthma

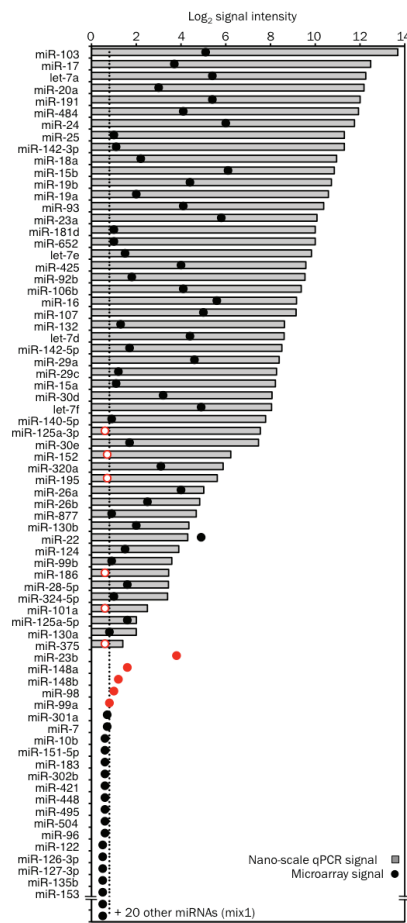


Figure 7. High concordance between nano-scale qPCR and microarray profiling data. RNA extracted from human Th2 cells was used for parallel profiling by both nano-scale PCR and microarray method. Fifty nanograms (ng) of RNA was used for the microarray method and cDNA from 1 ng (~1000 cell equivalent) of RNA, pre-amplified by 18 cycle PCR reaction, was used for miRNA detection by the nano-scale qPCR method (mix 1). The graph displays the intensity of the detection signals obtained by nano-scale qPCR and microarray method for 72 out of the 92 miRNAs that were assayed by qPCR. PCR signal intensity (grey bars) was calculated by subtracting the threshold cycle of detection (Ct) value for each miRNA from Ct of 28 (typical background signal on the Fluidigm Biomark). Array signal intensity (black dots) was calculated as the difference between the log2 intensity and the background signal measured for control probes. The miRNAs that were false positives in the

microarray method are displayed as closed red dots. The miRNAs that were detected by nano-scale qPCR but not by microarray (false negatives) are displayed as open red dots.

ers [11] have observed the need to reduce the annealing temperature during the PCR reaction to 55 °C from the 65 °C used in the pre-amplification step. The lower annealing temperature can result in non-specific product formation, especially when using the pre-amplified samples that have >100 residual unused primers from the 96-plex PCR reaction. Non-specific product formation can reduce the sensitivity and specificity of the assay. To overcome this problem, removing primer and dNTP contaminants has recently been shown to improve the specificity of the assay [18]. To optimize yield and reproducibility while minimizing sample cross-contamination, we developed a high-throughput method for cleaning up pre-amplified samples. We used ExoSAP™ reagent that utilizes two hydrolytic enzymes, Exonuclease I and Shrimp Alkaline Phosphatase to remove unwanted dNTPs and primers from the pre-amplified PCR template (Figure 6A). Exonuclease I degrades excess single-stranded primers and any extraneous single-stranded DNA produced in the PCR reaction. Shrimp Alkaline Phosphatase dephosphorylates remaining dNTPs from the PCR mixture. Free nucleotide monophosphates that result from ExoSAP treatment were then removed with gel filtration spin columns (G50) in single or 96-well plate form.

To compare the effectiveness of the various clean up steps, we divided a single pre-amplified product into 4 parts and subjected each part to a specific clean-up method: polyacrylamide gel electrophoresis (PAGE) purification, ExoSAP treatment only, ExoSAP treatment followed by column purification, and no clean-up. We then used nano-scale qPCR to profile 94 miRNAs concurrently for all 4 samples. Clean-up by exonuclease treatment followed by column purification improved the signal (Ct values) of the miRNAs detected when compared to the no clean-up sample (Figure 6B). This clean-up procedure yielded results that are highly comparable with PAGE purification, a low throughput gold standard (Figure 6C, top panel). The addition of a column purification step had a modest but definite improvement in the sensi-

Nano-scale miRNA profiling in asthma

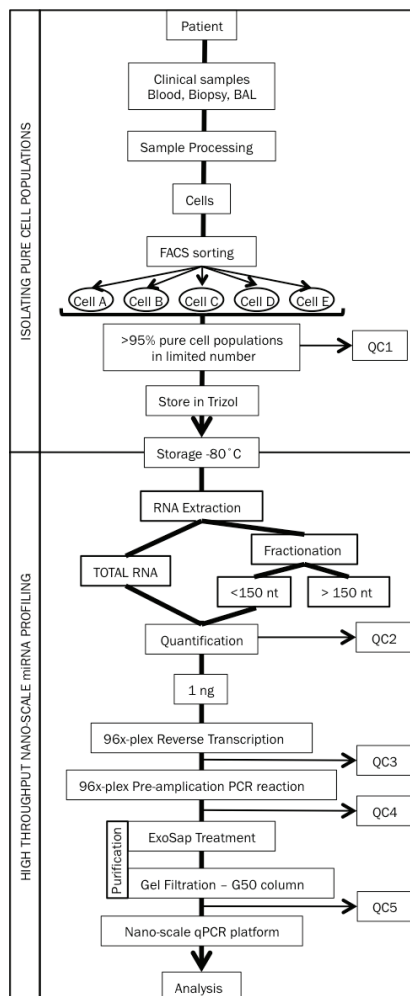


Figure 8. Experimental overview of our nano-scale approach to profiling miRNA in clinical samples from asthma patients. QC 1 to 5 are five mandatory quality control steps included in our approach.

tivity of the assay (**Figure 6C**, bottom panel). We conclude that cleaning-up pre-amplified samples critically improves the sensitivity and specificity of qPCR profiling. We routinely perform this optimized and efficient enzymatic and column purification method for all clinical samples.

Nano-scale qPCR is comparable to microarray-based profiling

We next analyzed the concordance in results obtained by nano-scale qPCR and miRNA microarrays. Fifty-one out of the 92 miRNAs assayed in 1 ng of RNA from *in vitro* derived human T helper type 2 (Th2) cells [19] were detected by nano-scale qPCR. Of these, 45 were detected by microarray analysis of 50 ng of the same RNA sample (**Figure 7**), including the 32 miRNAs with the strongest signal intensities on the nano-scale qPCR platform (**Figure 7**). As previously described, qPCR delivered globally higher signal intensities above background than microarrays, which suffer from considerable data compression as well as signal variability due to differences in hybridization to short miRNA probes [20]. The 6 miRNAs detected only by nano-scale qPCR had microarray signals very close to background (**Figure 7**). We confirmed a low level of expression in Th2 cells for four of these miRNAs by single-plex qRT-PCR on a conventional thermocycler, though miR-375 and miR-101a remained at or below the limit of detection (data not shown). We also found supporting evidence for the expression of all six of these miRNAs in published sequencing data for human T cells [21].

Nano-scale qPCR failed to detect miR-23b, miR-148a, miR-148b, miR-99a and miR-98, even though these miRNAs gave weak positive signals on the microarray and in single-plex qPCR on a conventional thermocycler (**Figure 7**). Nano-scale qPCR detected high levels of miRNAs with close sequence homology (miR-23a, miR-152, miR-99b and let-7 family) in the same samples, suggesting inhibitory primer or template competition among closely related miRNA assays. It has been shown that stem-loop qPCR can distinguish closely related miRNAs [11]. These results strongly suggest the qPCR data were accurate, whereas false positives arose in microarray analyses due to cross-hybridization of related miRNAs.

miRNA profile of T lymphocyte subtypes in blood from asthma patients

To demonstrate the utility of our nano-scale approach in identifying disease-associated miRNA signatures, we first profiled miRNA expression in circulating CD4⁺ T cells subtypes from patients with mild or moderate asthma

Nano-scale miRNA profiling in asthma

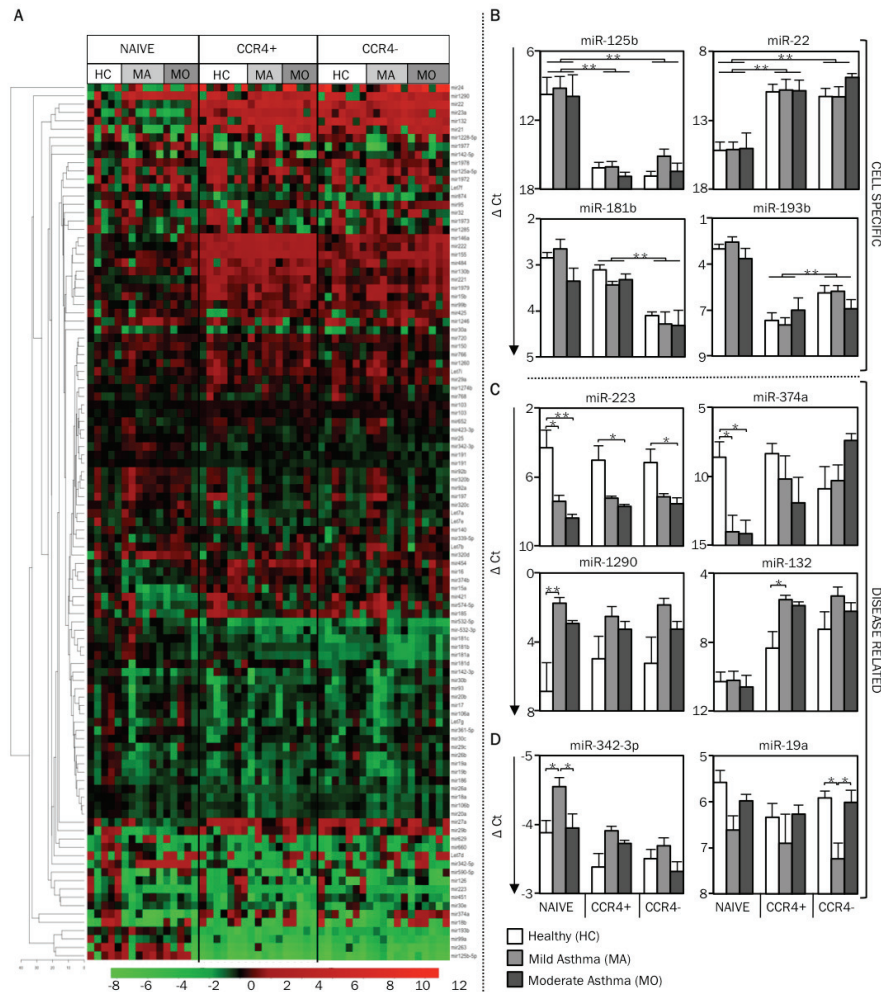


Figure 9. miRNA profile of circulating T cell subtypes in human asthma. **A** Using nano-scale PCR, miRNA expression levels were measured in circulating CD4⁺ T cell subtypes (naïve, memory CCR4⁺, and memory CCR4⁻) from 7 healthy subjects (HC), 6 mild asthmatic (MA) and 6 moderate asthmatic (MO) subjects. The heat map displays the expression levels of miRNAs in each sample (all cell types from every study subject shown) relative to the expression levels seen in naïve T cells of healthy control subjects. Expression levels of miRNAs (Δ Ct) in each sample was first calculated by subtracting the Ct value of the miRNA from the mean Ct value of the housekeeping miRNAs, miR-103 and miR-191, in that sample. The relative expression levels ($\Delta\Delta$ Ct), displayed in the heat map, were calculated by subtracting the Δ Ct values for each miRNA from the average Δ Ct values of the same miRNA in naïve T cells of healthy control subjects. The miRNAs are hierarchically clustered using Euclidean distance with average linkage. The samples are in a fixed order, sorted by cell type, then disease group. **B** The graph displays the mean (+SEM) expression levels of miR-125b, miR-22, miR-181b, and miR-193b to illustrate cell type-specific differences in miRNA expression levels. (**C**, **D**) The graph displays the mean (+SEM) expression levels of miR-223, miR-374a, miR-1290, miR-132, miR-342-3p and miR-19a to illustrate disease-related differences in miRNA expression levels. *p*-values were obtained by ANOVA, * *p* < 0.01, ** *p* < 0.001.

Nano-scale miRNA profiling in asthma

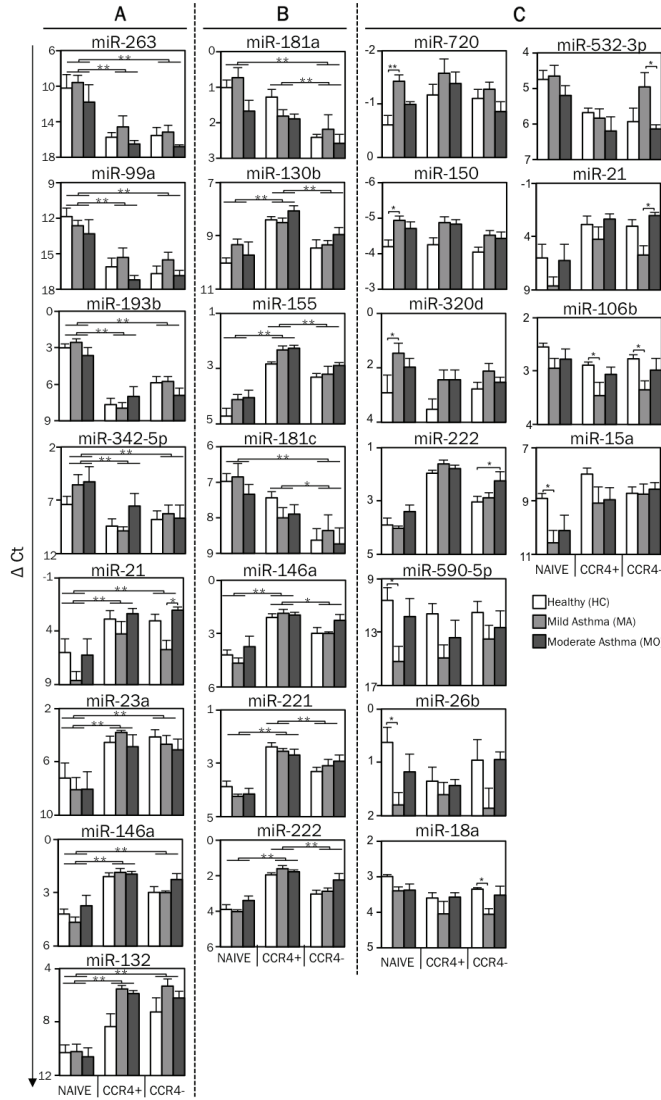


Figure 10. miRNA profile of circulating T cell subtypes in human asthma. A. Using nano-scale PCR, miRNA expression levels were measured in circulating CD4+ T cell subtypes (naïve, memory CCR4+, and memory CCR4-) from 7 healthy subjects (HC), 6 mild asthmatic (MA) and 6 moderate asthmatic (MO) subjects. Expression levels of miRNAs (Δ Ct) in each sample was first calculated by subtracting the Ct value of the miRNA from the mean Ct value of the housekeeping miRNAs, miR-103 and miR-191, in that sample. The graph displays the mean (+SEM) expression levels of miR-263, miR-21, miR-99a, miR-23a, miR-193b, miR-146a, miR-342-5p and miR-132 to illustrate cell type-specific differences in miRNA expression levels between naïve and memory T cells. B. The graph displays the mean (+SEM) expression levels of miR-181a, miR-181c, miR-130b, miR-146a, miR-155, miR-221, and miR-222 to illustrate cell type-specific differences in miRNA expression levels between CCR4+ and CCR4- memory T cells. C. The graph displays the mean (+SEM) expression levels of miR-720, miR-590-5p, miR-150, miR-26b, miR-320d, miR-18a, miR-222, miR-18a, miR-222, miR-15a, miR-532-3p, miR-21 and miR-106b to illustrate disease-related differences in miRNA expression levels. *p*-values were obtained by ANOVA, * *p* < 0.01, ** *p* < 0.001.

and healthy control subjects (overall strategy outlined in **Figure 8**). In view of their central role in asthma pathogenesis, we compared enriched Th2 cells (CCR4+) with the remaining non-Th2 cells (CCR4-) and circulating naïve helper T cells (CD45RA+). We restricted our qPCR assays to the 188 miRNAs detected in human CD4+ T cells based on published sequencing data and

microarray profiling (data not shown) [21]. We separated primers for closely related miRNAs into two 96-plex pools for the multiplex RT and pre-amplification reactions (mix 2 and 3; data not shown). This approach allowed us to profile 190 miRNAs in each individual subject with just 2 nanograms (~2000 cell equivalent) of RNA. Since Ct values for miR-103 and miR-191 var-

Nano-scale miRNA profiling in asthma

Table 1. Statistical analysis of miRNA expression levels in cell types. Values listed in the columns under cell types are the difference (Δ Ct) between the Ct value for each miRNA and the mean of Ct values for these two housekeeping miRNAs (miR-103, miR-191) in the same sample. miRNAs with a fold change >2 are shown. (FDR – False discovery rate)

Naive vs CCR4-	Healthy Controls		Mild Asthma		Moderate asthma		Statistics		
	Naive	CCR4-	Naive	CCR4-	Naive	CCR4-	M (Δ Ct)	Fold Change	FDR
mir24	13.80	9.69	13.78	9.78	10.39	5.34	4.39	20.9	0.030
mir22	15.17	11.25	15.11	11.28	15.01	9.87	4.27	19.3	0.000
mir132	10.29	7.24	10.21	5.32	10.57	6.20	4.04	16.5	0.000
mir21	6.00	3.03	8.62	5.71	6.23	2.04	3.49	11.2	0.000
mir23a	7.23	4.11	8.08	4.67	8.05	5.08	3.21	9.3	0.000
mir374a	8.60	10.90	14.02	10.31	14.15	7.41	2.76	6.8	0.031
mir29b	5.22	3.64	7.93	5.23	5.43	3.79	2.11	4.3	0.004
mir27a	8.89	6.72	8.81	7.30	9.79	7.35	2.04	4.1	0.001
mir146a	4.22	2.97	4.67	2.98	3.75	2.26	1.49	2.8	0.000
mir15a	8.91	8.72	10.58	8.72	10.09	8.57	1.23	2.3	0.001
mir421	8.61	7.99	8.91	7.27	10.09	8.62	1.22	2.3	0.011
mir1979	1.82	0.63	1.53	-0.01	1.17	0.44	1.14	2.2	0.000
mir155	4.69	3.29	4.13	3.18	4.01	2.90	1.13	2.2	0.000
mir222	3.90	3.04	4.03	2.88	3.39	2.26	1.05	2.1	0.000
mir221	3.87	3.31	4.23	3.08	4.13	2.90	0.98	2.0	0.000
mir532-5p	5.63	7.35	5.81	6.43	6.71	7.80	-1.17	-2.2	0.002
mir181b	2.87	4.09	2.64	4.27	3.35	4.32	-1.28	-2.4	0.000
mir181a	1.99	3.41	1.73	3.17	2.65	3.58	-1.29	-2.4	0.000
mir181c	6.98	8.63	6.85	8.36	7.33	8.74	-1.54	-2.9	0.000
mir874	4.00	5.49	3.88	6.54	3.61	4.64	-1.72	-3.3	0.001
mir342-5p	7.39	8.78	5.56	8.25	5.25	8.68	-2.55	-5.8	0.008
mir193b	3.00	5.89	2.55	5.78	3.63	6.91	-3.15	-8.8	0.000
mir99a	11.86	16.69	12.63	15.51	13.31	16.86	-3.77	-13.5	0.000
mir263	10.22	15.56	9.58	15.16	11.79	16.81	-5.35	-41.7	0.000
mir125b-5p	9.78	16.87	9.25	15.14	9.93	16.48	-6.57	-90.9	0.000
Naive vs CCR4+	Naive	CCR4+	Naive	CCR4+	Naive	CCR4+	M (Δ Ct)	Fold Change	FDR
mir22	15.17	10.92	15.11	10.78	15.01	10.83	4.24	18.9	0.000
mir21	6.00	2.87	8.62	4.23	6.23	2.35	3.94	15.3	0.000
mir132	10.29	8.34	10.21	5.52	10.57	5.87	3.57	11.8	0.000
mir23a	7.23	4.55	8.08	3.78	8.05	4.85	3.39	10.5	0.000
mir146a	4.22	2.10	4.67	1.87	3.75	1.95	2.25	4.8	0.000
mir222	3.90	1.96	4.03	1.61	3.39	1.77	1.99	4.0	0.000
mir27a	8.89	6.49	8.81	7.84	9.79	7.83	1.86	3.6	0.002
mir29b	5.22	4.17	7.93	5.09	5.43	4.39	1.80	3.5	0.019
mir155	4.69	2.81	4.13	2.30	4.01	2.27	1.77	3.4	0.000
mir221	3.87	2.38	4.23	2.56	4.13	2.69	1.56	3.0	0.000
mir130b	10.52	8.91	9.85	9.01	10.23	8.55	1.34	2.5	0.000
mir15a	8.91	7.98	10.58	9.08	10.09	8.95	1.32	2.5	0.001
mir454	8.09	7.19	8.96	7.38	7.69	6.51	1.24	2.4	0.001
mir1979	1.82	0.36	1.53	0.29	1.17	0.55	1.12	2.2	0.000
mir185	9.47	8.06	9.53	9.34	9.83	8.37	1.07	2.1	0.032
mir15b	7.98	6.61	7.63	6.51	7.47	6.75	1.07	2.1	0.004
mir421	8.61	7.48	8.91	8.30	10.09	8.91	1.04	2.1	0.032
mir30b	0.51	2.02	1.18	2.10	0.79	1.43	-1.02	-2.0	0.026
mir-532-3p	4.74	5.70	4.63	5.83	5.19	6.21	-1.05	-2.1	0.001
mir532-5p	5.63	7.04	5.81	7.68	6.71	7.55	-1.34	-2.5	0.001
mir342-5p	7.39	9.41	5.56	9.86	5.25	7.53	-2.95	-7.8	0.002
mir99a	11.86	16.11	12.63	15.35	13.31	17.21	-3.61	-12.2	0.000
mir193b	3.00	7.69	2.55	7.97	3.63	7.03	-4.55	-23.3	0.000
mir263	10.22	15.76	9.58	14.59	11.79	16.51	-5.16	-35.7	0.000
mir125b-5p	9.78	16.16	9.25	16.07	9.93	16.89	-6.72	-111.1	0.000
CCR4- vs CCR4+	CCR4-	CCR4+	CCR4-	CCR4+	CCR4-	CCR4+	M (Δ Ct)	Fold Change	FDR
mir181b	4.09	3.09	4.27	3.44	4.32	3.29	0.97	2.0	0.000
mir193b	5.89	7.69	5.78	7.97	6.91	7.03	-1.40	-2.6	0.027

Nano-scale miRNA profiling in asthma

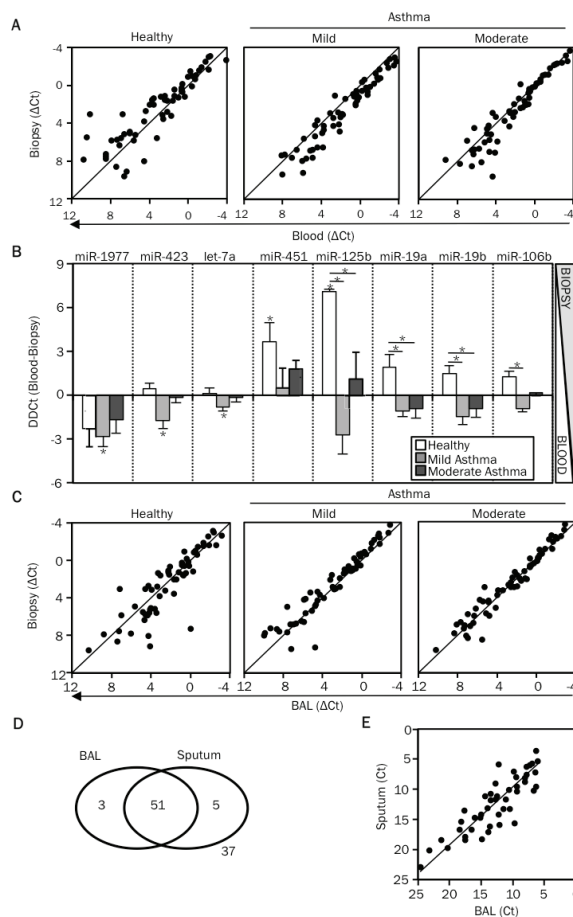


Figure 11. Airway T cells have a distinct miRNA signature compared to circulating T cells. A. Using nano-scale PCR, miRNA expression levels were measured in CD3⁺ T cells isolated from matched bronchial biopsy, BAL and blood specimens of 3 healthy controls, 6 mild and 6 moderate asthmatic patients. Expression levels of miRNAs (Δ Ct) in each sample were first calculated by subtracting the Ct value of the miRNA from the mean Ct value of the housekeeping miRNAs, miR-103 and miR-191, in that sample. The dot-plot displays the correlation in miRNA expression levels (Δ Ct) between T cells obtained from bronchial biopsy and blood specimens, across the study groups. B. The graph displays the difference in the expression levels ($\Delta\Delta$ Ct) between blood and bronchial biopsy T cells ($\Delta\Delta$ Ct = Δ Ct blood - Δ Ct bronchial biopsy). All miRNAs indicated on the figure were differentially expressed in airway T cells compared to blood T cells *i.e.* airway-specific are shown. miR-125b, miR-19a, miR-19b and miR-106b had expression values ($\Delta\Delta$ Ct) significantly different between healthy subjects and asthmatic patients. *p*-values were obtained by ANOVA, * *p* < 0.01. C. Dot-plots display the correlation in miRNA expression levels between T cells obtained from bronchial biopsy and BAL specimens, across the study groups. D. A panel of 96 miRNAs (mix 2) was measured in BAL and sputum supernatant samples by using the nano-scale PCR method. The venn diagram illustrates the overlap in the miRNAs detected in the two samples. E. The dot-plot displays the correlation in miRNA expression levels (Ct values) between BAL and sputum supernatant samples.

ied little among the many RNA samples, we expressed miRNA abundance as the difference (Δ Ct) between the Ct value for each miRNA and the mean of the Ct values for these two housekeeping miRNAs in the same sample [22]. Quantile normalization and delta-Ct methods yielded very similar results (data not shown).

Overall, miRNA expression patterns of circulating T cells were influenced more by T cell subtype than disease status (Figure 9A). *In vivo* differentiation of memory T cells was associated with major changes in miRNA expression in all subject groups. Among the many miRNAs that were significantly different, miR-125b, miR-

263, miR-193b, miR-99a and miR-342-5p were down-regulated over 10-fold in both subsets of memory T cells compared with their shared naïve precursors, while miR-22, miR-21, miR-132, miR-23a and miR-146a were upregulated to a similar degree (Figure 9B, 10A and Table 1). Nine miRNAs (miR-181a, b, c, miR-222, miR-130b, miR-146a, miR-155, miR-221 and miR-193b) were differentially expressed in the Th2-enriched CCR4⁺ versus Th2-depleted CCR4⁻ memory cell subsets (Figure 9B, 10B and Table 1). The full spectrum of miRNA expression changes seen in the freshly isolated T cells was not observed in *in vitro*-differentiated Th2 cells, supporting the rationale for study-

Nano-scale miRNA profiling in asthma

Table 2. List of miRNA detected in Sputum and BAL supernatants

Sputum and BAL (51)	BAL ONLY(3)	Sputum ONLY (5)
Let7b	mir100	Let7f
Let7d	mir378	mir122
Let7g	mir663b	mir1977
mir103		mir263
mir106a		mir874
mir1228 5p		
mir125 5p		
mir1260		
mir130b		
mir140		
mir142 5p		
mir146a		
mir150		
mir151 5p		
mir15b		
mir16		
mir17		
mir181c		
mir181d		
mir186		
mir18b		
mir191		
mir193b		
mir195		
mir1972		
mir1979		
mir199 5p		
mir19b		
mir20b		
mir222		
mir26b		
mir29b		
mir29c		
mir30a		
mir30e		
mir320c		
mir339 5p		
mir342 3p		
mir345		
mir374a		
mir451		
mir483 5p		
mir532 3p		
mir574 5p		
mir590 3p		
mir629		
mir660		
mir92a		
mir93		
mir95		
mir99a		

ing *in vivo*, rather than *in vitro* differentiated cells (data not shown).

Most importantly, isolating functionally relevant T cell subsets aided the identification of asthma-associated miRNA expression patterns (**Figure 9C, 10C**). miR-223 was significantly downregulated in subjects with mild or moderate asthma compared to healthy controls in all subsets, especially naïve T cells (**Figure 9C**). Like miR-223, miR-374a showed an asthma-associated reduction in naïve T cells, but the opposite pattern was observed in CCR4⁺ memory T cells. miR-1290, a primate-specific miRNA, was the most significantly upregulated miRNA in subjects with mild asthma. This difference was significant only in naïve T cells, though a similar pattern was observed in both memory subsets (**Figure 9C**). Interestingly, asthma-associated changes in miR-132 expression were seen only in the Th2-enriched CCR4⁺ memory T cell population (**Figure 9C**). These examples illustrate how our approach enabled the identification of asthma-associated miRNAs while also revealing the cell types in which miRNA levels are perturbed in diseased states.

Four miRNAs (miR-342-3p, miR-19a, miR-21 and miR-532-3p) were differentially expressed between mild asthmatic subjects who had never received corticosteroid treatment and moderate asthmatic subjects whose symptoms were controlled with inhaled corticosteroids (**Figure 9D, 10C**). Intriguingly, these miRNAs displayed similar patterns in moderate asthmatic subjects and healthy controls, suggesting that their dysregulated expression in asthma, as revealed in mild corticosteroid-naïve asthmatic subjects, may be corrected by corticosteroid treatment.

miRNA profile of asthmatic airway T cells

To test whether tissue-specific programming events shape the miRNA profile of T cells in asthma, we compared the miRNA profile of T cells from bronchial tissue and blood. The expression of most miRNAs correlated closely in these two compartments for all subject groups (**Figure 11A**). However, a small group of miRNAs exhibited tissue-specific expression in one or more subject groups (**Figure 11B**). miR-125b and miR-451 were significantly increased in airway T cells in healthy subjects, while miR-1977, miR-423 and let-7a were decreased in

Nano-scale miRNA profiling in asthma

the airway T cells of mild asthmatic subjects (**Figure 11B**). We next tested whether the effect of airway tissue residence on miRNA expression was significantly different between healthy and asthmatic subjects. Indeed, four miRNAs (miR-125b, miR-19a, miR-19b and miR-106b) exhibited decreased airway-specific expression in mild asthmatic subjects compared to healthy controls (**Figure 11B**). Intermediate levels of airway-specific expression were observed in moderate asthmatic subjects (**Figure 11B**). Differences in the expression of miRNAs in both blood and airway T cells contributed to asthma-associated changes.

Finally, we compared airway luminal T cells collected from BAL with airway tissue T cells sorted from bronchial biopsies. miRNA expression was highly correlated in T cells sorted from these distinct lung compartments, though a few miRNAs (miR-106b, miR-92b and miR-25) highly expressed in BAL T cells, were slightly but significantly less abundant in tissue-infiltrating T cells from biopsies (**Figure 11C**).

Airways lining fluids, sputum and BAL, have comparable miRNA profiles

Profiling miRNAs in serum has proven a useful and popular method for disease biomarker discovery [23]. We used nano-scale qPCR to measure 96 miRNAs in fluids lining diseased lung tissue, as these samples are more likely to provide disease-specific information than serum. BAL and induced sputum supernatants contained a diverse and abundant pool of miRNAs (**Figure 11D** and **Table 2**). Moreover, their miRNA profiles correlated closely, supporting the use of noninvasively obtained sputum supernatant as a surrogate for BAL, which requires bronchoscopy (**Figure 11E**). These data demonstrate that the fluid fractions of sputum and BAL samples are a rich source of miRNAs that can be profiled by nano-scale qPCR for biomarker discovery in various lung diseases, including asthma.

Discussion

The nearly ubiquitous involvement of the miRNA pathway in mammalian development, tissue homeostasis, and pathology has spurred an enormous effort to catalogue and characterize miRNA expression and function in a large variety of experimental and clinical settings.

Research into mechanisms and markers of human disease is frequently constrained by the limited amount of tissue available for research purposes. In addition, tissue heterogeneity may obscure disease-associated gene expression signals unless the effort is made to isolate and study individual cell types that are involved in disease pathogenesis. This process further limits the number of cells available for analysis, especially for diseases driven by relatively small populations of infiltrating inflammatory cells. Therefore, it is vitally important to develop techniques to study tissue responses and signatures of disease at a miniaturized scale. To meet this need, we developed a novel integrated approach for profiling miRNA expression in very small numbers of cells obtained from clinical specimens. Our approach couples cell sorting from dispersed tissues with a high fidelity and high throughput qRT-PCR method that delivers sensitive and quantitative miRNA detection in RNA samples from as little as 100 cells.

We applied our integrated approach to discover differentially expressed miRNAs in FACS sorted peripheral blood and airway-infiltrating T lymphocytes in a cross-sectional study of human asthma. A prior analysis of miRNA expression patterns in lung biopsy samples failed to identify asthma or corticosteroid treatment-associated miRNAs, possibly due to the heterogeneous cellular content of tissue biopsies [24]. Consistent with this possibility, analysis of airway brushings, which are highly enriched for epithelial cells, uncovered dramatically altered miRNA expression patterns in asthmatic subjects [25]. Employing cell sorting to isolate pathologically relevant inflammatory cells with nano-scaled assays for miRNA profiling in very small cell samples, we were able to identify several miRNAs associated with cell type, disease status, and tissue of origin. Major differences in miRNA expression were observed between isolated human naïve and memory T cell subtypes. These data extend previous observations, both in *in vitro* and mouse models, that memory T cell differentiation involves extensive miRNA repertoire reprogramming [21, 26-29]. Since the relative frequency of T cell subtypes varies significantly among individuals, this dominant pattern of cell type-specific differences in miRNA expression could have confounded comparisons between healthy and asthmatic

Nano-scale miRNA profiling in asthma

subjects. However, isolating homogenous cell populations prior to profiling, considerably reduced this source of variation and allowed us to identify miRNA expression patterns associated with asthma.

This report provides a generic experimental framework and tools to facilitate the discovery of miRNAs that are associated with human diseases. The miRNA signatures identified in this study may be extended and refined by further analysis of miRNA expression in relation to asthma susceptibility, severity, active Th2 inflammation, and response to therapy. By focusing on freshly isolated pathogenic T cells present in the blood and airways, we greatly increased the probability that the differentially expressed miRNAs discovered in our study regulate immune functions that contribute to asthma pathology. Regardless of whether the perturbations in miRNA expression are the cause or effect of disease, they represent attractive drug targets and/or biomarkers for asthma.

Acknowledgments

We thank the staff at the Wellcome Trust Clinical Research Facility (University of Southampton, UK) where samples were acquired from volunteers; Richard Jewel and Carolann McGuire for providing assistance in the flow cytometry facility; Andrea Barczak and Rebecca Barbeau at the SABRe Functional Genomics core facility; and Alain Mir at Fluidigm for helpful discussions and assistance with the Biomark instrument. This project was funded by the Dana Foundation (K.M.A.), the UCSF Program for Breakthrough Biomedical Research (K.M.A. & D.J.E.), GSK National Clinician Scientist Fellowship Award and Peel Travel Fellowship Award (P.V.). L.J.S. is a National Science Foundation Graduate Research Fellow.

Author Contributions

G.S., P.V., K.M.A. conceived the work, designed, performed and analyzed experiments, and wrote the paper; G.S. and P.V. obtained clinical specimens and performed experiments; N.O., L.K., M.N., A.P.G. recruited patients, helped obtain clinical specimens and, as well as L.S., performed some experiments; P.G.W. and J.V.F. recruited patients, obtained, and prepared BAL and sputum supernatants; R.D. provided support and direction for obtaining and processing

clinical specimens; R.B. and F.M. designed miRNA primers and shared multiplex qRT-PCR protocols prior to their publication; C.E. & D.E. performed statistical analysis.

Address correspondence to: K Mark Ansel, 513 Parnassus Avenue, UCSF Box 0414, San Francisco, CA 94143-0414. Tel: +1-415-476-5368; Fax: +1-415-502-4995; E-mail: mark.ansel@ucsf.edu

References

- [1] O'connell RM, Rao DS, Chaudhuri AA and Baltimore D. Physiological and pathological roles for microRNAs in the immune system. *Nat Rev Immunol* 2010; 10: 111-122.
- [2] Lanford RE, Hildebrandt-Eriksen ES, Petri A, Persson R, Lindow M, Munk ME, Kauppinen S and Orum H. Therapeutic silencing of microRNA-122 in primates with chronic hepatitis C virus infection. *Science* 2010; 327: 198-201.
- [3] Lu J, Getz G, Miska EA, Alvarez-Saavedra E, Lamb J, Peck D, Sweet-Cordero A, Ebert BL, Mak RH, Ferrando AA, Downing JR, Jacks T, Horvitz HR and Golub TR. MicroRNA expression profiles classify human cancers. *Nature* 2005; 435: 834-838.
- [4] Chen X, Ba Y, Ma L, Cai X, Yin Y, Wang K, Guo J, Zhang Y, Chen J, Guo X, Li Q, Li X, Wang W, Wang J, Jiang X, Xiang Y, Xu C, Zheng P, Zhang J, Li R, Zhang H, Shang X, Gong T, Ning G, Zen K and Zhang CY. Characterization of microRNAs in serum: a novel class of biomarkers for diagnosis of cancer and other diseases. *Cell Res* 2008; 18: 997-1006.
- [5] Castanotto D and Rossi JJ. The promises and pitfalls of RNA-interference-based therapeutics. *Nature* 2009; 457: 426-433.
- [6] Wang Q, Wang Y, Minto AW, Wang J, Shi Q, Li X and Quigg RJ. MicroRNA-377 is up-regulated and can lead to increased fibronectin production in diabetic nephropathy. *FASEB J* 2008; 22: 4126-4135.
- [7] Li Z, Zhang S, Huang C, Zhang W, Hu Y and Wei B. MicroRNAome of splenic macrophages in hypersplenism due to portal hypertension in hepatitis B virus-related cirrhosis. *Exp Biol Med* 2008; 233: 1454-1461.
- [8] Vijayanand P, Durkin K, Hartmann G, Morjaria J, Seumois G, Staples KJ, Hall D, Bessant C, Bartholomew M, Howarth PH, Friedmann PS and Djukanovic R. Chemokine receptor 4 plays a key role in T cell recruitment into the airways of asthmatic patients. *J Immunol* 2010; 184: 4568-4574.
- [9] Pauwels RA, Buist AS, Calverley PM, Jenkins CR and Hurd SS. Global strategy for the diagnosis, management, and prevention of chronic obstructive pulmonary disease. *NHLBI/WHO*

Nano-scale miRNA profiling in asthma

- Global Initiative for Chronic Obstructive Lung Disease (GOLD) Workshop summary. *Am J Respir Crit Care Med* 2001; 163: 1256-1276.
- [10] Vijayanand P, Seumois G, Pickard C, Powell RM, Angco G, Sammut D, Gadola SD, Friedmann PS and Djukanovic R. Invariant natural killer T cells in asthma and chronic obstructive pulmonary disease. *N Engl J Med* 2007; 356: 1410-1422.
- [11] Tang F, Hajkova P, Barton SC, O'Carroll D, Lee C, Lao K and Surani MA. 220-plex microRNA expression profile of a single cell. *Nat Protoc* 2006; 1: 1154-1159.
- [12] Gentleman RC, Carey VJ, Bates DM, Bolstad B, Dettling M, Dudoit S, Ellis B, Gautier L, Ge Y, Gentry J, Hornik K, Hothorn T, Huber W, Iacus S, Irizarry R, Leisch F, Li C, Maechler M, Rossini AJ, Sawitzki G, Smith C, Smyth G, Tierney L, Yang JY and Zhang J. Bioconductor: open software development for computational biology and bioinformatics. *Genome Biol* 2004; 5: R80.
- [13] Robinson DS, Hamid Q, Ying S, Tsicopoulos A, Barkans J, Bentley AM, Corrigan C, Durham SR and Kay AB. Predominant Th2-Like Bronchoalveolar Lymphocyte-T Population in Atopic Asthma. *N Engl J Med* 1992; 326: 298-304.
- [14] Vijayanand P, Seumois G, Pickard C, Powell RM, Angco G, Sammut D, Gadola SD, Friedmann PS and Djukanovic R. Invariant natural killer T cells in asthma and chronic obstructive pulmonary disease. *N Engl J Med* 2007; 356: 1410-1422.
- [15] Vijayanand P, Durkin K, Hartmann G, Morjaria J, Seumois G, Staples KJ, Hall D, Bessant C, Bartholomew M, Howarth PH, Friedmann PS and Djukanovic R. Chemokine receptor 4 plays a key role in T cell recruitment into the airways of asthmatic patients. *J Immunol* 2010; 184: 4568-4574.
- [16] Spurgeon SL, Jones RC and Ramakrishnan R. High throughput gene expression measurement with real time PCR in a microfluidic dynamic array. *PLoS One* 2008; 3: e1662.
- [17] Chen C, Ridzon DA, Broomer AJ, Zhou Z, Lee DH, Nguyen JT, Barbisin M, Xu NL, Mahuvakar VR, Andersen MR, Lao KQ, Livak KJ and Guegler KJ. Real-time quantification of microRNAs by stem-loop RT-PCR. *Nucleic Acids Res* 2005; 33: e179.
- [18] Moltzahn F, Olshen AB, Baehner L, Peek AS, Fong L, Stoppler HJ, Simko J, Hilton JF, Carroll PR and Blieloch R. Microfluidic based multiplex qRT-PCR identifies diagnostic and prognostic microRNA signatures in sera of prostate cancer patients. *Cancer Res* 2010.
- [19] Sandig H, McDonald J, Gilmour J, Arno M, Lee TH and Cousins DJ. Human Th2 cells selectively express the orexigenic peptide, pro-melanin-concentrating hormone. *Proc Natl Acad Sci U S A* 2007; 104: 12440-12444.
- [20] Git A, Dvinge H, Salmon-Divon M, Osborne M, Kutter C, Hadfield J, Bertone P and Caldas C. Systematic comparison of microarray profiling, real-time PCR, and next-generation sequencing technologies for measuring differential microRNA expression. *RNA* 2010; 16: 991-1006.
- [21] Barski A, Jothi R, Cuddapah S, Cui K, Roh TY, Schones DE and Zhao K. Chromatin poises miRNA- and protein-coding genes for expression. *Genome Res* 2009; 19: 1742-1751.
- [22] Bargaje R, Hariharan M, Scaria V and Pillai B. Consensus miRNA expression profiles derived from interplatform normalization of microarray data. *RNA* 2010; 16: 16-25.
- [23] Mitchell PS, Parkin RK, Kroh EM, Fritz BR, Wyman SK, Pogosova-Agadjanyan EL, Peterson A, Noteboom J, O'Brian KC, Allen A, Lin DW, Urban N, Drescher CW, Knudsen BS, Stirewalt DL, Gentleman R, Vessella RL, Nelson PS, Martin DB and Tewari M. Circulating microRNAs as stable blood-based markers for cancer detection. *Proc Natl Acad Sci U S A* 2008; 105: 10513-10518.
- [24] Williams AE, Larner-Svensson H, Perry MM, Campbell GA, Herrick SE, Adcock IM, Erjefalt JS, Chung KF and Lindsay MA. MicroRNA expression profiling in mild asthmatic human airways and effect of corticosteroid therapy. *PLoS One* 2009; 4: e5889.
- [25] Solberg OD, Ostrin EJ, Love MI, Peng JC, Bhakta NR, Hou L, Nguyen C, Solon M, Barczak AJ, Zlock LT, Blagev DP, Finkbeiner WE, Ansel KM, Arron JR, Erle DJ and Woodruff PG. Airway Epithelial miRNA Expression is Altered in Asthma. *American journal of respiratory and critical care medicine* 2012.
- [26] Monticelli S, Ansel KM, Xiao C, Socci ND, Krichevsky AM, Thai TH, Rajewsky N, Marks DS, Sander C, Rajewsky K, Rao A and Kosik KS. MicroRNA profiling of the murine hematopoietic system. *Genome Biol* 2005; 6: R71.
- [27] Merkerova M, Belickova M and Bruchova H. Differential expression of microRNAs in hematopoietic cell lineages. *Eur J Haematol* 2008; 81: 304-310.
- [28] Kuchen S, Resch W, Yamane A, Kuo N, Li Z, Chakraborty T, Wei L, Laurence A, Yasuda T, Peng S, Hu-Li J, Lu K, Dubois W, Kitamura Y, Charles N, Sun HW, Muljo S, Schwartzberg PL, Paul WE, O'Shea J, Rajewsky K and Casellas R. Regulation of microRNA expression and abundance during lymphopoiesis. *Immunity* 2010; 32: 828-839.
- [29] Wu H, Neilson JR, Kumar P, Manocha M, Shankar P, Sharp PA and Manjunath N. miRNA profiling of naive, effector and memory CD8 T cells. *PLoS One* 2007; 2: e1020.

Publishing Agreement

It is the policy of the University to encourage the distribution of all theses, dissertations, and manuscripts. Copies of all UCSF theses, dissertations, and manuscripts will be routed to the library via the Graduate Division. The library will make all theses, dissertations, and manuscripts accessible to the public and will preserve these to the best of their abilities, in perpetuity.

Please sign the following statement:

I hereby grant permission to the Graduate Division of the University of California, San Francisco to release copies of my thesis, dissertation, or manuscript to the Campus Library to provide access and preservation, in whole or in part, in perpetuity.

Laura Simpson

Author Signature

March 16, 2015

Date